SINGLE MOLECULE STUDIES OF BRANCHED POLYMER DYNAMICS

BY

DANIELLE J. MAI

DISSERTATION

Submitted in partial fulfillment of the requirements
for the degree of Doctor of Philosophy in Chemical Engineering
in the Graduate College of the
University of Illinois at Urbana-Champaign, 2016

Urbana, Illinois

Doctoral Committee:

Associate Professor Charles M. Schroeder, Chair
Professor Jonathan J. L. Higdon
Assistant Professor Randy H. Ewoldt
Assistant Professor Charles E. Sing

ABSTRACT

Polymer architecture plays a major role on the emergent physical and chemical properties of materials such as elasticity and wettability. Branched polymers exhibit strikingly different rheological behavior (*e.g.* enhanced stress dissipation and strain hardening) compared to linear polymers. In recent years, the dynamic properties of branched polymers have been studied using bulk rheological techniques (Chapter 1), but we still lack a full understanding of how molecular-scale interactions give rise to macroscopic properties for topologically complex polymers. Single molecule studies enable the direct observation of polymer chain dynamics at the molecular level; however, the vast majority of single polymer studies have only focused on linear DNA molecules (Chapter 2).

In this dissertation, we extend single molecule techniques to study the dynamics of branched polymers, which effectively bridges the gap between bulk-scale rheological properties and molecular scale behavior. In particular, we explore the synthesis, characterization, single molecule dynamics, and Brownian dynamics simulations of DNA-based branched polymers. This approach enables us to interrogate the impact of distributions in molecular size and architecture, thereby holding the potential to fundamentally change our understanding of the rheological response of topologically complex polymers.

We first developed a two-step synthesis method to generate branched polymers for single molecule visualization (Chapter 3). Here, we use a graft-onto synthesis method by linking side branches onto DNA backbones, thereby producing star, H-shaped, and comb-shaped polymers. In these experiments, DNA-based branched polymers are designed to contain short branches (1-10 kilobase pairs) and long backbones (10-40 kilobase pairs), where the branches and backbones are

monodisperse and the branch distribution can be controlled in an average sense. Following synthesis and purification, we utilize single molecule fluorescence microscopy to observe the dynamics of these molecules, in particular by tracking the side branches and backbones independently (Chapter 4). In this way, this imaging method allows for characterization of these materials at the single molecule level, including quantification of polymer contour length and branch distributions for varying synthetic conditions.

Moving beyond characterization, we study the dynamics of single branched polymers in flow using a molecular rheology approach. In one experiment, we study the dynamics of asymmetric star, H-shaped, and comb-shaped DNA polymers tethered to the surface in a microfluidic flow cell (Chapter 4). In this way, we study the impact of branch frequency and position on backbone chain relaxation from high stretch. In a second experiment, we utilize a microfluidic cross-slot device to hydrodynamically 'trap' branched DNA molecules in planar extensional flow, thereby studying the impact of branching on relaxation in solution, as well as transient and steady-state dynamics in flow (Chapter 5). We present results for branched polymer dynamics as functions of branch frequency and flow strength. We also conduct Brownian dynamics simulations based on a coarse-grained model for comb polymers (Chapter 6). Results from simulations and experiments agree qualitatively, and branched polymers exhibit a weaker dependence of relaxation on total polymer molecular weight in comparison to linear polymers.

Overall, this work presents molecular-scale investigations of branched polymer dynamics. From a broad perspective, this research provides a molecular-based understanding of topologically complex polymers in flow, thereby holding the potential to advance the large-scale production of polymers. Importantly, this platform can be further extended to study branched polymers in

alternate flow fields such as simple shear flow or linear mixed flows, semi-dilute solutions, and concentrated solutions. These experiments will provide a molecular basis for phenomena observed in branched polymers, from viscosity modification of blended branched polymer solutions to hierarchical relaxation mechanisms of entangled branched polymers to enhanced strain hardening of comb polymer melts.

dedicated to my family
and to the memory of my beloved mother

ACKNOWLEDGMENTS

I would like to thank my research advisor Dr. Charles Schroeder for his curiosity, vision, and guidance through a challenging and rewarding course of research. Charles has inspired me to dive deeper into science than I ever imagined, and I greatly appreciate his support and mentorship. I would also like to thank Dr. Charles Sing for bringing new perspectives to my work, keeping his door open for countless discussions, and providing access to his computational resources. I thank the members of my preliminary exam and dissertation committees, Drs. Jonathan Higdon, Deborah Leckband, and Randy Ewoldt, for insightful questions and suggestions. I am especially grateful to Drs. Rohit Bhargava and Alex Scheeline for advice in navigating the academic landscape.

The Department of Chemical & Biomolecular Engineering has been particularly supportive, and I acknowledge campus resources including the Roy J. Carver Biotechnology Center, Metabolomics Research Center, and Dr. Kenis's clean room. I am indebted to funding that enabled freedom in my research pursuits, including an Illinois Distinguished Fellowship, a National Science Foundation Graduate Research Fellowship, and the Mavis Future Faculty Fellows Program.

I have enjoyed friendship and growth with the entire Schroeder research group, with special thanks for mentorship from Chris, Amanda, Folarin, Arnab, Eric, and Melikhan, daily entertainment working alongside Dan, Utsav, Luke, Kaiwen, Anish, and Subha, and fresh ideas from our newest members, Peter, Songsong, Bo, and Shivani. Immeasurable thanks to Kejia for her codes, which saved months of staring at the ends of DNA molecules. I am particularly thankful for the opportunity to work with motivated and talented undergraduate researchers, Lily Chen, Sarah Kuhl, and Zhiwei Zhang.

To my closest friends at Illinois – Yelena and Kate – thank you for sharing the good times, the bad times, and many lunches on the quad with squirrels; may we never finish enough red wine or coloring books with Jillian, Liz, Meg, and Laura. Thanks to my climbing partners, Matt and Dylan, for mutual trust. Thanks to Bill and Jill, Andy and Catherine, Andrea, and Nick for their company in drives between Champaign and Ann Arbor. Thanks to countless other friends at Illinois in ChBE, GradSWE, weSTEM, iFEAT, the rogue book club, and the Ewoldt research group. I am appreciative of the graduate community at Illinois for making this experience so enjoyable.

Entering a graduate program would not have been possible without a series of mentors in science and engineering – Lisa Harbour, Drs. John Goudie, Silvia Rossbach, Ben Hamilton, Jason Daida, Nina Lin, Elijah Petersen, Sharon Soong, and Jason McMullan – thank you for helping dreams come true.

Finally, I thank my family for their love, patience, and encouragement. My sister Kim paved the way for me growing up, in a way that I always have and will look up to her. My parents made everything possible, in every sense of the phrase. Mom, I miss you every day. Dad, I am grateful for your unending enthusiasm and love. Most of all, I would like to express my love and gratitude to my husband Jonathan, who is the stable force in my life. Thank you for always knowing how to make me smile, laugh, and keep perspective, even from 350 miles away.

TABLE OF CONTENTS

1 GENERAL INTRODUCTION

Fundamental studies of polymer dynamics at the molecular level are critical for improved processing and large-scale production of polymers [1]. Commercial polymers frequently contain entangled and/or branched molecules, which result in strikingly different rheological properties compared to dilute solutions of linear polymer molecules [2, 3]. Recent interest in rheological studies has focused on branched polymers such as low-density polyethylene, which is widely used in packaging applications. The influence of branching on flow properties, such as dissipation of stress, plays an intimate role in energy requirements and processing conditions for polymer production.

Current approaches for studying branched polymers include advanced techniques for polymer synthesis (*e.g.* living anionic polymerization, atom transfer radical polymerization), new purification methods based on molecular architecture (*e.g.* thermal gradient interaction chromatography), characterization of linear and non-linear viscoelastic rheology, and the development of molecular-scale simulations and theories [4]. Molecular-scale dynamics ultimately determines the macroscopic response of polymeric materials, so it is of critical importance to develop a clear understanding of microstructural dynamics in topologically complex polymer systems. In this work, we aim to extend single molecule experimental techniques to the study of branched polymers.

1.1 POLYMER CHAIN ARCHITECTURE

Polymer chain architecture encompasses a wide range of shapes and chain types, including linear polymers, branched polymers, ring polymers, and polymer networks [5]. Linear polymer chains

have only two ends, and extensive studies of linear polymers in polymer science include solution/melt thermodynamics, stability diagrams and phase behavior, bulk viscoelasticity, and investigations of single molecule dynamics. Branched polymers are defined as having additional polymeric chains attached to a linear molecule, resulting in a variety of architectures: star, H-shaped, pom-pom, and comb-shaped. Examples of polymer architectures are shown in **Figure 1.1**.

Recent work has focused on the impact of macromolecular branching on polymer dynamics and rheological behavior [3, 4]. The properties of branched polymers traverse a wide parameter space, including molecular weight, branch distribution, and architectural and molar mass dispersity [6]. In an entangled solution or melt of comb polymers, branches and branch points are known to dramatically slow down the overall relaxation of a material, especially as the branch molecular weight increases [2]. This complex topology leads to a spectrum of relaxation times related to movement of branches, segments between branches, and the entire molecular backbone. Thus, chain branching can result in extremely complex flow properties; for example, comb polymers in uniaxial extensional flow exhibit strain hardening under relatively low strain rates, whereas linear polymers do not [7].

Comb polymers have attracted recent interest due to advances in the chemical synthesis and purification of precisely structured molecules. Examples of model comb polymers include high-vacuum anionic polymerization of an ‘exact comb’ polyisoprene with three branches, in which the middle branch has twice the molecular weight of two other external branches [8], and thermal gradient interaction chromatographic isolation of combs with 3-5 branches [9]. The linear backbone within a comb polymer also permits a direct, molecular-scale comparison to a linear polymer. The isolation of precisely branched polymers launched an emerging sub-field of

branched polymer molecular rheology [6-17] that explores the role of architectural dispersity on flow.

The linear and non-linear viscoelastic response of comb polymer melts has been investigated using integrated approaches combining theory [1, 18, 19], simulations [4, 10, 11, 17], and bulk rheological experiments [7, 9-17]. Various techniques have uncovered a 'hierarchical' stress relaxation mechanism for comb polymer molecules that arises due to branched molecular architectures, such that sub-molecular relaxation processes take place over varying timescales [7, 12-14, 16, 17]. **Figure 1.2** illustrates a proposed series of relaxation processes for an entangled comb polymer after strain. This mechanism, however, has yet to be directly observed at the molecular level. Furthermore, a majority of branched polymer synthesis techniques result in structural heterogeneity, such that branch length, frequency, and location can vary greatly from molecule to molecule. These impurities blur the macroscopic rheological response of branched polymer melts [4, 6], and the non-linear behavior of branched polymers generally lacks description by a universal constitutive model, unlike linear [19], pom-pom [18], or model comb [20] polymers.

In our approach, biochemical synthetic techniques facilitate the synthesis of comb-shaped architectures by enabling a broad design space of chain lengths and branching densities. Precise structures may also be achieved by capitalizing on the template-based nature of nucleic acids. We seek to understand the relationship between the molecular parameters within this design space, molecular-scale chain behavior, and rheological phenomena in order to improve predictive tools for polymer engineering and overall control of polymer processing.

1.2 SINGLE POLYMER DYNAMICS USING DNA MOLECULES

Deoxyribonucleic acid (DNA) is frequently utilized as a model for single polymer molecules in flow [21-24]; moreover, single polymer experiments have allowed for the direct observation of unexpected phenomena such as molecular individualism [25] and conformational hysteresis [26]. While most studies of DNA as a model polymer have relied on its natural linear architecture [21], macromolecular DNA stars and pom-poms have been previously synthesized via sequence hybridization at a branched junction [27, 28]. Disadvantages associated with hybridized junctions include thermodynamic base-pair fluctuations, necessity of sequence specificity, and limited structural control. For these reasons, a more robust method to synthesize branched DNA structures is required for single molecule studies.

Single molecule experiments reveal a richness of information due to the inherent ability to observe individual dynamic molecular trajectories. Single molecule fluorescence microscopy enables the observation of molecular conformations, the direct measurement of end-to-end distance, and the ability to identify molecular sub-populations [24]. Furthermore, single molecule results can be compared to bulk-level experimental data, which intrinsically average over the structural heterogeneity in a sample.

1.3 DISSERTATION OVERVIEW

This dissertation describes our progress towards extending single molecule studies of polymer dynamics to branched polymer architectures. Chapter 2 outlines the current state of single molecule dynamics of topologically complex polymers, emphasizing the important but vastly unexplored space around branched polymers. Chapter 3 describes the synthesis, purification, and bulk-scale characterization of branched DNA polymers. Chapter 4 presents the single molecule

characterization and dynamics of branched polymers tethered to a surface. Here, we demonstrate our ability to control branch frequency distributions of DNA comb polymers, and we directly observe topology-controlled relaxation dynamics in branched DNA polymers. Chapter 5 extends the work of Chapters 3 and 4, exploring dilute solution relaxation of DNA comb polymers and stretching dynamics in planar extensional flow. Chapter 6 presents a method for modeling branched polymers via Brownian dynamics simulations, as well as preliminary data in support of experimental findings. Chapter 7 concludes this dissertation with closing remarks and a discussion of future directions.

1.4 FIGURES

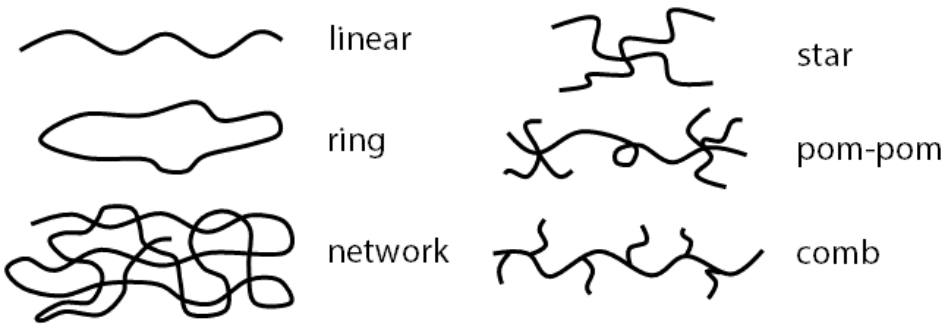

Figure 1.1. Examples of polymer architectures.

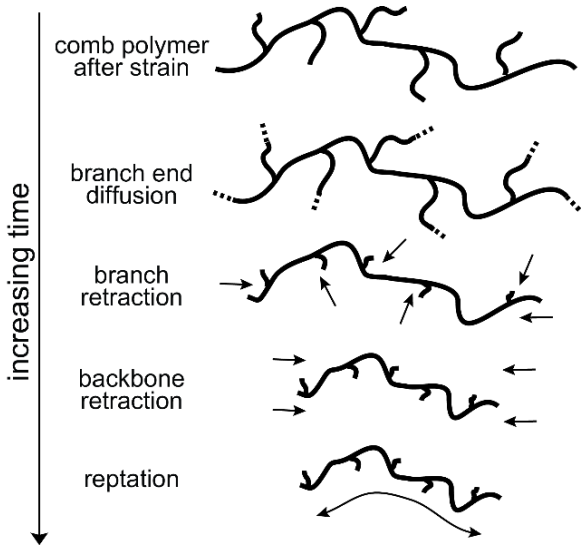

Figure 1.2. Hierarchical relaxation in a comb polymer melt.

1.5 REFERENCES

[1] Larson RG. The Structure and Rheology of Complex Fluids. New York: Oxford University Press; 1998.

[2] Dealy JM, Larson RG. Structure and Rheology of Molten Polymers. Cincinnati, OH: Hanser Publications; 2006.

[3] Larson RG. Predicting the Flow of Real Polymers. Science. 2011;333:1834-5.

[4] van Ruymbeke E, Lee H, Chang T, Nikopoulou A, Hadjichristidis N, Snijkers F, et al. Molecular rheology of branched polymers: decoding and exploring the role of architectural dispersity through a synergy of anionic synthesis, interaction chromatography, rheometry and modeling. Soft matter. 2014.

[5] Hiemenz PC, Lodge TP. Polymer Chemistry. 2nd ed. Boca Raton, FL: CRC Press; 2007.

[6] Snijkers F, van Ruymbeke E, Kim P, Lee H, Nikopoulou A, Chang T, et al. Architectural Dispersity in Model Branched Polymers: Analysis and Rheological Consequences. Macromolecules. 2011;44:8631-43.

[7] Lentzakis H, Vlassopoulos D, Read D, Lee H, Chang T, Driva P, et al. Uniaxial extensional rheology of well-characterized comb polymers. Journal of Rheology (1978-present). 2013;57:605-25.

[8] Ratkanthwar K, Hadjichristidis N, Lee S, Chang T, Pudukulathan Z, Vlassopoulos D. Synthesis and characterization of an exact comb polyisoprene with three branches having the middle branch twice the molecular weight of the other two identical external branches. Polymer Chemistry. 2013;4:5645-55.

[9] Chambon P, Fernyhough CM, Im K, Chang T, Das C, Embery J, et al. Synthesis, Temperature Gradient Interaction Chromatography, and Rheology of Entangled Styrene Comb Polymers. Macromolecules. 2008;41:5869-75.

[10] Daniels DR, McLeish TCB, Crosby BJ, Young RN, Fernyhough CM. Molecular Rheology of Comb Polymer Melts. 1. Linear Viscoelastic Response. Macromolecules. 2001;34:7025-33.

[11] Kapnistos M, Vlassopoulos D, Roovers J, Leal LG. Linear Rheology of Architecturally Complex Macromolecules: Comb Polymers with Linear Backbones. Macromolecules. 2005;38:7852-62.

[12] Kapnistos M, Kirkwood KM, Ramirez J, Vlassopoulos D, Leal LG. Nonlinear rheology of model comb polymers. Journal of Rheology (1978-present). 2009;53:1133-53.

[13] Kempf M, Ahirwal D, Cziep M, Wilhelm M. Synthesis and Linear and Nonlinear Melt Rheology of Well-Defined Comb Architectures of PS and PpMS with a Low and Controlled Degree of Long-Chain Branching. Macromolecules. 2013;46:4978-94.

[14] Ruocco N, Dahbi L, Driva P, Hadjichristidis N, Allgaier J, Radulescu A, et al. Microscopic Relaxation Processes in Branched-Linear Polymer Blends by Rheo-SANS. Macromolecules. 2013;46:9122-33.

[15] Snijkers F, Vlassopoulos D, Ianniruberto G, Marrucci G, Lee H, Yang J, et al. Double Stress Overshoot in Start-Up of Simple Shear Flow of Entangled Comb Polymers. ACS Macro Letters. 2013;2:601-4.

[16] Snijkers F, Vlassopoulos D, Lee H, Yang J, Chang T, Driva P, et al. Start-up and relaxation of well-characterized comb polymers in simple shear. Journal of Rheology (1978-present). 2013;57:1079-100.

[17] Bačová P, Lentzakis H, Read DJ, Moreno AJ, Vlassopoulos D, Das C. Branch-Point Motion in Architecturally Complex Polymers: Estimation of Hopping Parameters from Computer Simulations and Experiments. Macromolecules. 2014;47:3362-77.

[18] McLeish TCB, Larson RG. Molecular constitutive equations for a class of branched polymers: The pom-pom polymer. Journal of Rheology (1978-present). 1998;42:81-110.

[19] McLeish TCB. Tube theory of entangled polymer dynamics. Advances in Physics. 2002;51:1379-527.

[20] Lentzakis H, Das C, Vlassopoulos D, Read DJ. Pom-pom-like constitutive equations for comb polymers. Journal of Rheology. 2014;58:1855-75.

[21] Latinwo F, Schroeder CM. Model systems for single molecule polymer dynamics. Soft Matter. 2011;7:7907-13.

[22] Mai DJ, Brockman C, Schroeder CM. Microfluidic systems for single DNA dynamics. Soft matter. 2012;8:10560-72.

[23] Marciel AB, Schroeder CM. New directions in single polymer dynamics. Journal of Polymer Science Part B: Polymer Physics. 2013;51:556-66.

[24] Shaqfeh ESG. The dynamics of single-molecule DNA in flow. Journal of Non-Newtonian Fluid Mechanics. 2005;130:1-28.

[25] Perkins TT, Smith DE, Chu S. Single Polymer Dynamics in an Elongational Flow. Science. 1997;276:2016-21.

[26] Schroeder CM, Babcock HP, Shaqfeh ES, Chu S. Observation of polymer conformation hysteresis in extensional flow. Science. 2003;301:1515-9.

[27] Heuer DM, Saha S, Archer LA. Electrophoretic dynamics of large DNA stars in polymer solutions and gels. ELECTROPHORESIS. 2003;24:3314-22.

[28] Saha S, Heuer DM, Archer LA. Electrophoretic mobility of linear and star-branched DNA in semidilute polymer solutions. ELECTROPHORESIS. 2006;27:3181-94.

2 KNOTS, LOOPS, AND JUNCTIONS: SINGLE POLYMER DYNAMICS OF TOPOLOGICALLY COMPLEX DNA*

2.1 INTRODUCTION

Topological constraints in polymeric materials have long been considered as fascinating and challenging problems in polymer physics [1-3]. In mathematics, topology refers to the preservation of spatial properties upon continuous deformation such as stretching or bending. In some cases, shape and conformation are independent of topology, and topological constraints arise from the uncrossability of physically connected elements, such as entangled polymer chains [1]. In the field of polymer science, topology adopts a broad definition, generally referring to intramolecular shape (*e.g.* branched or circular chains) and/or intermolecular interactions (*e.g.* entangled chains), both of which are impacted by polymer sequence, molecular weight, architecture, and chain connectivity [4]. These microstructural and physical features provide non-chemical handles that can be leveraged to drive structure–property relationships in polymeric materials. For example, polymers with brush-like topologies have recently been used to prepare soft, solvent-free networks [5]. Here, tuning the polymer branch length and density resulted in single-component materials with superior elasticity and extensibility compared to designer hydrogels for biological applications.

Molecular-scale connectivity is known to play a key role in determining the relationship between molecular topology and the emergent physical properties of polymeric materials. Rheological studies of branched polymers with architectural dispersity have revealed the sensitivity of

*Adapted from D. J. Mai and C. M. Schroeder, *Current Opinion in Colloid and Interface Science*, *submitted* (2016).

viscoelastic response to topological impurities in entangled polymers [6]. Similarly, conflicting reports of ring polymer melt viscoelasticity have been attributed to trace linear impurities [7]. Topological defects in networks, such as dangling ends or loops, directly impact the mechanical properties of gels, in some cases preventing gel formation altogether [8]. Despite numerous advances in chemical synthesis, a grand challenge remains in achieving large-scale, precise control over complex polymer sequences and architectures [9].

In nature, these challenges are overcome by dynamic regulation of microscopic topological events in biological macromolecules with remarkably high frequency and precision. Biopolymers as deoxyribonucleic acid (DNA) undergo knotting and unknotting events, circularization and supercoiling, or the formation of branched junctions for replication [10]. These topological transitions are aided by the double stranded and double-helical nature of DNA strands, which imparts an intrinsic twist (or combination of twist and writhe) along DNA backbones. In living systems, DNA topology is regulated by a class of enzymes called topoisomerases, which are known to generate transient breakages along DNA strands to alter topology while preserving sequence [11]. Single molecule techniques have enabled deeply insightful biophysical studies of DNA topology, uncovering the structural dynamics of individual Holliday junctions [12] and mechanisms for supercoiling [13]. Nevertheless, the dynamics of polymers with complex topologies has not yet been fully characterized using single polymer techniques, and this nascent area of research is a particular exciting new direction in the field.

In this Chapter, we highlight the use of DNA to study the impact of topology on single polymer dynamics. This review covers recent experimental, computational, and theoretical advances in knotted, circular, and branched polymers. DNA serves as a powerful system for single polymer

dynamics, in particular due to an established understanding of the physical properties and preparation methods, including facile fluorescent labeling, compatibility with aqueous buffers, and templated synthesis of monodisperse polymers. For single molecule studies of linear DNA dynamics, we refer readers to recent reviews on DNA in hydrodynamic flows [14], electrophoresis [15], and confinement [16]. Here, we focus on the physics of polymer chain topology, namely its influence on single polymer dynamics at equilibrium and under non-equilibrium flows.

2.2 DNA KNOTS

Knots are central to the theory of mathematical topology [17], and naturally occurring knots have been discovered in various macromolecules and biopolymers [18]. Knots can also be generated by chemical and physical means, wherein the latter has been studied in the context of knots in single polymers. Rigorous definitions of knots exist only for closed structures, but knotting is observed on both open chains and closed loops in single DNA molecules. Knots may be classified in several ways, most commonly using the Alexander-Briggs notation [17]. Here, a knot is first designated by the number of self-crossings, followed by an arbitrary index to distinguish topologically different knots with the same number of crossings. A single loop with no knots (the 'unknot') is designated 0_1, and the simplest non-trivial knot (trefoil) is labeled 3_1. Knot complexity and topological uniqueness increase with the crossing number, such that five crossings give rise to two unique knots (5_1 and 5_2), six crossings to three unique knots (6_1, 6_2, 6_3), seven crossings to seven knots, and so on.

Further classifications for knots include torus, twist, and chiral or achiral knots. Torus knots encompass the family of knots with notation $(2n + 1)_1$; these knots can be represented as closed curves on the surface of a torus. Twist knots are an example of supercoiling and are formed by

twisting and folding a loop repeatedly before closing its ends. Finally, chirality describes whether a knot is equivalent to its mirror image.

Although natural occurrences of numerous knot topologies have been detected and classified since the late 1970s [18], the first demonstration of actively tying a molecular knot was not reported until 1999 [19]. The ability to simultaneously generate and visualize knots using optical tweezers enabled a seminal paper quantifying the behavior of knots in fluorescently labeled DNA molecules [20]. Quake and co-workers observed a strong influence of topology on the size and mobility of single knots in DNA (**Figure 2.1a-d**). Perhaps not surprisingly, knots with increasingly complex topologies diffused more slowly along DNA. Calculations of drag coefficients for single knots correlated with predictions for ideal, tight knots, thereby demonstrating the validity of DNA as a robust polymeric system for studying knotting phenomena.

These findings further sparked broad interest in the physics of knotted polymer molecules, which encompasses a wide design space, from equilibrium properties to topology-dependent behavior to knotting and unknotting dynamics. These topics have motivated detailed computational investigations of knots on open chains. For tight, localized knots, such as those generated by optical tweezers, loop closure and subsequent knot classification are relatively straightforward. Robust and efficient closure of complex knots generated *in silico*, however, poses a non-trivial problem. To address this challenge, Tubiana *et al.* developed a minimally interfering closure method to characterize entangled knots along an open polymer [21]. This method enabled many of the recent computational studies on single knotted chains in the past half-decade, several of which are highlighted in this section.

2.2.1 Knots in semiflexible polymers: considerations for knotted DNA

It is well known that double stranded DNA molecules are semiflexible polymers and exhibit notably different behaviors in comparison to truly flexible polymers [22]. Chain flexibility is often defined by the persistence length ℓ_p, which can be viewed as the distance along a polymer backbone over which local tangent vectors become uncorrelated. The bare, non-electrostatic persistence length of double stranded DNA is $\ell_p \cong 50$ nm, in contrast to $\ell_p < 1$ nm for many synthetic organic polymers. Knots are intrinsically bent and twisted, and the resulting knotted structures will be intimately affected by molecular properties such as chain thickness and flexibility. From this view, we begin our discussion of knots in DNA with a brief evaluation of the role of semiflexibility on knot properties and dynamics.

Grosberg and Rabin predicted that semiflexible wormlike chains form metastable knots, which spontaneously adopt a well-defined size, diffuse along a polymer, and eventually release from the chain end [23]. The knot contour is described as occupying a confining tube that has (itself) been pulled into a tight knot. Knot formation results in a free energy penalty with competing contributions from the bending energy and confining energy of the polymer, which lead to knot swelling and contracting, respectively.

Doyle and coworkers studied metastable knots with Monte Carlo simulations of long, linear semiflexible polymers [24]. This work determined the probability and size distributions of trefoil knots along chains of zero thickness with contour length $L_c > 400\ \ell_p$. With these dimensions, roughly one quarter of the chains formed trefoil knots, with a peak knot size of 12 ℓ_p. The most probable knot size was also shown to be independent of L_c, in agreement with the Grosberg–Rabin predictions. Conversion of knotting probabilities to a potential of mean force resulted in a local

minimum at the most probable knot size, whereas the global minimum corresponds to the unknotted state. The potential well was relatively broad, such that chains accommodate large knots with highly variable size; the depth of the potential well (~6 kT) indicates that unknotting events may be more likely to occur via knot diffusion than swelling of the entire chain.

More realistic polymers were also simulated by modifying the Grosberg-Rabin theory to accommodate nonzero chain width [24]. As the polymer thickness increased, knotting probability monotonically decreased, the potential well became more shallow, and the most probable knot size increased. These trends reveal the interplay between length scales in real, semiflexible chains. With consideration of appropriate scaling relations, it is possible that the understanding gained from studies of knotted DNA can be applied to polymers of varying flexibility.

2.2.2 Dynamics of knotted DNA polymers in nanoconfinement

Advances in DNA nanotechnology have motivated recent investigations of knotting in polynucleotides, from preventing knot formation during genetic barcoding [25] to determining viral packaging mechanisms [26]. DNA knots are enhanced by spatial confinement, whether by a viral capsid, intracellular environment, or nanofluidic device. Under confinement, DNA chains may be more prone to forming loops, internal folds, and self-entanglements.

Nanoconfinement geometries are defined by the number of dimensions with nanoscale features, such that 1D, 2D, and 3D confinement correspond to slits, channels, and cavities, respectively. A polymer is considered confined when the nanofeature dimension d is smaller than a molecule's radius of gyration R_g, such that $d < R_g$. In slits and channels, two primary regimes describe the

strength of confinement: weaker de Gennes confinement ($\ell_p \ll d < R_g$) and stronger Odijk confinement ($\ell_p \approx d$).

Knotting behavior differs in the de Gennes and Odijk regimes, as well as in the transition region between these two regimes. Micheletti, Marenduzzo, Orlandini, and co-workers have generated a large body of computational work [26-31] that explores confinement in both regimes and the transition region. Specifically, they applied numerical methods and simulations to characterize the equilibrium and dynamic behavior of DNA confined in spheres [26], tubes [27, 29-31], and slits [28, 31]. In these studies, d ranged from 40 nm to 1 μm and DNA contour lengths L_c ranged from 1.2 – 4.8 μm, corresponding to 24 – 96 persistence lengths or 3.5 – 14.0 kilobase pairs (kbp) of unstained DNA.

Monte Carlo simulations collectively revealed that the probability of knot formation and resulting knot topologies depend largely on d, L_c, and the confining geometry [26-28, 31]. The physical underpinnings of these trends were explored by applying Brownian dynamics (BD) simulations to observe time-dependent unknotting and knotting events along DNA strands in nanochannels [29, 30].

The probability of finding a knot along an equilibrium polymer conformation increased with the number of confining dimensions, such that the most knots were detected in spherical confinement, followed by channel-like and slit-like confinements [26-28, 31]. Overall, single polymers formed more complex knot topologies in channels compared to chains in slits: in cases of maximum knotting (L_c = 4.8 μm, d = 70 nm), simple trefoil knots (3_1) accounted for ~65% of the knots in slits but only ~50% of knots formed in channels [31].

Both nanoslit and nanochannel confinement resulted in non-monotonic knotting probabilities with respect to d [27, 28, 31]. Starting from wide channels and slits (d = 1.0 μm), the probability of knotting gradually increased as a polymer became more confined, eventually reaching a maximum and sharply decreasing upon approaching strong confinement (d < 75 nm). BD simulations revealed that major knotting and unknotting events occurred when polymer ends had atypically large backfolds [29]. Polymers under very strong confinement are known to minimize entropy by elongation; this spontaneous extension hinders backfolding and looping events, thereby resulting in fewer knotting events in narrower channels. Moreover, knots in strong confinement generally form at shallower depths along the chain, persist for shorter residence times, and adopt simpler topological conformations compared to knots in deeper channels. Analysis of dynamic transitions between various knot topologies revealed successive knotting events to form higher order knots (*e.g.* 5_1 knot topologies are only accessible by multiple passes of a strand through a loop). In this way, complex knots rarely form in the strongest confinement conditions, even if an existing knot persists for an extended period.

Perhaps not surprisingly, it was found that the probability of encountering a knot increases with increasing L_c, differing by an order of magnitude between L_c = 1.2 and 4.8 μm [31]. Longer chains also accommodate more complex knot topologies. In a BD study of knots in a strongly confined tube (d = 56 nm) [30], the average knot size increased slightly with L_c, but with a weaker dependence in comparison to unconfined chains. Here, the most probable knot size was relatively constant across L_c, agreeing with Grosberg–Rabin theory and indicating that test chains were not prohibitively short for studying knotting dynamics. Interestingly, increases in L_c resulted in longer average knot residence times (τ_{knot}) while having negligible effects on the duration of unknotted

chain events (τ_{unknot}). The disconnect between τ_{unknot} and L_c was elucidated by detailed analysis of spontaneous knot formation, which revealed that tying and untying events occurred exclusively near the ends of DNA chains in strong confinement. In this way, the frequency of knotting and unknotting events is independent of length. This finding was supported by the probability distribution of short-lived knots, which was also independent of L_c. Dynamic trajectories indicate the longer *average* values of τ_{knot} are dominated by rare events in which knots on longer chains travel deep into the chain and achieve long dwell times.

Overall, these recent computational studies have provided additional insight into the mechanisms of knotting in confinement. One major shortcoming, however, is the apparent disconnect between simulation parameters and common experimental approaches. Fabricated nanofluidic channels are typically rectangular in dimensional cross-section and may exhibit interactions and soft repulsions with DNA, which may differ from hard, confining cylindrical tubes commonly used in simulations. Moreover, the polymers studied in these simulations generally have much smaller contour lengths compared to DNA commonly used in single polymer experiments, for example lambda phage DNA (λ-DNA, 48.5 kbp, 16 μm unstained or 21.1 μm under typical fluorescent labeling with YOYO-1) [32].

In order to resolve these apparent differences between experiments and simulations, Doyle and coworkers studied metastable knot size in rectangular nanochannels [33]. Monte Carlo simulations of relatively long chains ($L_c = 400\ell_p$, ~20 μm for dsDNA) in channels with square cross sections reproduced non-monotonic knot sizes with respect to confinement strength. Rigorous comparison to Grosberg–Rabin theory captured trends between the most probable knot size, chain width, and confining dimension. Even though these simulations mirrored realistic experimental conditions,

the feature sizes encountered in DNA knots remain difficult, if not impossible, to resolve using diffraction-limited fluorescence imaging techniques.

Small feature sizes encountered in polymeric knots is further evident in experimental observations of DNA topology in nanochannel confinement [25]. In single molecule genetic barcoding, topological events can lead to misreads and decreased data quality. To understand the nature of these events, single molecules of genomic DNA from *E. coli* were loaded onto a nanochannel array, and molecules were driven by electrophoresis and pre-stretched in an obstacle array to promote uniform loading into nanochannels. Reference labels were introduced to generate unique barcode labels for DNA, and DNA was lightly stained with YOYO-1 to detect topological anomalies (**Figure 2.1e**). In these experiments, measurements consist of dual-color snapshots, and the absence of temporal data is compensated by high throughput, such that this study included 189,153 DNA molecules.

Despite pre-stretching, topological events were detected on 7% of the DNA molecules [25]. Over half of these events occur at the leading edge of a DNA molecule driven into a nanochannel. The remaining events were evenly distributed along the length of a molecule, with a slight increase near the trailing edge. The increase at trailing edges likely corresponds to spontaneous knotting and unknotting events as described by Brownian dynamics simulations [30]. Topological event intensities are normalized to adjacent regions of DNA, and relative fluorescence emission intensities are mapped into probability distributions. Events at leading edges exhibit relative fluorescence intensities of ~2, which corresponds to a polymer folding event within a nanochannel. Interestingly, other events show a ~3.3× average increase in intensity relative to adjacent regions of similar size. This increase could correspond to DNA backfolding within a channel or formation

of a trefoil knot. These events also skew toward higher intensities, which suggests complex knot formation; unfortunately, rigorous classification of individual topological events is generally not possible using diffraction-limited imaging. Although the initial goal of this work was to study the impact of topology on genome mapping, it is possible that this experimental platform could be leveraged to compare knotting topologies to computational results.

2.2.3 Mechanical response of self-entangled DNA polymers

Knots in confined polymers arise due to highly specialized scenarios, in which spontaneous knot formation is a result of the interplay between backfolds, loops, and entropic-driven extension. Aside from confined polymers, how does a knot behave in non-confined systems? As mentioned in Section 1, this problem has been studied using optical tweezing of dual-tethered DNA molecules [20]; however, a drawback to this approach was the low throughput of knot formation: Bao *et al*. note that of 100 successful knotting events, only one third provided useful data.

Doyle and coworkers reported a technique to form knotted DNA in dilute solutions by applying a uniform electric field to single DNA molecules [34]. It was observed that strong electric fields result in isotropically compressed DNA coils, which presumably promotes the generation of a self-entangled polymer. Following the removal of the electric field, single DNA molecules are observed to relax back to non-compressed coils. Relaxation dynamics were categorized into two distinct re-expansion behaviors according to changes in R_g. In the first category, R_g smoothly and continuously returned to the expected equilibrium average; these cases were characterized as unentangled coils. In the second category, expansion was characterized by a three-stage process: (1) an initial arrested state with minimal conformational fluctuations, (2) a nucleation event leading to a second arrested state with a visible compact core, and (3) rapid vanishing of the core and

recovery of the equilibrium R_g. The stage-wise relaxation mechanism is attributed to the formation of self-entanglements during compression. Coupling electrohydrodynamic compression with low molecular weight polymer additives enables quick and reliable generation of self-entangled molecules [35].

The impact of self-entanglements on polymers was further probed using single molecule stretching experiments (**Figure 2.1f**) [36] and simulations (**Figure 2.1g**) [37]. A planar elongational electric field was generated in a microfluidic cross-slot device, according to Eq. 2.1, where v_x and v_y are velocity in the x and y directions, and $\dot{\varepsilon}$ is the strain rate of the field.

$$v_x = \dot{\varepsilon}x;\ v_y = -\dot{\varepsilon}y \qquad (2.1)$$

The strength of the deformation rate can be characterized by the Weissenberg number, $Wi = \dot{\varepsilon}\tau_1$, where τ_1 is the longest polymer relaxation time. Linear polymers are known to undergo a coil-to-stretch transition (CST) at $Wi \approx 0.5$ in elongational fields. In this way, DNA polymers in initially relaxed or initially self-entangled conformations were transiently stretched (**Figure 2.2a-d**) [36].

Across a wide range of dimensionless flow rates ($1 < Wi < 5$), self-entangled polymers stretched over drastically longer timescales compared to unentangled polymers (**Figure 2.2e-f**). Progressive, stage-wise dynamics were observed, in analogy to the expansion of compressed polymers described before. Unentangled polymer stretching trajectories included a near-immediate transient stretching process followed by steady-state extension, in agreement with prior studies of stretching dynamics [14]. Self-entangled polymer stretching trajectories were characterized in a three-stage process (**Figure 2.1f**): (1) an initial metastable arrested state, (2) a nucleation event followed by transient stretching, and (3) steady-state extension.

Decomposition of traces as a function of stage revealed 50% slower transient stretching of self-entangled molecules compared to unentangled molecules. Self-entangled DNA also contained bright spots that localized and persisted through the stretching trajectories, indicative of knot formation. Moreover, knotted polymers reached shorter steady-state extensions compared to unentangled polymers; this difference was characterized as the excess knot length $\langle L_{knot} \rangle$ due to the contour contained in self-entanglements. $\langle L_{knot} \rangle$ decreased with increasing *Wi*, consistent with the tightening of a knot under tension.

The single molecule dynamics of self-entangled polymers were qualitatively described using a simple, non-Brownian dumbbell model [36]. Here, a polymer molecule's contour is divided into free and entangled portions, L_f and L_e. The deformation field acts only upon L_f, and a transient Weissenberg number accounts for the changing relaxation time of the free contour according to Eq. 2.2.

$$Wi_f = Wi \left(\frac{L_f}{L_c}\right)^2 \tag{2.2}$$

For fixed $\dot{\varepsilon}$, *Wi* is constant, but Wi_f grows as the polymer changes from its initial entangled state ($L_e \gg L_f$) to progressively freeing of ends ($\langle L_{knot} \rangle \sim L_e \ll L_f$). The details of the model are based on transport mechanisms of the polymer contour, which are proposed as diffusive release of entanglements and convective transport of ends (*i.e.*, pulling ends out of an entangled region). Despite the simplicity of this model, a rough estimate of knot friction matched optical tweezer measurements of friction in complex knots [20].

Although the dynamics of specific knot topologies cannot be probed after electrohydrodynamic collapse, simulations again provide a deeper look into the impact of topology on single polymer

dynamics. Renner and Doyle applied BD simulations to study knots on short DNA molecules (3 μm) in elongational flow [37]. Specifically, knot position was tracked while applying extensional flow on an initially knotted chain (**Figure 2.1g**). Under a range of dimensionless flow strengths ($1.6 < Wi < 24$), 1D motion of the knots was shown to be strongly dependent on knot topology and nearly independent of tension.

Knot topology was found to impact both diffusive and convective regimes of motion, with particularly interesting dynamics arising in the convection-dominated regime. All knot positions lagged the deformation of the applied flow, and knot topology dictated the degree of lag. In fact, torus knots exhibited much faster convection than non-torus knots, and conformations of torus knots revealed a "corkscrew" translation mechanism of global, sustained rotations along the chain. Conversely, all non-torus knots had similar rates of convection, despite drastically differing sizes. This trend suggests topological self-interference, where convection rates are related to the rate of self-reptation of a knot along a chain.

The majority of recent work has focused on stretching dynamics of self-entangled polymers in strong flows $Wi > 1$, but we anticipate interesting dynamics at lower field strengths, particularly in the vicinity of the CST. Several key questions remain to be addressed. Does the presence of a self-entanglement shift the CST? Would weak deformation allow for unknotting events, such as the diffusive expansion of compressed coils? Finally, studies of self-entanglements introduced by electrohydrodynamic compression would immensely benefit from a method to elucidate knot topology.

2.3 RING POLYMERS

Ring polymers exhibit remarkably different dynamics compared to linear chains and are a topic of current and growing interest in the field. The introduction of a single topological constraint via ring closure drastically changes the dynamic response of circular polymers in flow [7, 38-40]. Moreover, the rheological behavior of melts of circular polymers are highly sensitive to linear contaminants, leading to conflicting experimental reports from bulk-scale techniques [7, 38]. For these reasons, several open questions remain regarding the physical mechanisms in these systems. Single molecule techniques are uniquely suited to study these effects by direct visualization of polymer topology and conformation [39-48].

Several years ago, Smith and coworkers developed a collection of circular DNA molecules spanning two orders of magnitude in molecular weight (2.7–289 kbp) that can be propagated in bacterial cell hosts [49]. Standard molecular cloning techniques enable reasonable yields from laboratory scale bacterial cultures and control over linear, relaxed circular, and supercoiled chain topologies during sample preparation. As a result, recent and ongoing work is aimed at probing the impact of polymer topology on single molecule diffusion [41-48], relaxation [39, 48, 50], and elongation [39, 40, 43, 44].

In addition to single chain dynamics, circular polymers are rich in topological phenomena. In closed loops, knots have rigorous definitions [17]. For closed circular DNA, the double helical backbone can accommodate twists and writhes, which can lead to supercoiled structures [10, 11]. While several open questions remain in these systems, this section of our review focuses on the use of circular DNA as a model polymer in dilute, entangled, and topologically heterogeneous polymer solutions.

2.3.1 Dynamics of unentangled ring polymers

2.3.1.1 Diffusion in free solution

Early single molecule studies of circular DNA confirmed the topological independence of power-law scaling behavior for center-of-mass chain diffusion [41]. The diffusion coefficient D follows an inverse power-law scaling with molecular weight such that $D \sim R_g^{-1} \sim L_c^{-\nu}$, where the scaling exponent $\nu = 0.5$ in theta solvents and $\nu \cong 0.588$ for good solvents [2]. Diffusion measurements obtained for multiple molecular weight samples spanning 6–290 kbp resulted in $\nu_L = 0.571 \pm 0.014$, $\nu_C = 0.589 \pm 0.018$, and $\nu_S = 0.571 \pm 0.057$ for linear, relaxed circular, and supercoiled circular DNA, respectively.

Despite the near-identical molecular weight scaling behavior of topologically distinct polymers, circular polymers diffuse more quickly than linear polymers of identical length ($D_{circular}/D_{linear} \cong 1.32$). Qualitatively, faster diffusion of rings is attributed to the constraint of ring closure, which decreases a polymer's mean square end-to-end distance. Quantitatively, the exact value of this ratio is still unclear, as a recent study by Habuchi and coworkers reported measurements indicating a ratio of $D_{circular}/D_{linear} \cong 1.1$ [42]. Current models predict ratios ranging from 1.1 – 1.45, exhibiting sensitivity to solvent conditions, molecular weight, hydrodynamic interactions (HI), and excluded volume (EV) effects [41].

The study by Habuchi and coworkers revisited single polymer diffusion primarily to verify a new method of image analysis called cumulative area (CA) tracking [42]. This method tracks the cumulative area occupied by a molecule over time and capitalizes on the connection between temporal fluctuations and molecular size, diffusion, and chain conformation. CA tracking resulted

in reportedly precise measurements of diffusion coefficients and holds potential to clarify discrepancies in measured ratios of $D_{circular}/D_{linear}$.

2.3.1.2 Enhanced polymer mobility in crowded solutions

In cells, DNA exists in a crowded microenvironment due to surrounding macromolecules, thereby prohibiting DNA molecules from freely diffusing in dilute solution as described in Section 2.1.1. Macromolecular crowding agents drive biological functions while varying in size, shape, and chemistry; for these reasons, understanding DNA dynamics in the context of the cellular environment remains a challenge across several scientific disciplines [51].

Robertson-Anderson and coworkers have begun to map the topological aspects of this problem, specifically by measuring and comparing the mobility of linear and circular DNA in crowded solutions [43, 44]. Dextran, an inert branched polysaccharide, is a crowding agent commonly used to mimic intracellular proteins [51]. It was observed that the diffusion coefficient D decreased with increasing dextran size and volume fraction Φ; however, crowding-induced mobility reduction was independent of DNA length *and* topology above a critical dextran volume fraction Φ_C. As expected, dextran increased solution viscosities η; however, DNA molecules universally diffused more quickly than predicted by the Stokes–Einstein relation ($D \sim \eta^{-1}$).

Enhanced mobility in dextran solutions was attributed to crowder-induced conformational changes. Linear DNA adopted elongated conformations rather than random coils, thereby maximizing crowder volume and the overall system entropy despite the fact that the linear polymer chain enters a lower entropic state [44]. Although isotropic compaction would further enhance entropic volume effects, it was not observed in these experiments due to the entropic cost of charge

repulsion at physiological salt conditions. Circular DNA molecules adopted compacted conformations while exhibiting the same mobility enhancement in crowded solutions as linear DNA [43]. In contrast to linear DNA, elongated circular DNA conformations would be more energetically costly due to close alignment of two negatively charged strands and significant bending energy at the folded "ends."

Interestingly, both linear and circular DNA molecules "breathe" between conformational states, as characterized by the time and length scales associated with conformational fluctuations [43]. In dilute cases, ring polymer fluctuations took place over ~1.3× shorter time and length scales compared to linear polymers, corresponding to ~1.3× faster diffusion of ring polymers [41]. In the presence of crowding agents, the fluctuations approached a topology-independent timescale above ~2.5Φ_C. Topology-independent fluctuation relaxation times were coupled with topology-independent fluctuation length scales, wherein fluctuations normalized by R_{max} remained relatively constant with increasing Φ. In this way, changing time scales due to crowding were coupled with changing "step sizes" of a DNA molecule's random walk, in turn enhancing mobility.

2.3.1.3 Ring polymers in non-equilibrium flows

As described in Section 2.2.3, studies of self-entangled polymers in extensional flow clearly demonstrate the impact of topology on single polymer molecules in non-equilibrium flows. Recent work in this area has focused on the dynamics of circular and linear DNA polymers in planar extensional flow [39, 40]. As described by Eq. 2.1 (Section 2.2.3), a planar extensional field is characterized by a principal axis of compression and an orthogonal axis of extension. Extensional flows are generally considered strong flows, such that polymers can be highly stretched and oriented. Here, planar extensional flow was generated using pressure-driven flow in a microfluidic

cross-slot device, and single polymers were confined for extended periods using a hydrodynamic trap [52, 53].

Using this approach, single polymer relaxation and stretching dynamics were studied in extensional flow. The longest relaxation time τ_1 of single polymer molecules was measured as a function of molecular weight, specifically comparing 25, 45, and 114.8 kbp circular DNA [39]. Here, a molecule is stretched to ~70% of its effective contour length, such that $L_{eff} = L_c$ for linear DNA and $L_{eff} = L_c/2$ for circular DNA to account for connectivity of a ring polymer. Upon cessation of flow, the time-dependent maximum projected polymer extension $x(t)$ is fit to:

$$\left(\frac{\langle x(t)\rangle}{L_c}\right)^2 = A \exp\left(\frac{-t}{\tau_1}\right) + B \qquad (2.3)$$

where A and B are fitting constants. The fit is performed over the linear entropic force regime where $\langle x(t)\rangle/L_{eff} < 0.3$, except in the case of 25 kbp circular DNA, where the fit is performed over $\langle x(t)\rangle/L_{eff} < 0.5$ to account for imaging resolution over a shorter effective length [40].

Ring polymers relaxed faster than linear chains of the same molecular weight; this difference is attributed to an altered relaxation mode structure in the absence of free ends [40]. Power law scaling behavior was also observed for both circular and linear polymer relaxation. Zimm scaling predicts $\tau_1 \sim L_c^{3\nu}$, such that $3\nu = 1.5 – 1.76$ for solvent quality varying between theta and good solvents [2]. Scaling for linear ($3\nu_L = 1.71 \pm 0.05$) and ring ($3\nu_R = 1.58 \pm 0.10$) polymers were within this predicted range, and the smaller exponent for ring polymers suggests a decrease in EV effects, perhaps due to the shorter L_{eff} [39].

Ring polymers also show a coil-stretch transition in extensional flow, though the behavior was found to differ from linear polymers. Here, the steady-state extension of single ring polymers was

studied as a function of *Wi*, and it was observed that the onset of ring polymer stretch required a higher critical flow strength compared to linear polymers ($Wi_{c,ring} \cong 1.25 Wi_{c,linear}$) [39]. In this way, rings required stronger flows to match the degree of stretch of linear polymers, and rescaling all steady-state extension data by a factor of $Wi_{c,ring}/Wi_{c,linear} \cong 1.25$ superimposed the curves for linear and circular polymer topologies. BD simulations reproduced the shift in $Wi_{c,ring}$ in the presence of HI [40]. Analysis of specific forces within a ring polymer suggest a strong influence of intramolecular HI for circular polymers, such that parallel "strands" of the ring exert secondary backflows on each other during stretch (**Figure 2.3a**). The proposed coupling mechanism between HI and chain topology is further supported by 3D conformations generated by BD simulations, which reveal a stretched 'loop' conformation wherein rings open into the z-direction orthogonal to the planar extensional field (**Figure 2.3b**).

Interestingly, transient dynamics of ring polymers revealed two primary stretching pathways: continuous elongation and interrupted elongation (**Figure 2.3c**) [39]. These behaviors contrast the spectrum of conformations observed for linear polymers: dumbbell, half-dumbbell, kinked, and folded states. This reduced degree of molecular individualism of circular DNA relative to linear DNA is consistent with the notion that circular molecules have fewer degrees of freedom due to their connectivity. Experimentally, interrupted elongation pathways appeared to form transient knots that hindered stretch until their eventual release. This behavior was reproduced in BD simulations, in which hairpins and loops in the *z*-direction are associated with slow unfolding behaviors (**Figure 2.3b**) [40].

2.3.2 Diffusion of entangled ring polymers

A single, linear polymer molecule in an entangled solution or melt is known to move by reptation, wherein polymers diffuse through an effective confining potential or confining tube by a snake-like motion [2, 54]. Circular polymers, however, have no ends. Clearly, ring polymers must utilize a fundamentally different mechanism to move and translate in entangled solutions.

In synthetic organic polymer chemistry, the preparation of topologically pure solutions or melts of ring polymers is a challenging problem. Furthermore, trace quantities of linear polymers are known to drastically change the rheological behavior of entangled ring polymers. Even with recent advances in synthesis and purification, bulk measurement techniques lack the molecular resolution needed to fully understand ring polymer mechanisms [7, 38]. Enzymatic transformations enable topological control over DNA molecules [41, 49], which further emphasizes the suitability of DNA as a suitable system for studying entangled ring polymers. Single molecule studies of ring and linear polymer self-diffusion in topologically pure and heterogeneous (blended) solutions provide direct evidence of new mechanisms for ring polymer motion, in addition to clarifying anomalous behavior of rings in the presence of linear impurities.

Upon demonstrating the facile preparation of topologically pure, entangled DNA solutions, Robertson and Smith thoroughly investigated the impacts of topology, molecular weight, and concentration on chain diffusion [45-47]. Systematic studies of fluorescent tracer molecules entangled in a background matrix probed several topological combinations of linear and circular polymers, as depicted in **Figure 2.4a**: a linear polymer matrix containing tracer molecules of linear (L-L) or circular (C-L) topology, as well as a circular polymer matrix containing linear (L-C) or circular (C-C) tracer molecules.

Self-diffusion measurements revealed the greatest overall effect between different matrix polymer topologies (**Figure 2.4b**) [45, 46], where linear or circular tracers in an entangled circular matrix diffused orders of magnitude more quickly than linear or circular tracers in an entangled linear matrix. In unentangled matrices (lower concentration or molecular weight DNA), the effect of topology was negligible and diffusion coefficients of all combinations were maintained within a factor of two. Overall findings for diffusion coefficients in entangled solutions where $D_{C\text{-}C} \gtrsim D_{L\text{-}C} \gg D_{L\text{-}L} \gg D_{C\text{-}L}$, which led to several predictions for the molecular motions of ring polymers: first, linear polymers are capable of pinning or threading through rings, slowing ring diffusion until release of the linear constraint ($D_{C\text{-}L} \ll D_{L\text{-}L}$); second, constraint release involving a threaded linear chain is a slower process than reptation in these systems; third, constraint release is negligible in pure ring matrices.

Habuchi and coworkers further explored these predictions by applying CA tracking (Section 2.1.1) to entangled DNA [48], which enabled simultaneous characterization of molecular motion at various length scales and conformational relaxation times. Molecular motions were used to determine diffusion coefficients of C-C, C-L, and L-L polymer combinations, resulting in the same trends where $D_{C\text{-}C} \gg D_{L\text{-}L} \gg D_{C\text{-}L}$ (**Figure 2.4c**).

Modes of diffusion were determined by comparison of mean CA trajectories to 1D and 2D random motions, which correspond to different molecular models for ring polymers [48]. 1D random motions indicate reptation or double-folded reptation, whereas 2D random motions suggest a lattice-animal model in which cyclic chains adopt double-folded linear conformations with multiple loops. Dilute polymers diffused via 2D motion only, as expected for Brownian motion,

and all entangled combinations recovered 2D random motion and random walks at long length scales.

Conformational relaxation times were determined by analyzing temporal fluctuations of the area occupied by a molecule, such that autocorrelation functions of molecular fluctuations were fit to a single exponential decay. Pure entangled ring polymers (C-C) exhibited similar conformational relaxation times in comparison to dilute rings, despite slower diffusion. At short length scales, diffusive motions followed neither 1D nor 2D random motions, suggesting a different mechanism for ring polymer motion than predicted by either reptation or lattice animal models. Habuchi and coworkers suggest *mutual relaxation* of ring polymers, where intermolecular constraints are negligible because rings do not thread each other. All data acquired for pure entangled linear polymers (L-L) agreed with reptation motion, including 1D diffusive behavior at short length scales. Surprisingly, only 2D motion was observed for C-L systems, such that cyclic molecules exhibited isotropic motion in linear polymer backgrounds. Heterogeneity in diffusion coefficients revealed larger distributions in $D_{C\text{-}L}$ compared to other cases, suggesting heterogeneous molecular-level interactions, such as variable threading of linear polymers through a tracer ring polymer [48].

An investigation of blends of linear and circular DNA by Robertson-Anderson and coworkers supports the notion of variable threading [47]. Self-diffusion coefficients of linear and circular tracers were measured at varying concentrations below, near, and above the entanglement concentration in blends of linear and ring polymers, as depicted for linear tracers in **Figure 2.4d**. Blend fractions were incremented from pure circular (ϕ_C = 1.0, ϕ_L = 0) to pure linear (ϕ_L = 1.0, ϕ_C = 0) in steps of 0.1. Diffusion coefficients were independent of blend composition in all unentangled solutions. Near or above entanglement, ring polymer tracers diffused quickly when

ϕ_L = 0; upon increasing ϕ_L, D_C rapidly decreased by orders of magnitude before slowly and monotonically decreasing. This behavior is consistent with measurements in topologically pure solutions, as well as a minimal constraint model for binary blends of ring and linear polymers [55].

Unexpectedly, D_L responded non-monotonically to changes in blend composition, reaching a minimum near $\phi_C \sim \phi_L \cong 0.5$ [47]. This behavior was not predicted by the minimal constraint model, rather, slight modifications incorporating the impact of ring threading on linear polymers were required to capture the experimental findings. Briefly, the relaxation times of circular and linear polymers are modeled as functions of blend composition ($\tau_R(\phi_L)$ and $\tau_L(\phi_L)$, respectively), with contributions from the average number of entanglements per molecule in a linear melt and the average number of linear polymers threading a ring [55]. Numerical evaluation of this model uncovered criteria for non-monotonic behavior, such that a crossover must occur between D_C and D_L [47].

Intuitively, the trends in diffusion coefficients can be explained by considering the transition between pure circular and linear solutions. At $\phi_L \approx 0$, a small fraction of rings are threaded by linear polymers while most rings diffuse freely. As ϕ_L increases, both the fraction of threaded rings and number of threads per ring increase, monotonically increasing τ_C until threading events plateau as ϕ_L approaches unity. Considering the opposite transition for linear polymers, when ϕ_L = 1, all polymers have the same relaxation time τ_L. When one background linear polymer is replaced with a ring polymer, the solution has exchanged a somewhat mobile constraint with a less mobile, threaded ring polymer, and $\tau_L(\phi_L)$ increases. As more constraints are replaced (ϕ_L decreases from 1), $\tau_R(\phi_L)$ concurrently decreases, reaching some point at which $\tau_R(\phi_L) = \tau_L(\phi_L)$. As ϕ_L decreases from this point, the exchange between constraining molecules introduces more mobile rings, so

$\tau_L(\phi_L)$ decreases. This competition between structure and dynamics results in a maximum in $\tau_L(\phi_L)$ or a minimum in $D_L(\phi_L)$, and supports proposed mechanisms of variable threading between linear and circular polymers in topologically heterogeneous mixtures.

Based on these studies, it is clear that a simple change in polymer topology (ring closure) leads to a wealth of interesting and unexpected dynamic behavior at the single molecule level. Moving forward, additional studies focusing on the nonequilibrium dynamics of rings and topologically complex polymers in entangled solutions will undoubtedly reveal new physics.

2.4 BRANCHED DNA POLYMERS

Connectivity in polymer chains can be considered in terms of molecular branching or chemical or physical networks [3, 5, 6, 8, 54, 56]. Networks are formed by chemical or physical crosslinks, which impart topological constraints and elasticity in gels, plastics, and rubbers. Branched polymers are defined as having secondary polymer chains linked to a primary backbone, resulting in a variety of polymer architectures such as star, H-shaped, pom-pom, and comb-shaped polymers.

The molecular properties of branched polymers can be described by a wide parameter space, including chemical structure, backbone molecular weight, branch molecular weight, and branching density. From this view, branched polymers can exhibit broad chemical versatility, thereby giving rise to potentially dramatic changes in rheological behavior [5, 6, 8, 56]. In an entangled solution of combs or comb polymer melts, branch points are known to substantially slow down the overall relaxation processes within the material, especially for high molecular weight branches. Branching often results in a spectrum of relaxation times related to movement of branches, segments between

branches, and the entire molecular backbone [6]. In this way, chain branching is thought to result in extremely complex behaviors at equilibrium and in response to flow.

Recent single molecule studies of branched polymers have only begun to scratch the surface of these phenomena. Although branched structures naturally form in DNA during replication and recombination, these intermediate states are intrinsically transient and generally not suitable as models for covalently linked branched polymers [57]. In this section, we review two independent approaches for synthesis and single molecule studies of branched DNA polymers.

2.4.1 Star DNA polymers

The instability of branched junctions in DNA (*e.g.* the Holliday junction) stems from sequence symmetry around a DNA branch point. Asymmetric sequences can be used to generate artificial, immobilized nucleic acid junctions [57]. This technology enabled structural characterization of DNA junctions [58], inspired the burgeoning field of DNA origami [59], and provided a method to create stable branched DNA polymers [60].

Archer and coworkers carried out initial studies of branched DNA using single polymer techniques [60-62]. This early work reported important findings and represents a few of only a handful of investigations on single branched polymers. Here, branched DNA was generated by forming a star core of hybridized oligonucleotides with sticky overhangs complementary to the 5'-overhang of λ-DNA (**Figure 2.5a**). λ-DNA molecules were hybridized to the sticky overhangs and ligated to produce DNA stars. This method was also extended to create pom-pom polymers by connecting two stars with a λ-DNA crossbar.

Conformational dynamics and electrophoretic mobility μ of star DNA polymers were measured in solutions of linear polyacrylamide [60, 61] and polyethylene oxide [62], as well as in agarose and polyacrylamide gels [60]. In dilute solutions, DNA conformations and μ were independent of topology, such that both star and DNA molecules migrated as random coils [60, 62]. In unentangled, semi-dilute solutions, star DNA exhibited inverted squid-like conformations upon interacting with the surrounding polymers (**Figure 2.5b**). Star DNA arms outstretched in the direction of the electric field, pulling star cores through the solution. Despite major conformational differences between linear and star DNA, μ was relatively insensitive to topology; instead, μ was found to depend on the molecular weight and concentration of the background polymer [62].

DNA architecture was found to play a more significant role on μ in entangled solutions of linear polymer backgrounds [60, 61]. Here, linear DNA oriented and aligned with the electric field, migrating with μ independent of background polymer molecular weight. In contrast, star DNA adopted more drastic versions of the inverted squid-like conformations as cores entangled with polymers in the surrounding solution. Star DNA migrated more slowly as the background polymer molecular weight increased [61]. The most drastic conformational difference between stars and linear polymers occurred in gels. Here, it was observed that large DNA stars simply could not migrate through a fixed surrounding network. When driven toward an interface between a semi-dilute polymer solution and a gel, the core of the DNA star was trapped by the fixed constraints of the gel [60].

These studies began to reveal the impact of branching on single polymer dynamics, albeit in the context of electrophoresis rather than solution-based fluid flows. Moreover, the hybridization-based synthesis approach was not exceedingly efficient, with Archer and coworkers noting overall

yields of 5-10% after purification by gel extraction [60]. Although hybridized DNA junctions have proven useful for oligonucleotide assembly and DNA origami [59], the two-step process of hybridizing and ligating very large arms to a core of small oligonucleotides is kinetically slow, ultimately prohibiting the widespread use of hybridization-based branched DNA for single polymer dynamics.

2.4.2 Graft-onto branched DNA polymers

A major challenge in single molecule studies of branched DNA is the synthesis of polymers with precisely controlled architectures with suitable properties for fluorescence imaging. Schroeder and coworkers recently introduced new strategies to address these issues [63, 64].

Template-directed enzymatic synthesis of DNA was combined with grafting techniques from synthetic organic chemistry (**Figure 2.5c**, left). In this way, DNA "building blocks" of precise sequence and length were synthesized via polymerase chain reaction (PCR). The inclusion of chemically modified primers and non-natural nucleotides during PCR resulted in the incorporation of internal graft sites, terminal reactive sites, and fluorescent labels. Bioconjugation techniques enabled graft-onto reactions between end-functionalized branches and mid-functionalized backbones, thereby producing stable, branched DNA molecules.

This hybrid enzymatic-synthetic approach was used to synthesize relatively short DNA with precisely defined structures [63]. Backbone sequences were defined to include graft sites at specified locations, with exact control over the number and spatial arrangement of graft sites incorporated in product polymers during PCR. Topologies included three-arm star, H-shaped, and graft block polymers, with topological possibilities limited only by the template length (50-60 bp

in this study). In addition to structurally defined homopolymers, branched copolymers and miktoarm star polymers were also synthesized by grafting poly(ethylene glycol) side branches to DNA templates. Although these polymers generally had low molecular weights that would preclude direct single molecule imaging of molecular conformations, these precision materials hold strong potential for detailed studies of self-assembly and structure-function relationships in branched polymers and block copolymers. Furthermore, grafted DNA oligomers exhibited drastically hindered electrophoretic migration compared to linear polymers, in agreement with electrophoresis of large branched DNA constructs [60].

The two-step synthetic approach was further extended to generate long branched DNA for single molecule studies of comb polymers [64]. Here, exact control was maintained over branch length (1–10 kbp) and backbone length (10–30 kbp), with average control over the degree of branching by tuning stoichiometry using a graft-onto approach. As expected, branched DNA products exhibited decreased mobility during gel electrophoresis in comparison to linear DNA.

Inclusion of a chemically modified terminal linker on the backbone enabled specific attachment of branched DNA molecules to a surface, facilitating direct observation of single branched DNA without requiring extensive purification [64]. In one study, DNA comb polymers consisted of 10–20 kbp backbones and "short" branches (1 kbp) with covalently linked fluorescent labels. Here, molecular branch frequency distributions and polymer end-to-end distances were characterized via simultaneous visualization of polymer branches and backbones (**Figure 2.5c**, right). In regards to branching distributions, single molecule data showed that the number of branches added per backbone was generally less than expected based on simple stoichiometric arguments for incorporation of chemically modified nucleotides and addition of branches during graft-onto

reactions. In particular, average branch frequencies ranged from 1.5 – 10 per backbone, but the theoretical maximum number of graft sites ranged from 100 – 1200. The main source of this disparity likely lies in the discrimination of non-natural nucleotides against natural nucleotides during PCR, which can likely be overcome by tuning stoichiometry or chemical structure of modified nucleotides.

A separate study directly observed conformational relaxation of larger branched DNA, with 30 kbp backbones and 10 kbp branches (**Figure 2.5c**, bottom) [64]. Although the stretching dynamics were not investigated in full detail, it was clear that branched DNA exhibited a CST and stretched prior to relaxation upon cessation of flow.

Qualitatively, single molecule videos clearly showed that relaxation processes depend on molecular topology [64]. At early times in the relaxation process, the backbone and branches exhibited a simultaneous and rapid elastic recoil characterized by a sharp decrease in extension with respect to time. At intermediate times, branched polymers exhibited mixed relaxation dynamics of branches and backbones, such that branches explored various conformational "breathing modes" while the backbone relaxed. The mixing of relaxation modes was likely related to the similar branch and backbone molecular weights in this particular study. At long times, the longest mode of relaxation dominated the process, which corresponds to relaxation of the main chain backbone. These visual observations empirically suggest that at least two dominant time scales govern the relaxation process, including an intermediate branch relaxation time and the longest backbone relaxation time.

These time scales were quantified in a similar method as described in Section 2.1.3 and Eq. 2.3, where the time-dependent backbone end-to-end distance was fit to a single exponential decay over

the longest relaxation time and length scales, $\langle x(t) \rangle / L_c < 0.3$, or intermediate time and length scales, $0.3 < \langle x(t) \rangle / L_c < 0.5$. The longest relaxation time generally increased with an increasing number of branches, which reflects an increase in friction along the DNA backbone due to pre-relaxed side branches. Intermediate timescales were much more sensitive to the number of branches, as well as branch position. Interestingly, polymers with a single branch behaved similarly to linear polymers on average.

A deeper investigation of branch position revealed a strong dependence of intermediate relaxation time on distance between the branch and surface tether. Branches far from the tether slowed relaxation, whereas branches near the tether resulted in faster overall relaxation processes compared to a linear polymer. Schroeder and coworkers postulated that branches introduce a new modes of relaxation between the tether point and the branch end. In the case of a branch far from the tether, the contour length of a branched molecule is effectively increased. In the case of a branch near the tether, the branch relaxes more quickly than the main chain, potentially inducing local hydrodynamic flows that enhance relaxation of the main chain. From a broader perspective, it is important to note that single molecule techniques are quite powerful in revealing these topological effects via direct observation of polymer architecture.

Overall, the vast parameter space of branched polymeric systems remains relatively unexplored by single molecule techniques. The few studies that exist demonstrate the wealth of molecular-scale understanding to be gained by future investigations. Progress towards preparing branched DNA at high yield and purity will enable systematic molecular-scale exploration of the impact of branching on polymer structure, properties, and dynamics. In this way, an improved fundamental

understanding of recently observed rheological phenomena will provide insights toward the molecular-scale design of topologically complex polymers.

2.5 CONCLUSIONS

DNA is a remarkably versatile polymer for single polymer dynamics. In recent years, researchers have leveraged biological, biochemical, and synthetic tools to generate DNA-based polymers with complex molecular topologies. In this review, we summarize recent investigations of knotted, circular, and branched DNA, all of which provide a new fundamental understanding of the interplay between topology and dynamics. This approach can be followed to effectively link experiments, simulations, and theory in single polymer dynamics.

Simulations of knotted and confined DNA elucidate the conditions for knot formation [29], potentially informing the design of next-generation nanofabricated devices for genetic barcoding [25]. Self-entangled DNA exhibits new mechanical behavior, forming arrested states and stretching much more slowly in comparison to linear DNA [36]. Specific knot topology and dynamics are intimately related, and progress toward the resolution and classification of experimentally generated knots will enable the validation of knot models and theories.

Single molecule studies of polymer diffusion in entangled circular and/or linear DNA solutions have revealed the physical mechanisms underlying anomalous behavior in entangled ring solutions and melts. Entangled rings diffuse by non-reptative mechanisms [48], and threading of circular polymers by linear molecules dramatically reduces circular chain mobility [45-48]. In dilute solutions, a coupling between topology and hydrodynamic interactions governs ring polymer dynamics [39, 48], and new experimental techniques raise questions about ring polymer diffusion

[42]. Probing the non-equilibrium dynamics of entangled ring polymer solutions will undoubtedly reveal new physics surrounding topological complexity.

Single molecule studies of branched polymers have only begun to explore the vast parameter space of molecular architecture, but early work already demonstrates strong coupling between molecular topology and dynamics [64]. Overcoming challenges of scale-up and purification will enable rich studies of branched polymer dynamics in dilute, semi-dilute, and entangled solutions.

In all areas of topology, single polymer dynamics connect molecular-scale behaviors to emergent properties of polymeric materials. DNA has enabled these contributions, given facile preparation of monodisperse samples, topological control, and well-established experimental conditions. New developments in super-resolution imaging and fluorescently labeled synthetic polymers [65] have potential to drive progress in the field beyond DNA. Until then, DNA will continue to serve as the gold standard for single molecule dynamics of topologically complex polymers.

2.6 FIGURES

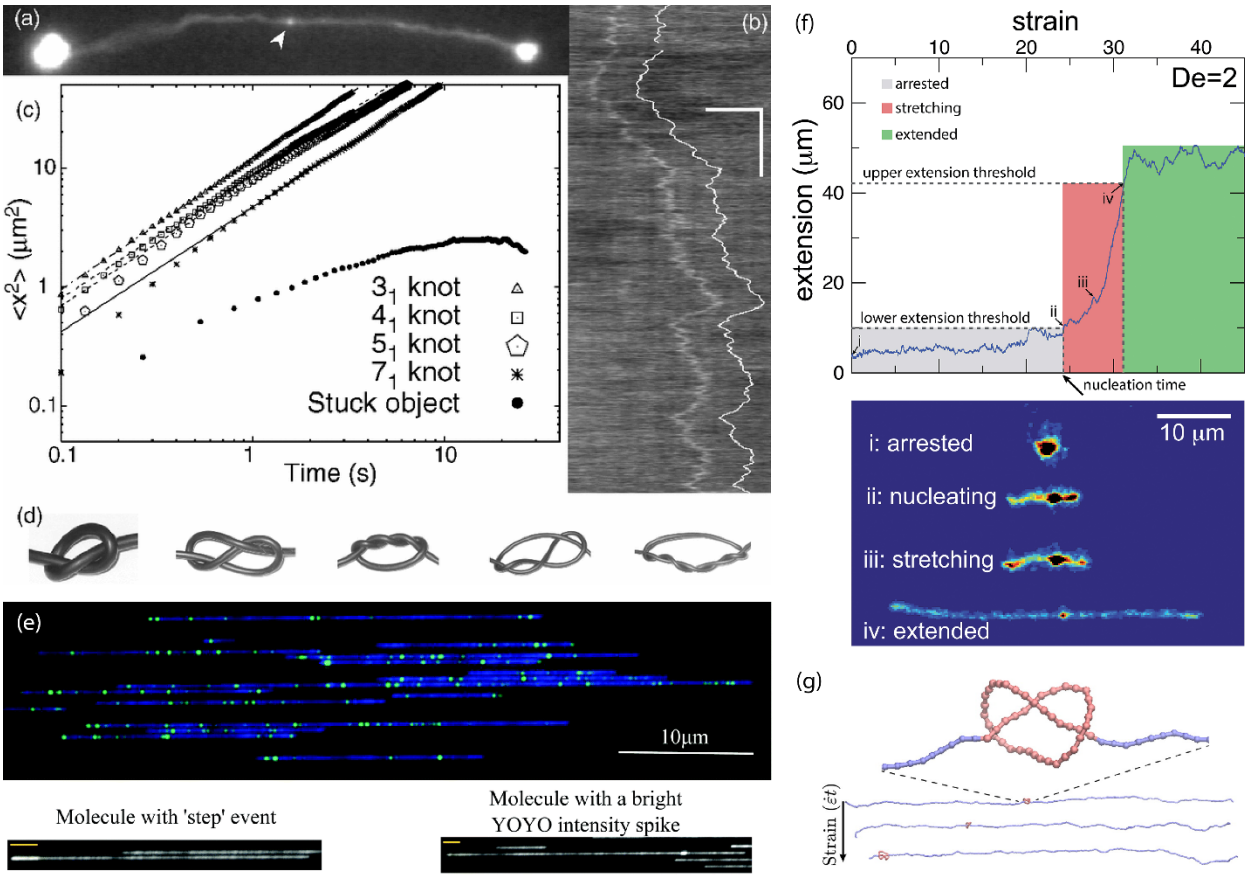

Figure 2.1. Visualization of DNA knots. (a) Knotted DNA appears as a diffraction-limited contour between two beads, with an increase in fluorescence at the knot (arrow). (b) A diffusive trace indicating a knot's trajectory. Scale bars, 5 μm (horizontal) and 5 s (vertical); scale of (a) is the same as the horizontal scale of (b). (c) Mean squared distance of knot traveled as a function of time *t*. (d) Topologies of single open knots, from left to right: 3_1, 4_1, 5_1, 5_2, and 7_1. (e) Two-color imaging of DNA in a nanochannel array, with barcodes shown in green and YOYO-1 in blue. Examples of topological events are shown below, specifically a fold at a leading edge fold (left) and high intensity event (right). (f) Stages of stretching self-entangled DNA. (g) Trefoil knots along a bead-rod chain. Reprinted (a)-(d) with permission from X. R. Bao, H. J. Lee, and S. R. Quake, *Physical Review Letters*, **91**, 265506. Copyright (2003) by the American Physical Society. Adapted (e) from Ref. 26 with permission of The Royal Society of Chemistry under CC BY 3.0. Reproduced (f) from Ref. 37 with permission of The Royal Society of Chemistry under CC BY-NC 3.0. Reprinted (g) with permission from C. B. Renner and P. S. Doyle, *ACS Macro Letters*, **3**(10), 963-967. Copyright (2014) American Chemical Society.

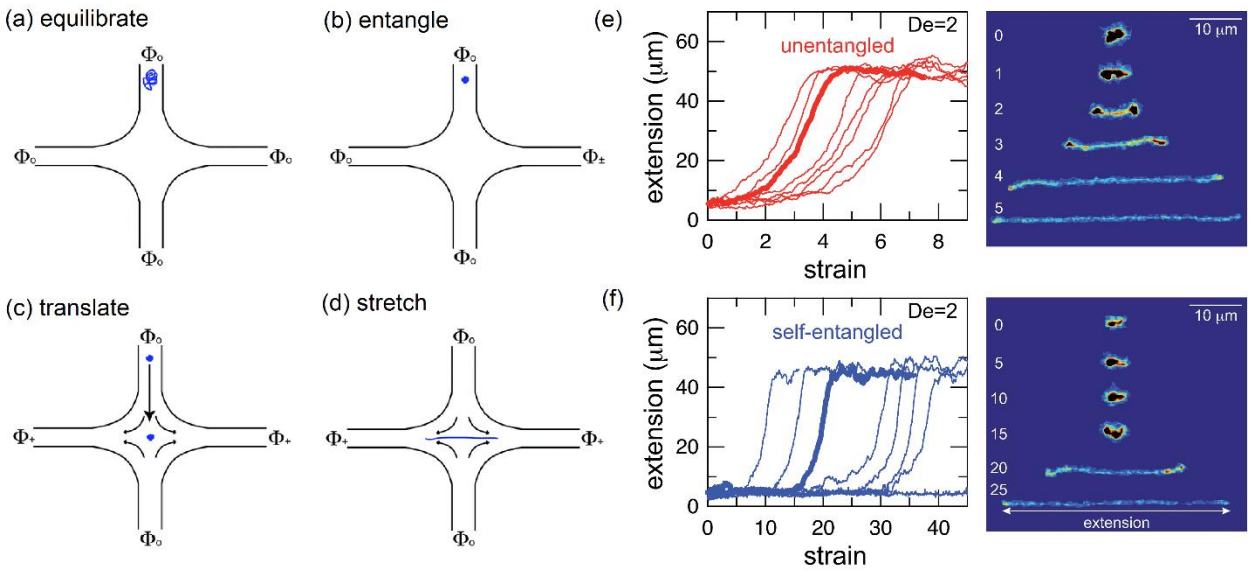

Figure 2.2. Stretching unentangled and self-entangled DNA. Schematic of experiment, single molecule trajectories, and single molecule snapshots of the stretching process are shown for self-entangled DNA molecules. (a) A molecule is equilibrated under no field before (b) self-entanglement via electrohydrodynamic compression, (c) translation to the center of the cross-slot device, and (d) stretch in planar extension. Unentangled molecules are translated, equilibrated, and then stretched. Extension versus strain trajectories for (e) unentangled and (f) self-entangled molecules (note different x-axis scales). Bold trajectories correspond to single molecule snapshots, in which the accumulated strains are displayed in white. Adapted from Ref. 37 with permission of The Royal Society of Chemistry under CC BY-NC 3.0.

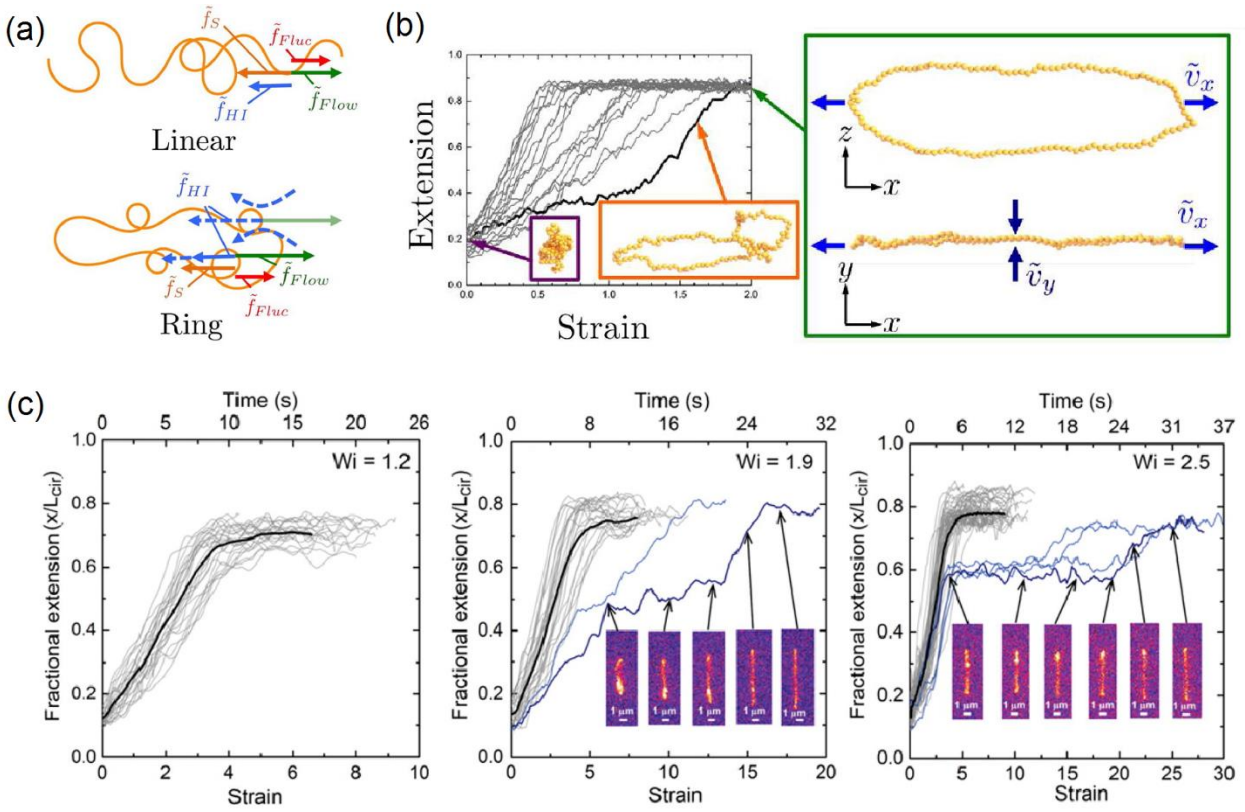

Figure 2.3. Stretching of ring polymers in planar extensional flow. (a) Schematic of the forces on moderately stretched linear and ring polymers. In both cases, the Brownian and entropic spring forces are essentially the same. The ring experiences stronger hydrodynamic forces, where two stretching portions of the ring polymer exert backflows felt by the opposite strand, and a stronger applied fluid flow is required to maintain the same stretch. (b) 3D conformations from Brownian dynamics simulations demonstrating hairpin and looped conformations of transiently stretching ring polymers. Note that loop extension in the *z*-direction is orthogonal to the *xy*-flow plane. (c) Single molecule experimental transient stretch of DNA rings as functions of time and strain ($\varepsilon = \dot{\varepsilon}t$) for Wi = 1.2, 1.9, and 2.5. Bold curves represent ensemble averages ($\langle x(t)\rangle/L_{eff}$). Interrupted stretching trajectories are blue, and continuously stretching trajectories are gray. Single molecule images demonstrate the formation and release of transient knotting events. Adapted (a) and (b) with permission from Hsiao, Schroeder, and Sing, *Macromolecules*, 49(5), 1961-1971. Copyright (2016) American Chemical Society. Adapted (c) with permission from Li, Hsiao, Brockman, Yates, Robertson-Anderson, Kornfield, San Francisco, Schroeder, and McKenna, *Macromolecules*, 48(16), 5997-6001. Copyright (2015) American Chemical Society.

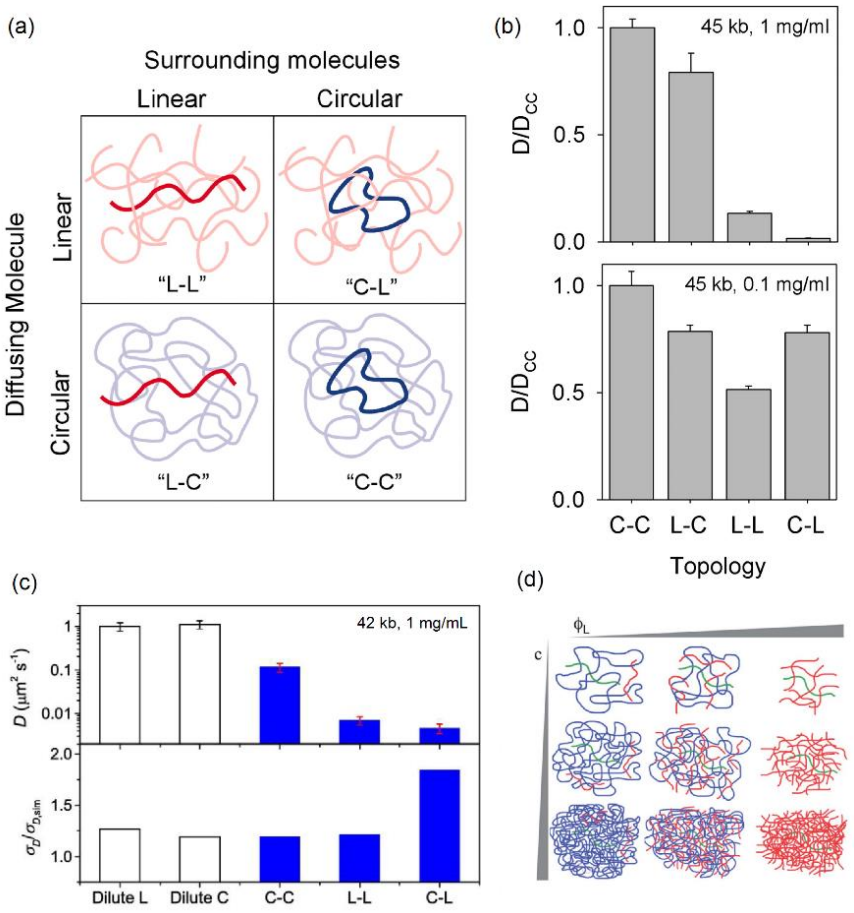

Figure 2.4. Single molecule diffusion of circular and linear DNA. (a) Topological combinations of linear or circular tracer molecules (bold) in a background matrix of linear or circular polymers. (b) DNA self-diffusion coefficients as a function of topology in entangled (1 mg/mL, top) and unentangled (0.1 mg/mL, bottom) solutions. (c) DNA self-diffusion coefficients (top) and distributions (bottom) measured by CA tracking. (d) Schematic of the concentration and blend composition parameter space for a linear tracer molecule (green) surrounded by circular and/or linear DNA. The same parameter space is tested using circular tracers. Adapted (a) and (b) from Robertson and Smith, *Proceedings of the National Academy of Sciences*, **104**(12), 4824-4827. Copyright (2007) National Academy of Sciences, USA. Adapted (c) with permission from Abadi, Serag, and Habuchi, *Macromolecules*, **48**(17), 6263-6271. Copyright (2015) American Chemical Society. Adapted (d) with permission from Ref. 47 with permission of the Royal Society of Chemistry.

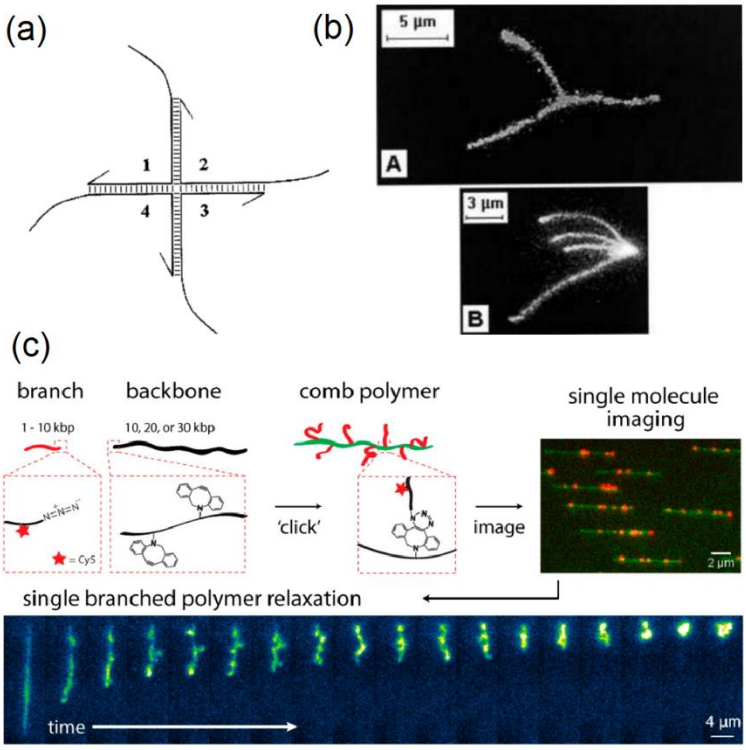

Figure 2.5. Synthesis and single molecule imaging of branched DNA. (a) Schematic of a four-arm star core generated by hybridization of oligonucleotides. (b) Large DNA star conformations in concentrated polymer solutions; (top) no applied electric field, (bottom) an electric field is applied with the positive electrode on the left. (c) Synthesis, imaging, and relaxation of graft-onto branched polymers. Reproduced (a) and (b) from Ref. 60 with permission of John Wiley and Sons, Inc. Reprinted (c) with permission from D. J. Mai, A. B. Marciel, C. E. Sing, and C. M. Schroeder, *ACS Macro Letters*, **4**(4), 446-452. Copyright (2015) American Chemical Society.

2.7 REFERENCES

[1] Grosberg A, Nechaev S. Polymer topology. Polymer Characteristics. Berlin, Heidelberg: Springer Berlin Heidelberg; 1993. p. 1-29.

[2] Doi M, Edwards SF. The Theory of Polymer Dynamics: Clarendon Press; 1988.

[3] Flory PJ. Principles of Polymer Chemistry: Cornell University Press; 1953.

[4] Peurifoy SR, Guzman CX, Braunschweig AB. Topology, assembly, and electronics: three pillars for designing supramolecular polymers with emergent optoelectronic behavior. Polymer Chemistry. 2015;6:5529-39.

[5] Daniel WFM, Burdynska J, Vatankhah-Varnoosfaderani M, Matyjaszewski K, Paturej J, Rubinstein M, et al. Solvent-free, supersoft and superelastic bottlebrush melts and networks. Nat Mater. 2016;15:183-9.

[6] van Ruymbeke E, Lee H, Chang T, Nikopoulou A, Hadjichristidis N, Snijkers F, et al. Molecular rheology of branched polymers: decoding and exploring the role of architectural dispersity through a synergy of anionic synthesis, interaction chromatography, rheometry and modeling. Soft Matter. 2014;10:4762-77.

[7] Kapnistos M, Lang M, Vlassopoulos D, Pyckhout-Hintzen W, Richter D, Cho D, et al. Unexpected power-law stress relaxation of entangled ring polymers. Nat Mater. 2008;7:997-1002.

[8] Zhou H, Woo J, Cok AM, Wang M, Olsen BD, Johnson JA. Counting primary loops in polymer gels. Proceedings of the National Academy of Sciences. 2012;109:19119-24.

[9] Lutz J-F, Ouchi M, Liu DR, Sawamoto M. Sequence-Controlled Polymers. Science. 2013;341.

[10] Bates AD, Maxwell A. DNA Topology: Oxford University Press; 2005.

[11] Schoeffler AJ, Berger JM. DNA topoisomerases: harnessing and constraining energy to govern chromosome topology. Quarterly Reviews of Biophysics. 2008;41:41-101.

[12] McKinney SA, Declais A-C, Lilley DMJ, Ha T. Structural dynamics of individual Holliday junctions. Nat Struct Mol Biol. 2003;10:93-7.

[13] Koster DA, Crut A, Shuman S, Bjornsti M-A, Dekker NH. Cellular strategies for regulating DNA supercoiling: A single-molecule perspective. Cell. 2010;142:519-30.

[14] Mai DJ, Brockman C, Schroeder CM. Microfluidic systems for single DNA dynamics. Soft Matter. 2012;8:10560-72.

[15] Dorfman KD. DNA electrophoresis in microfabricated devices. Reviews of Modern Physics. 2010;82:2903-47.

[16] Dai L, Renner CB, Doyle PS. The polymer physics of single DNA confined in nanochannels. Advances in Colloid and Interface Science. 2015:in press.

[17] Adams CC. The Knot Book: An Elementary Introduction to the Mathematical Theory of Knots. Providence, RI: American Mathematical Society; 2004.

[18] Lim NCH, Jackson SE. Molecular knots in biology and chemistry. Journal of Physics: Condensed Matter. 2015;27:354101.

[19] Arai Y, Yasuda R, Akashi K-i, Harada Y, Miyata H, Kinosita K, et al. Tying a molecular knot with optical tweezers. Nature. 1999;399:446-8.

[20] Bao XR, Lee HJ, Quake SR. Behavior of Complex Knots in Single DNA Molecules. Physical Review Letters. 2003;91:265506.

[21] Tubiana L, Orlandini E, Micheletti C. Probing the Entanglement and Locating Knots in Ring Polymers: A Comparative Study of Different Arc Closure Schemes. Progress of Theoretical Physics Supplement. 2011;191:192-204.

[22] Latinwo F, Schroeder CM. Model systems for single molecule polymer dynamics. Soft Matter. 2011;7:7907-13.

[23] Grosberg AY, Rabin Y. Metastable Tight Knots in a Wormlike Polymer. Physical Review Letters. 2007;99:217801.

[24] Dai L, Renner CB, Doyle PS. Metastable Tight Knots in Semiflexible Chains. Macromolecules. 2014;47:6135-40.

[25] Reifenberger JG, Dorfman KD, Cao H. Topological events in single molecules of E. coli DNA confined in nanochannels. Analyst. 2015;140:4887-94.

[26] Marenduzzo D, Orlandini E, Stasiak A, Sumners DW, Tubiana L, Micheletti C. DNA–DNA interactions in bacteriophage capsids are responsible for the observed DNA knotting. Proceedings of the National Academy of Sciences. 2009;106:22269-74.

[27] Micheletti C, Orlandini E. Knotting and metric scaling properties of DNA confined in nano-channels: a Monte Carlo study. Soft Matter. 2012;8:10959-68.

[28] Micheletti C, Orlandini E. Numerical Study of Linear and Circular Model DNA Chains Confined in a Slit: Metric and Topological Properties. Macromolecules. 2012;45:2113-21.

[29] Micheletti C, Orlandini E. Knotting and Unknotting Dynamics of DNA Strands in Nanochannels. ACS Macro Letters. 2014;3:876-80.

[30] Antonio S, Enzo O, Cristian M. Knotting dynamics of DNA chains of different length confined in nanochannels. Journal of Physics: Condensed Matter. 2015;27:354102.

[31] Orlandini E, Micheletti C. Knotting of linear DNA in nano-slits and nano-channels: a numerical study. Journal of Biological Physics. 2013;39:267-75.

[32] Schroeder CM, Babcock HP, Shaqfeh ESG, Chu S. Observation of Polymer Conformation Hysteresis in Extensional Flow. Science. 2003;301:1515-9.

[33] Dai L, Renner CB, Doyle PS. Metastable Knots in Confined Semiflexible Chains. Macromolecules. 2015;48:2812-8.

[34] Tang J, Du N, Doyle PS. Compression and self-entanglement of single DNA molecules under uniform electric field. Proceedings of the National Academy of Sciences. 2011;108:16153-8.

[35] Renner CB, Du N, Doyle PS. Enhanced electrohydrodynamic collapse of DNA due to dilute polymers. Biomicrofluidics. 2014;8:034103.

[36] Renner CB, Doyle PS. Stretching self-entangled DNA molecules in elongational fields. Soft Matter. 2015;11:3105-14.

[37] Renner CB, Doyle PS. Untying Knotted DNA with Elongational Flows. ACS Macro Letters. 2014;3:963-7.

[38] Yan Z-C, Costanzo S, Jeong Y, Chang T, Vlassopoulos D. Linear and Nonlinear Shear Rheology of a Marginally Entangled Ring Polymer. Macromolecules. 2016;49:1444-53.

[39] Li Y, Hsiao K-W, Brockman CA, Yates DY, Robertson-Anderson RM, Kornfield JA, et al. When Ends Meet: Circular DNA Stretches Differently in Elongational Flows. Macromolecules. 2015;48:5997-6001.

[40] Hsiao K-W, Schroeder CM, Sing CE. Ring Polymer Dynamics Are Governed by a Coupling between Architecture and Hydrodynamic Interactions. Macromolecules. 2016;49:1961-71.

[41] Robertson RM, Laib S, Smith DE. Diffusion of isolated DNA molecules: Dependence on length and topology. Proceedings of the National Academy of Sciences. 2006;103:7310-4.

[42] Serag MF, Abadi M, Habuchi S. Single-molecule diffusion and conformational dynamics by spatial integration of temporal fluctuations. Nat Commun. 2014;5.

[43] Gorczyca SM, Chapman CD, Robertson-Anderson RM. Universal scaling of crowding-induced DNA mobility is coupled with topology-dependent molecular compaction and elongation. Soft Matter. 2015;11:7762-8.

[44] Chapman CD, Gorczyca S, Robertson-Anderson RM. Crowding Induces Complex Ergodic Diffusion and Dynamic Elongation of Large DNA Molecules. Biophysical Journal. 2015;108:1220-8.

[45] Robertson RM, Smith DE. Strong effects of molecular topology on diffusion of entangled DNA molecules. Proceedings of the National Academy of Sciences. 2007;104:4824-7

[46] Robertson RM, Smith DE. Self-Diffusion of Entangled Linear and Circular DNA Molecules: Dependence on Length and Concentration. Macromolecules. 2007;40:3373-7.

[47] Chapman CD, Shanbhag S, Smith DE, Robertson-Anderson RM. Complex effects of molecular topology on diffusion in entangled biopolymer blends. Soft Matter. 2012;8:9177-82.

[48] Abadi M, Serag MF, Habuchi S. Single-Molecule Imaging Reveals Topology Dependent Mutual Relaxation of Polymer Chains. Macromolecules. 2015;48:6263-71.

[49] Laib S, Robertson RM, Smith DE. Preparation and Characterization of a Set of Linear DNA Molecules for Polymer Physics and Rheology Studies. Macromolecules. 2006;39:4115-9.

[50] Robertson RM, Smith DE. Direct Measurement of the Confining Forces Imposed on a Single Molecule in a Concentrated Solution of Circular Polymers. Macromolecules. 2007;40:8737-41.

[51] Zimmerman SB, Minton AP. Macromolecular Crowding: Biochemical, Biophysical, and Physiological Consequences. Annual Review of Biophysics and Biomolecular Structure. 1993;22:27-65.

[52] Tanyeri M, Schroeder CM. Manipulation and Confinement of Single Particles Using Fluid Flow. Nano Letters. 2013;13:2357-64.

[53] Shenoy A, Rao CV, Schroeder CM. Stokes trap for multiplexed particle manipulation and assembly using fluidics. Proceedings of the National Academy of Sciences. 2016.

[54] Larson RG. The Structure and Rheology of Complex Fluids: OUP USA; 1999.

[55] Subramanian G, Shanbhag S. Self-Diffusion in Binary Blends of Cyclic and Linear Polymers. Macromolecules. 2008;41:7239-42.

[56] Snijkers F, Pasquino R, Olmsted PD, Vlassopoulos D. Perspectives on the viscoelasticity and flow behavior of entangled linear and branched polymers. Journal of Physics: Condensed Matter. 2015;27:473002.

[57] Seeman NC, Kallenbach NR. Design of immobile nucleic acid junctions. Biophysical Journal. 1983;44:201-9.

[58] Duckett DR, Murchie AIH, Diekmann S, von Kitzing E, Kemper B, Lilley DMJ. The structure of the holliday junction, and its resolution. Cell. 1988;55:79-89.

[59] Returning to the fold. Nat Mater. 2016;15:245-.

[60] Heuer DM, Saha S, Archer LA. Electrophoretic dynamics of large DNA stars in polymer solutions and gels. ELECTROPHORESIS. 2003;24:3314-22.

[61] Saha S, Heuer DM, Archer LA. Electrophoretic mobility of linear and star-branched DNA in semidilute polymer solutions. ELECTROPHORESIS. 2006;27:3181-94.

[62] Saha S, Heuer DM, Archer LA. Effect of matrix chain length on the electrophoretic mobility of large linear and branched DNA in polymer solutions. ELECTROPHORESIS. 2004;25:396-404.

[63] Marciel AB, Mai DJ, Schroeder CM. Template-Directed Synthesis of Structurally Defined Branched Polymers. Macromolecules. 2015;48:1296-303.

[64] Mai DJ, Marciel AB, Sing CE, Schroeder CM. Topology-Controlled Relaxation Dynamics of Single Branched Polymers. ACS Macro Letters. 2015;4:446-52.

[65] Keshavarz M, Engelkamp H, Xu J, Braeken E, Otten MBJ, Uji-i H, et al. Nanoscale Study of Polymer Dynamics. ACS Nano. 2016;10:1434-41.

3 SYNTHESIS OF BRANCHED DNA POLYMERS[†]

3.1 INTRODUCTION

The development of advanced materials critically relies on the synthesis of structurally defined polymers. Precise control over the spatial position of branches along a polymer chain backbone holds the key to understanding the rheological consequences of branching in entangled polymer solutions and melts [1-3]. To this end, extensive efforts have been focused on the development of synthetic methods that can provide simultaneous control over polymer composition, topology, and chemical functionality with a high degree of polymer chain uniformity [4-6].

Several strategies have been developed in recent years to increase control over polymer chain topology. Specifically, atom transfer radical polymerizations (ATRP) and anionic living polymerization have been used to produce architecturally complex polymers including star, comb, brush, and hyperbranched polymers with controlled, narrow molecular weight distributions [7, 8]. Moreover, advanced separations techniques, such as thermal gradient interaction chromatography, have enabled the identification and removal of architectural impurities [4, 6]. These synthetic and separation techniques have been further paired with rheological characterization to provide molecular-based insights on the impact of branching on material response; however, macroscopic techniques inherently measure averaged behaviors of bulk materials.

Single polymer dynamics overcome these challenges by direct visualization of individual polymer molecules in flow [9-12]. Over the past two decades, researchers have used DNA as a model

[†]Adapted with permission from A. B. Marciel, D. J. Mai, C. M. Schroeder, *Macromolecules*, **48**, 1296-1303, 2015 and D. J. Mai, A. B. Marciel, C. E. Sing, C. M. Schroeder, *ACS Macro Letters*, **4**, 446-452, 2015. Copyright (2015) American Chemical Society.

system to study polymer dynamics using single molecule methods [13, 14]. DNA serves as a powerful system for single polymer dynamics, in particular due to an established understanding of the physical properties and preparation methods, including facile fluorescent labeling, compatibility with aqueous buffers, and templated synthesis of monodisperse polymers. Despite these key advantages, however, natural DNA lacks the broad chemical diversity generally provided by synthetic polymers that are routinely employed as functional materials.

In order to incorporate chemical functionality into nucleic acid polymers, DNA can be readily modified using a variety of approaches. DNA block-copolymers (DBCs) have been synthesized via covalent attachment of oligonucleotides to synthetic organic polymers, thereby allowing for self-assembly and tuning of behavior by controlling one or both blocks. [15] Recently, amphiphilic DBCs exhibiting micelle-like assembly behavior have been synthesized, and these structures have proven useful for applications in biotechnology and nanomedicine [16-18].

The first generation of DBCs was based on a linear chain architecture, whereas many rheological phenomena are observed using synthetic organic polymers with exceedingly complex topologies. An alternative class of DBCs with branched architectures was subsequently synthesized consisting of synthetic polymer backbones with randomly grafted DNA side chains. This strategy has been used to synthesize comb polymer architectures based on poly(acrylic acid) backbones for single-nucleotide polymorphism detection [19], ROMP-derived backbones for DNA detection [20, 21], biodegradable polypeptide backbones for hydrogel formation [22], and poly(peptide) nucleic acid amphiphiles for nanoparticle formation [23]. In a related approach, a handful studies have focused on synthesizing DNA backbones with grafted polymer side-chains. Here, DNA intercalators can be used to crosslink double-stranded DNA upon UV irradiation, followed by covalent attachment

of synthetic polymers [24-26]. A subsequent investigation used the ability of DNA polymerase to incorporate non-natural nucleotide triphosphates containing large polymer modifications in a template-dependent manner [27], but nucleotides containing substantial chemical modifications exhibited exceedingly poor fidelity by a natural DNA polymerase, thereby inhibiting manipulation of branch length and chemical identity. From this perspective, there remains a strong need for the development of new techniques and methods allowing for the synthesis of DNA with controlled topologies for single polymer studies.

In prior work, we demonstrated a versatile synthesis method to produce monodisperse and architecturally precise branched polymers based on single-stranded DNA (ssDNA) backbones [28]. In particular, we used a hybrid enzymatic graft-onto synthesis method, thereby allowing for precise control over side branch placement along ssDNA backbones. First, we utilized the natural ability of *Pwo* superyield DNA polymerase to enzymatically incorporate chemically-modified DBCO-dUTP monomers in a template-directed fashion. Next, we employed copper-free 'click' chemistry to directly graft natural oligonucleotides or synthetic polymer side branches onto ssDNA backbones. In this way, we systematically produced a variety of branched ssDNA architectures including three-arm stars, H-polymers, and graft block copolymers with uniform composition, topology, and chemical identity. From a broad perspective, this synthetic strategy could provide a useful method for the facile production of polymers with model topologies for structure-property relationship studies.

In this Chapter, we describe the extension of this hybrid enzymatic graft-onto synthetic approach to generate branched DNA for single polymer dynamics [29]. In this way, template-directed synthesis is used to generate polymer backbones and branches with bio-orthogonal reactive groups,

followed by a ‘graft onto’ approach for covalently linking side branches to the main chain backbone (**Figure 3.1**). Backbones and side branches have controlled molecular weights, and long-range polymerases are utilized to synthesize high molecular-weight components appropriate for single molecule imaging. All materials are characterized via agarose gel electrophoresis, and branched polymers are purified for single molecule experiments using size exclusion chromatography.

3.2 MATERIALS AND METHODS

3.2.1 Materials and reagents

The following materials and reagents are used for synthesis and preparation of DNA-based branched polymers: bacteriophage λ-DNA (New England Biolabs, Ipswich, MA), PCR Extender System (5 PRIME, Gaithersburg, MD), *Taq* DNA Polymerase with Thermopol Buffer (New England Biolabs, Ipswich, MA), 5-DBCO-dUTP (Jena Bioscience GmbH, Germany), Cy5-dUTP-PCR (Jena Bioscience GmbH, Germany), deoxynucleotide (dNTP) solution (New England Biolabs, Ipswich, MA), custom oligonucleotide primers (**Table 3.1**, IDT DNA, Coralville, IA), QIAquick PCR Purification Kit (QIAGEN, Valencia, CA), Vivacon 2 with 100,000 MWCO Hydrosart Membrane (Vivaproducts, Littleton, MA), agarose (Thermo Fisher Scientific, Waltham, MA), 50× TAE Buffer (2.0 M Tris, 1.0 M acetic acid, 50 mM EDTA, Biorad, Hercules, CA), SYBR Gold Nucleic Acid Gel Stain (Invitrogen, Grand Island, NY), SYTOX Green Nucleic Acid Stain (Molecular Probes, Grand Island, NY).

3.2.2 Synthesis of linear DNA backbones and branches

Synthesis of linear DNA. Polymerase chain reaction (PCR) is used to enzymatically amplify target sequences from λ-phage DNA in the presence of chemically modified deoxyribonucleotides (dNTPs) and primers. In one reaction, DNA backbones (10, 20, 30, or 40 kbp) are synthesized with internal dibenzylcyclooctyne (DBCO) groups. In some cases, a terminal biotin tag is included for specific attachment to a surface. In a separate reaction, azide-terminated DNA branches (951 bp, 2200 bp, or 10 kbp) are synthesized using a chemically modified PCR primer to append an azide group to one branch terminus. In some cases, internal Cy5 dyes are directly incorporated into the low molecular weight branches (951 or 2200 bp) using modified Cy5-dTTP nucleotides. Specific conditions for PCR amplification of backbones, low molecular weight branches (951 and 2200 bp), and high molecular weight branches (10 kbp) are outlined in **Tables 3.2, 3.3, and 3.4**, respectively.

DNA purification. Branch PCR products are purified using QIAquick PCR Purification Kits, and backbone PCR products are purified using pre-rinsed Vivacon 2 columns. Manufacturer instructions are followed in both purification steps. The concentrations of all purified products are measured using a NanoDrop UV-Vis spectrophotometer (Thermo Scientific). During all preparation and handling steps, care is taken to minimize shearing or degradation of macromolecular structures.

Quantification of Cy5 dye incorporation in branches. Incorporation of Cy5 dyes during PCR is determined by measuring sample absorbance at 260 and 649 nm (A_{260} and A_{649}, respectively) using Eq. 3.1 with extinction coefficients ε_{DNA} = 6,600 $cm^{-1}M^{-1}$ and ε_{Cy5} = 250,000 $cm^{-1}M^{-1}$.

$$\frac{dyes}{base} = \frac{A_{649} \times \varepsilon_{DNA}}{(A_{260} - 0.05A_{649}) \times \varepsilon_{Cy5}} \quad (3.1)$$

3.2.3 Grafting reaction of DNA branches onto backbones

Graft-onto synthesis of branched DNA. Following PCR amplification and purification of precursor molecules, branch molecules are chemically grafted onto DNA backbones via strain-promoted [3+2] azide–alkyne cycloaddition (SPAAC), thereby generating branched DNA macromolecules suitable for single molecule fluorescence microscopy. Purified branch and backbone PCR products were mixed at varying concentrations in thin-walled PCR-type Eppendorf tubes. A wide range of reaction conditions was scanned for efficient conversion of SPAAC reactions. Following optimization, graft-onto reactions were generally carried out in 250 mM Tris (pH 8.0), 1.0 M NaCl, and 10 mM EDTA at 70 °C for 18 hours or longer.

Agarose gel electrophoresis. Gel electrophoresis is used to characterize linear precursors and SPAAC products. Agarose gels are prepared in 1× TAE buffer (1.0 wt% agarose, 40 mM Tris, 20 mM acetic acid, 1 mM EDTA). DNA samples are stained with SYBR Gold, and electrophoresed in 1× TAE buffer for 30 minutes at 120 V. After electrophoresis, agarose gels are imaged using an ethidium bromide filter using a Foto/Analyst FX (FotoDyne Incorporated). Dual-color agarose gels are imaged with SYBR Gold and Cy5 filters using a Typhoon 9400 imager (Amersham Bioscience/GE Healthcare). In all cases, samples are compared to a 1 kbp DNA ladder with λ-DNA as a size standard.

3.2.4 Purification of DNA comb polymers

Gel filtration chromatography was utilized to remove excess branches following SPAAC reactions, thereby enabling the study of single comb polymers in flow. A Tricorn 10/300 column

was packed with Sephacryl S-1000 gel filtration media and installed on an AKTA FPLC system (GE Healthcare Life Sciences). After equilibrating the column with an aqueous buffer system (200 mM NaCl, 30 mM Tris, 2 mM EDTA, filtered using 0.22 μm Millipore Stericup), SPAAC products are flowed through the column at a volumetric flow rate of 0.05 – 0.1 mL/min. The first peak to elute is identified as purified DNA comb polymer and concentrated using a Vivacon 2 column. Concentrated comb polymers are stored in 50% glycerol at –20 °C.

3.3 RESULTS AND DISCUSSION

Our hybrid enzymatic-synthetic approach allows for precise control over backbone and branch molecular weights. Following synthesis, branched DNA polymers are first characterized using agarose gel electrophoresis. The agarose gel in **Figure 3.2** shows both control and SPAAC reaction products based on a 10 kbp DNA backbone and Cy5-labeled 951 bp DNA branches. In all cases, negative controls show that DNA backbones without chemically modified DBCO-dNTPs do not react with azide-terminated DNA branches (Lane 2). However, branched polymers are formed by reacting DNA backbones with DBCO modifications (10% of dTTP replaced with 5-DBCO-dUTP) with azide-terminated DNA branches, which generally shows a noticeable shift in agarose gels (Lane 3). In this particular experiment, negative control and SPAAC reaction samples were both mixed with a ~20 molar excess of azide-terminated, Cy5-labeled branches (red emission), and the reactions were carried out in 250 mM Tris buffer (pH 8.0) and 1.0 M NaCl at 70 °C over the course of 70 hours, though significant conversion was observed after only a few hours (**Figures 3.3 and 3.4**).

Migration patterns in gel electrophoresis are indicative of polymer chain branching. The negative control sample shown in **Figure 3.2** exhibits green fluorescence emission (only) from the high

molecular weight band at 10 kbp, which indicates the absence of Cy5-labeled branch molecules co-migrating with natural DNA backbones. However, the presence of DNA comb polymers is indicated in Lane 3 by the co-migration of red and green fluorescence emission from the high molecular weight band corresponding to comb polymer. Moreover, the band corresponding to the molecular weight of the DNA backbone is absent in Lane 3, suggesting a near quantitative conversion to branched DNA polymers. Importantly, gel electrophoresis also shows a clear shift in the mobility of branched DNA compared to linear DNA. A decrease in electrophoretic mobility of comb polymers is consistent with previous reports of decreased mobility in DNA with branched architectures, such as stars [30, 31], pom-poms [30], and partial denaturation events [32]. This phenomenon is attributed to an increase in molecular weight of DNA combs and the generation of branch sites, which are known to impede the migration of polymers through gel networks due to chain stretch in the transverse direction of the electric field. This topologically driven motion prevents backbone reptation through matrix pores, entangles molecules in the gel network, and transiently traps branch junctions in the matrix, all of which results in a significantly reduced electrophoretic mobility for branched DNA molecules [30-32].

Optimization of SPAAC reaction conditions. Purified branch and backbone PCR products were mixed at varying concentrations in thin-walled PCR-type Eppendorf tubes. A wide range of reaction conditions was scanned for efficient conversion of SPAAC reactions. NaCl and Tris/Tris-HCl (pH 8.0) concentrations were selected based on a 25-fold molar excess of branches relative to backbones; reaction solutions were held at 70 °C for 18 hours. The resulting products are shown in **Figure 3.3**, which is fully described in **Table 3.5**. The condition shown in Lane 7 (250 mM Tris and 1.0 M NaCl) is used for all subsequent branch addition reactions. **Figure 3.4** and **Table 3.6**

show two-color fluorescent gel electrophoresis of 10 kbp and 20 kbp samples with Cy5-labeled 951 bp branches. Bulk absorbance measurements used to quantify the Cy5 dye loading along 951 bp DNA branches reveal an average of 7-8 Cy5 dyes per branch for these reaction conditions. As the ratio of molecular branches to backbones during SPAAC reactions is increased, bands corresponding to the linear branches and backbones disappear and decreases in branched product mobility become more apparent. Perhaps not surprisingly, these observations suggest higher degrees of branching following SPAAC reactions with a greater molar excess of branches.

Purification of DNA combs for solution-based single molecule experiments. **Figures 3.2-3.4** clearly show the presence of excess branches following SPAAC reactions. Size exclusion chromatography (SEC) was utilized to remove excess branches, thereby enabling the study of single comb polymers in flow. SEC is a liquid chromatography method that separates mixtures based on size [33]. The stationary phase consists of a porous packed column, and molecules undergo "reverse sieving," such that large molecules elute before smaller molecules. Here, small molecules interact with the porous matrix and become temporarily trapped, whereas large molecules bypass the pores to elute first.

SEC with an aqueous mobile phase is specifically referred to as gel filtration chromatography (GFC) [33]. We employ this technique to separate large branched DNA molecules from smaller, unreacted branches. A GFC trace of DNA combs with 30 kbp backbones and 951 bp branches is shown in **Figure 3.5**, where UV absorption (254 nm) and conductivity are measured as functions of volume. Selected fractions were combined, concentrated using Vivacon 2 columns, and analyzed using agarose gel electrophoresis, as shown in **Figure 3.6**. As expected, large branched DNA elutes prior to smaller unreacted branches, with some overlap between peaks in the GFC

trace. GFC is further applied to larger constructs (40 kbp backbone and 951 or 2200 bp branches). GFC traces and gel electrophoresis before and after GFC are shown in **Figures 3.7 and 3.8**, respectively.

3.4 CONCLUSIONS

In summary, we report a versatile approach to synthesize branched polymers appropriate for single molecule studies. The two-step enzymatic-synthetic method provides access to a wide design space of polymer backbone length, branch length, and branch density. Bioorthogonal DBCO branch sites are enzymatically incorporated by PCR, followed by direct grafting of azide-terminated branches to polymer backbones. Importantly, this method allows for synthesis of branched polymers with tunable molecular weights and topologies. In all cases, branched polymer architectures are characterized by agarose gel electrophoresis, which generally shows retardation of electrophoretic mobility as a function of branch length, branch number, and branch placement. We further purify and isolate the desired branched polymer structures from their linear template precursors via size-exclusion chromatography.

Recently, this synthetic method was also used to precisely control branch placement, branch number, and chemical identity of side branches in oligomeric DNA [28]. In this way, structure–function relations can be systematically studied and controlled polymer topologies can be used to drive assembly of new materials for biomedical and electronic materials applications. Finally, this platform offers the ability to study the effects of architectural defects on microstructural assembly. To this end, the unique ability to insert site-specific errors (*e.g.* missing branches or distinct chemical functionalities) holds the potential to enable systematic characterization of macromolecular behavior for advanced materials.

3.5 FIGURES AND TABLES

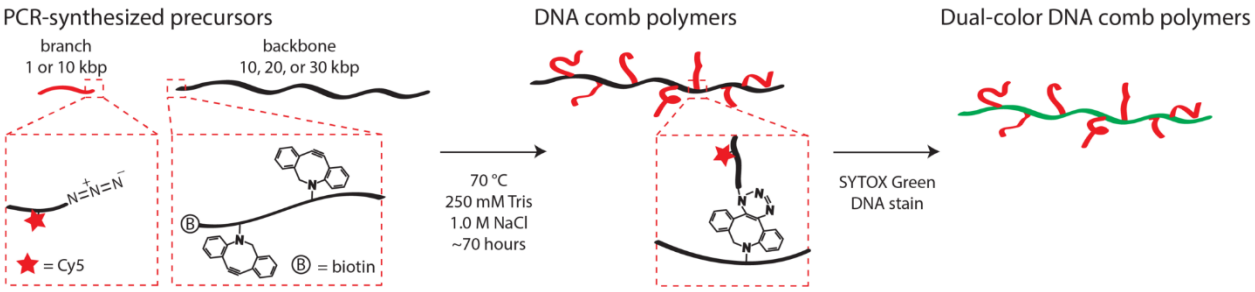

Figure 3.1. Synthesis scheme for DNA comb polymers. In some cases, dual-color branched polymers are synthesized by direct incorporation of Cy5 dyes into side branches, followed by labeling with an intercalating DNA dye such as SYTOX Green.

Table 3.1. Custom oligonucleotide primer sequences. 951 F, 951 R, and 2200 R were designed using VectorNTI software. The remaining primer sequences were based on targets identified by Fuller *et al*. [34]. Universal F and its variants are universal forward primers for long targets from λ-DNA.

Primer name	**Target length**	**Nucleic acid sequence (5' → 3')**	**Modification**
951 F	951 bp	GACAGCGTACAGCCCGTTCA	5'-azide
951 R	951 bp	TCGCGTCATTCATCCTCTCC	None
Univ F	n/a	CTGATGAGTTCGTGTCCGTACAACTGGCGTAATC	None
Univ F biotin	n/a	CTGATGAGTTCGTGTCCGTACAACTGGCGTAATC	5'-biotin
Univ F azide	n/a	CTGATGAGTTCGTGTCCGTACAACTGGCGTAATC	5'-azide
2200 R	2200 bp	CTGACCCAGCCACGGAACACATCG	None
10k R	10,052 bp	ATACGCTGTATTCAGCAACACCGTCAGGAACACG	None
20k R	20,052 bp	GTGCACCATGCAACATGAATAACAGTGGGTTATC	None
30k R	30,052 bp	GAAAGTTATCGCTAGTCAGTGGCCTGAAGAGACG	None
40k R	40,052 bp	TAATGCAAACTACGCGCCCTCGTATCACATGG	None

Table 3.2. PCR parameters: backbones, with or without internal DBCO modifications

Reaction composition				
50 uL per reaction 1X Tuning buffer with Mg^{2+} 0.4 uL PCR Extender Polymerase Mix 400 nM Univ F biotin or Univ F primer 400 nM 10k R, 20k R, 30k R, or 40k R primer 20 ng λ-DNA 500 uM dATP, dCTP, dGTP, dTTP[§]				
PCR step	10 kbp target	20 kbp target	30 kbp target	30 kbp target
Initial denaturation	93 °C / 3 min	93 °C / 3 min	93 °C / 3 min	93 °C / 3 min
*Denaturation	93 °C / 15 sec	93 °C / 15 sec	93 °C / 15 sec	93 °C / 15 sec
*Anneal	62 °C / 30 sec	62 °C / 30 sec	62 °C / 30 sec	62 °C / 30 sec
*Extension	68 °C / 8 min[†]	68 °C / 15 min	68 °C / 20 min	68 °C / 21 min
# cycles constant	10	10	10	10
# cycles ramping	8	8	8	8
Increase per cycle	+ 20 sec[†]	+ 20 sec	+ 20 sec	+ 20 sec

[§]dTTP was substituted with 5-DBCO-dUTP at 0.5, 1.0, 10, or 25% replacement
*steps included in cycling
[†]extension times increased by 50% for 25% replacement of dTTP with 5-DBCO-dUTP

Table 3.3. PCR parameters: 951 or 2200 bp azide-terminated branches

Unlabeled branches	Cy5-labeled branches	PCR step	Temp. / Time
50 uL per reaction 1X Thermopol buffer* 0.25 uL *Taq* DNA Polymerase 200 nM 951 F primer 200 nM 951 R primer 20 ng λ-DNA 200 uM dATP, dCTP, dGTP, dTTP	*20 uL per reaction* 1X Thermopol buffer 0.25 uL *Taq* DNA Polymerase 500 nM 951 F primer 500 nM 951 R primer 20 ng λ-DNA 100 uM dATP, dCTP, dGTP 75 uM dTTP 25 uM Cy5-dUTP	Initial denaturation *Denaturation *Anneal *Extension Final Extension *cycle steps 30x	95 °C / 30 sec 95 °C / 15 sec 60 °C / 30 sec 68 °C / 60 sec 68 °C / 120 sec
50 uL per reaction 1X Thermopol buffer* 0.25 uL *Taq* DNA Polymerase 200 nM Univ F azide primer 200 nM 2200 R primer 20 ng λ-DNA 200 uM dATP, dCTP, dGTP, dTTP	*20 uL per reaction* 1X Thermopol buffer 0.25 uL *Taq* DNA Polymerase 500 nM Univ F azide primer 500 nM 2200 R primer 20 ng λ-DNA 100 uM dATP, dCTP, dGTP 75 uM dTTP 25 uM Cy5-dUTP	Initial denaturation *Denaturation *Anneal *Extension Final Extension *cycle steps 30x	95 °C / 30 sec 95 °C / 15 sec 60 °C / 30 sec 68 °C / 60 sec 68 °C / 120 sec

*1X Thermopol buffer: 20 mM Tris-HCl, 10 mM $(NH_4)_2SO_4$, 10 mM KCl, 2 mM $MgSO_4$, 0.1% Triton X-100, pH 8.8.

Table 3.4. PCR parameters: 10 kbp azide-terminated branches

Reaction composition	PCR step	10 kbp target
50 uL per reaction	Initial denaturation	93 °C / 3 min
1X Tuning buffer with Mg^{2+}	*Denaturation	93 °C / 15 sec
0.4 uL PCR Extender Polymerase Mix	*Anneal	62 °C / 30 sec
400 nM Univ F azide primer	*Extension	68 °C / 8 min
400 nM 10k R primer	# cycles constant	10
20 ng λ-DNA	# cycles ramping	8
500 uM dATP, dCTP, dGTP, dTTP	Increase per cycle	+ 20 sec

*steps included in cycling

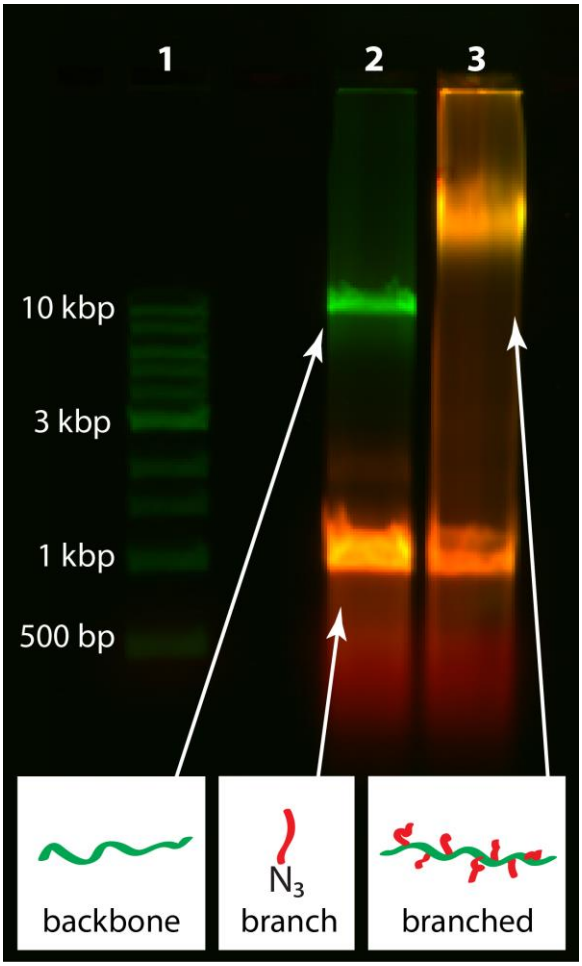

Figure 3.2. Agarose gel electrophoresis of DNA comb polymers formed by SPAAC. Lane 1: 1 kbp DNA ladder (New England Biolabs). Lane 2: negative control reaction of Cy5-labeled, azide-terminated branches (951 bp) and natural backbones (10 kbp). Lane 3: formation of dual-color branched DNA polymers (>10 kbp) via grafting Cy5-labeled, azide-terminated branches onto DBCO-modified backbones. Gels are stained with SYBR Gold (Invitrogen) and electrophoresed in 1.0% agarose in 1X TAE buffer for 30 minutes at 120 V.

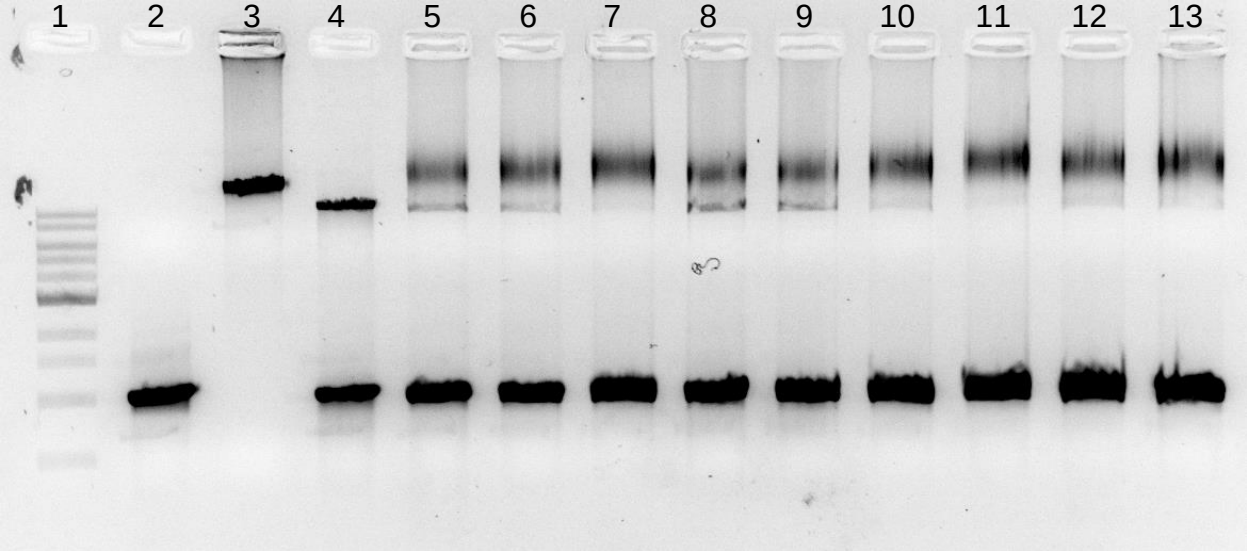

Figure 3.3. Optimizing SPAAC reaction conditions between azide-terminated branches and DBCO-modified backbones. The reaction conditions are described in **Table 3.5**. Samples are stained with SYBR Gold, followed by agarose gel electrophoresis (1.0% agarose) in 1X TAE buffer at 120 V for 30 minutes.

Table 3.5. SPAAC reaction conditions of samples in **Figure 3.3**.

Lane	Description
1	1 kbp ladder (New England Biolabs)
2	951 bp branch precursor
3	10 kbp backbone precursor
4	Control reaction, ddH_2O only
5	Reaction; 250 mM Tris, 250 mM NaCl
6	Reaction; 250 mM Tris, 500 mM NaCl
7	Reaction; 250 mM Tris, 1 M NaCl
8	Reaction; 500 mM Tris
9	Reaction; 500 mM Tris, 250 mM NaCl
10	Reaction; 500 mM Tris, 500 mM NaCl
11	Reaction; 500 mM Tris, 1 M NaCl
12	Reaction; 1 M Tris
13	Reaction; 1 M NaCl

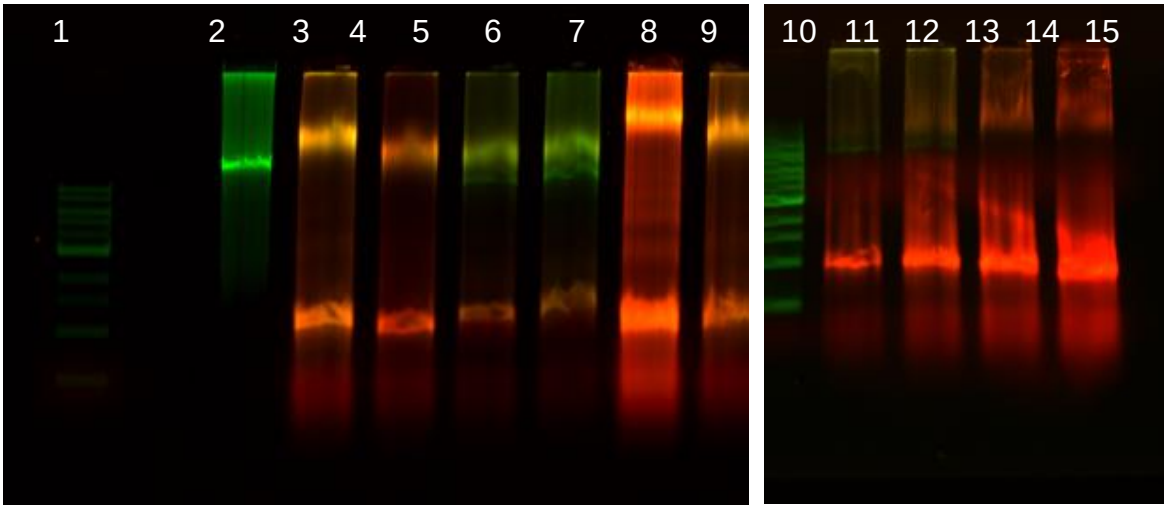

Figure 3.4. Two-color fluorescent gel electrophoresis images of branched DNA polymers with (left) 10 kbp backbones and (right) 20 kbp backbones. All samples were reacted at 70 °C for at least 80 hours in 250 mM Tris and 1.0 M NaCl; additional conditions are listed in **Table 3.6**. Samples are stained with SYBR Gold, followed by agarose gel electrophoresis (1.0% agarose) in 1X TAE buffer at 120 V for 30 minutes.

Table 3.6. SPAAC reaction conditions of samples in **Figure 3.4**. Percentage of DBCO indicates substitution of dTTP with dUTP-DBCO in the reaction mixture, ratios indicate molar excess of branches to backbones in the reaction solution.

Lane	Description	Lane	Description
1	1 kbp ladder	10	20 kbp backbone
2	10 kbp backbone	11	1 kbp ladder
3	10% DBCO, 20:1 br:bb	12	1% DBCO, 10:1 br:bb
4	10% DBCO, 10:1 br:bb	13	1% DBCO, 20:1 br:bb
5	10% DBCO, 5:1 br:bb	14	1% DBCO, 50:1 br:bb
6	10% DBCO, 3:1 br:bb	15	1% DBCO, 100:1 br:bb
7	25% DBCO, 50:1 br:bb		
8	25% DBCO, 20:1 br:bb		
9	25% DBCO, 10:1 br:bb		

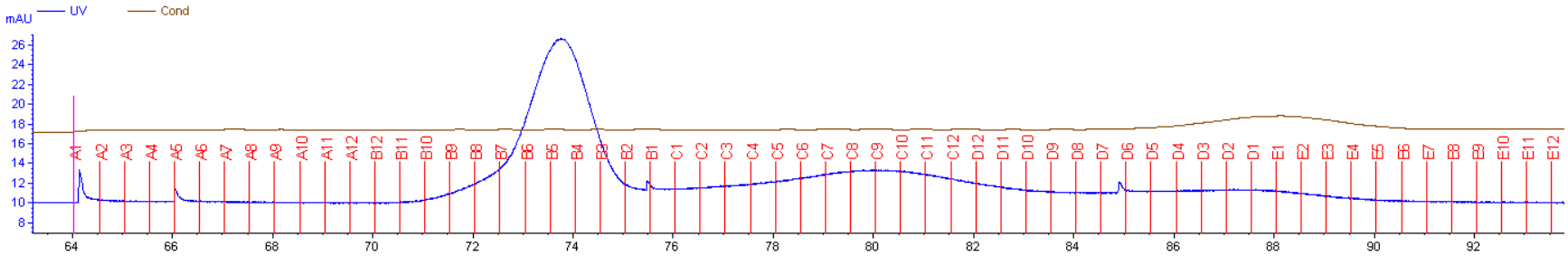

Figure 3.5. Sample GFC trace of DNA combs consisting of 30 kbp backbones with 1.0% replacement of dTTP with 5-DBCO-dUTP and 30-fold molar excess of 951 bp branches, reacted for 48 h at 70 °C. UV absorbance at 254 nm (a.u., blue) and conductivity (scale not shown, brown) are plotted as a function of volume passed through the GFC column (mL).

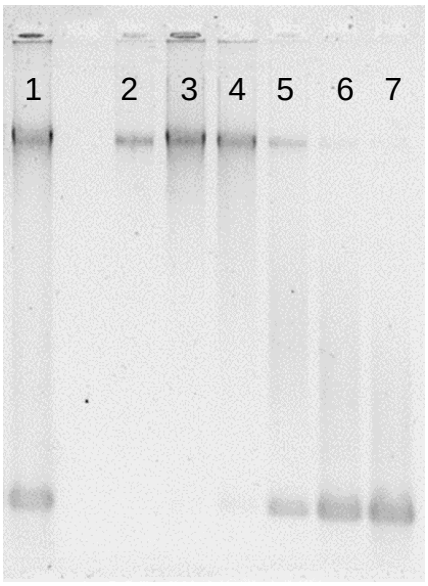

Figure 3.6. DNA combs before and after gel filtration chromatography. DNA combs consist of 30 kbp backbones with 1.0% replacement of dTTP with 5-DBCO-dUTP and 30-fold molar excess of Cy5-labeled 951 bp branches, reacted for 48 h at 70 °C (Lane 1). GFC fractions are collected over B7-B10 (Lane 2), B4-B6 (Lane 3), B1-B3 (Lane 4), C1-C4 (Lane 5), C5-C8 (Lane 6), and C9-C12 (Lane 7) and concentrated using Vivacon 2 columns. Samples are stained with SYBR Gold, followed by agarose gel electrophoresis (0.6% agarose) in 1X TAE buffer at 60 V for 180 minutes.

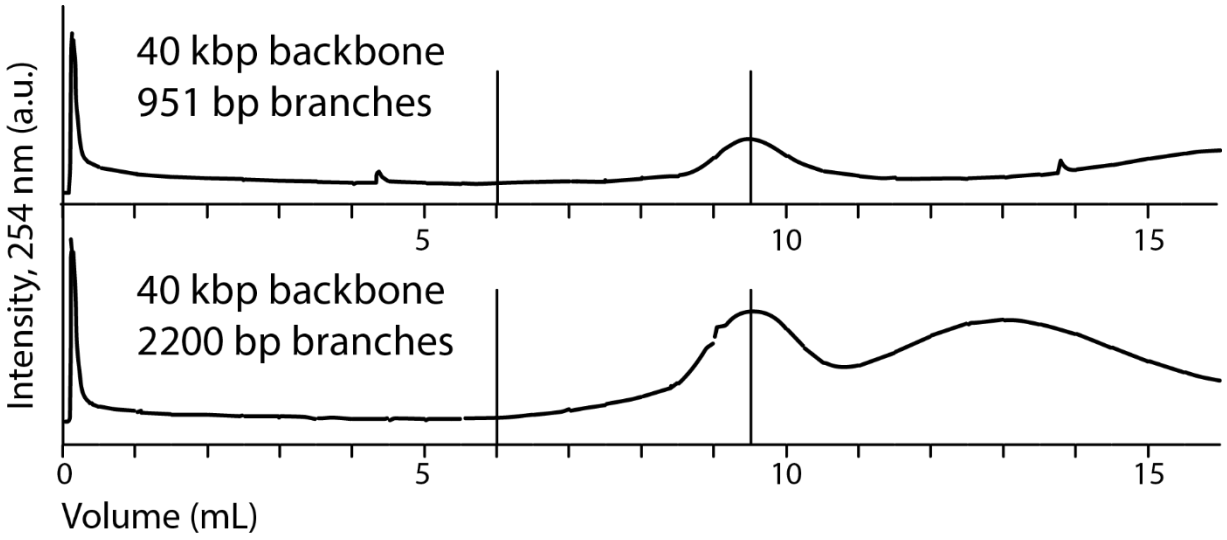

Figure 3.7. GFC traces of DNA combs. 40 kbp backbones with 0.5% replacement of dTTP with 5-DBCO-dUTP and 40-fold molar excess of Cy5-labeled 951 bp branches (top) or Cy5-labeled 2200 bp branches (bottom), reacted for 65 h at 70 °C. UV absorbance at 254 nm (a.u.) is plotted as a function of volume passed through the GFC column (mL). Fractions collected in the region between the vertical lines are combined and concentrated prior to single molecule fluorescence microscopy.

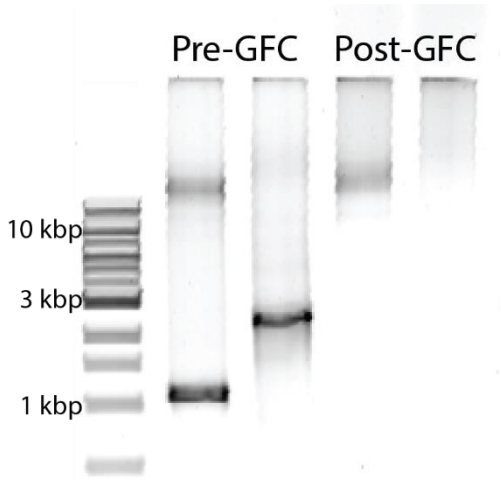

Figure 3.8. DNA combs before (Lanes 2 and 3) and after (Lan**e**s 4 and 5) gel filtration chromatography. A 1 kbp ladder with λ-DNA is shown for reference Lane 1. DNA combs consist of 40 kbp backbones with 0.5% replacement of dTTP with 5-DBCO-dUTP and 40-fold molar excess of Cy5-labeled 951 bp branches (Lanes 2 and 4) or Cy5-labeled 2200 bp branches (Lanes 3 and 5), reacted for 65 h at 70 °C. GFC fractions are collected as shown in **Figure 3.6** and concentrated using Vivacon 2 columns. Samples are stained with SYBR Gold, followed by agarose gel electrophoresis (1.0% agarose) in 1X TAE buffer at 120 V for 30 minutes.

3.6 REFERENCES

[1] Larson RG. The Structure and Rheology of Complex Fluids: OUP USA; 1999.

[2] Dealy JM, Larson RG. Structure and Rheology of Molten Polymers: From Structure to Flow Behavior and Back Again: Hanser Publishers; 2006.

[3] Snijkers F, Pasquino R, Olmsted PD, Vlassopoulos D. Perspectives on the viscoelasticity and flow behavior of entangled linear and branched polymers. Journal of Physics: Condensed Matter. 2015;27:473002.

[4] Snijkers F, van Ruymbeke E, Kim P, Lee H, Nikopoulou A, Chang T, et al. Architectural Dispersity in Model Branched Polymers: Analysis and Rheological Consequences. Macromolecules. 2011;44:8631-43.

[5] Lutz J-F, Ouchi M, Liu DR, Sawamoto M. Sequence-Controlled Polymers. Science. 2013;341.

[6] van Ruymbeke E, Lee H, Chang T, Nikopoulou A, Hadjichristidis N, Snijkers F, et al. Molecular rheology of branched polymers: decoding and exploring the role of architectural dispersity through a synergy of anionic synthesis, interaction chromatography, rheometry and modeling. Soft Matter. 2014;10:4762-77.

[7] Hadjichristidis N, Pitsikalis M, Pispas S, Iatrou H. Polymers with complex architecture by living anionic polymerization. Chemical reviews. 2001;101:3747-92.

[8] Matyjaszewski K, Xia J. Atom transfer radical polymerization. Chemical reviews. 2001;101:2921-90.

[9] Perkins T, Quake, Smith D, Chu S. Relaxation of a single DNA molecule observed by optical microscopy. Science. 1994;264:822-6.

[10] Perkins TT, Smith DE, Chu S. Single Polymer Dynamics in an Elongational Flow. Science. 1997;276:2016-21.

[11] Smith DE, Chu S. Response of Flexible Polymers to a Sudden Elongational Flow. Science. 1998;281:1335-40.

[12] Mai DJ, Brockman C, Schroeder CM. Microfluidic systems for single DNA dynamics. Soft Matter. 2012;8:10560-72.

[13] Latinwo F, Schroeder CM. Model systems for single molecule polymer dynamics. Soft Matter. 2011;7:7907-13.

[14] Tree DR, Muralidhar A, Doyle PS, Dorfman KD. Is DNA a Good Model Polymer? Macromolecules. 2013;46:8369-82.

[15] Kwak M, Herrmann A. Nucleic Acid/Organic Polymer Hybrid Materials: Synthesis, Superstructures, and Applications. Angewandte Chemie International Edition. 2010;49:8574-87.

[16] Cottenye N, Syga M-I, Nosov S, Muller AHE, Ploux L, Vebert-Nardin C. Biological-like vesicular structures self-assembled from DNA-block copolymers. Chemical Communications. 2012;48:2615-7.

[17] Ding K, Alemdaroglu FE, Börsch M, Berger R, Herrmann A. Engineering the Structural Properties of DNA Block Copolymer Micelles by Molecular Recognition. Angewandte Chemie International Edition. 2007;46:1172-5.

[18] Li Z, Zhang Y, Fullhart P, Mirkin CA. Reversible and Chemically Programmable Micelle Assembly with DNA Block-Copolymer Amphiphiles. Nano Letters. 2004;4:1055-8.

[19] Taira S, Yokoyama K. Self-assembly DNA-conjugated polymer for detection of single nucleotide polymorphism. Biotechnology and Bioengineering. 2004;88:35-41.

[20] Watson KJ, Park S-J, Im J-H, Mirkin CA. DNA−Block Copolymer Conjugates. Journal of the American Chemical Society. 2001;123:5592-3.

[21] Gibbs JM, Park S-J, Anderson DR, Watson KJ, Mirkin CA, Nguyen ST. Polymer−DNA Hybrids as Electrochemical Probes for the Detection of DNA. Journal of the American Chemical Society. 2005;127:1170-8.

[22] Chen P, Li C, Liu D, Li Z. DNA-Grafted Polypeptide Molecular Bottlebrush Prepared via Ring-Opening Polymerization and Click Chemistry. Macromolecules. 2012;45:9579-84.

[23] James CR, Rush AM, Insley T, Vuković L, Adamiak L, Král P, et al. Poly(oligonucleotide). Journal of the American Chemical Society. 2014;136:11216-9.

[24] Umeno D, Kawasaki M, Maeda M. Water-Soluble Conjugate of Double-Stranded DNA and Poly(*N*-isopropylacrylamide) for One-Pot Affinity Precipitation Separation of DNA-Binding Proteins. Bioconjugate Chemistry. 1998;9:719-24.

[25] Maeda M, Nishimura C, Umeno D, Takagi M. Psoralen-Containing Vinyl Monomer for Conjugation of Double-Helical DNA with Vinyl Polymers. Bioconjugate Chemistry. 1994;5:527-31.

[26] Umeno D, Maeda M. Poly(*N*-isopropylacrylamide) Carrying Double-Stranded DNA for Affinity Separation of Genotoxins. Analytical Sciences. 1997;13:553-6.

[27] Baccaro A, Marx A. Enzymatic Synthesis of Organic-Polymer-Grafted DNA. Chemistry – A European Journal. 2010;16:218-26.

[28] Marciel AB, Mai DJ, Schroeder CM. Template-Directed Synthesis of Structurally Defined Branched Polymers. Macromolecules. 2015;48:1296-303.

[29] Mai DJ, Marciel AB, Sing CE, Schroeder CM. Topology-Controlled Relaxation Dynamics of Single Branched Polymers. ACS Macro Letters. 2015;4:446-52.

[30] Heuer DM, Saha S, Archer LA. Electrophoretic dynamics of large DNA stars in polymer solutions and gels. ELECTROPHORESIS. 2003;24:3314-22.

[31] Saha S, Heuer DM, Archer LA. Electrophoretic mobility of linear and star-branched DNA in semidilute polymer solutions. ELECTROPHORESIS. 2006;27:3181-94.

[32] Sean D, Slater GW. Gel electrophoresis of DNA partially denatured at the ends: What are the dominant conformations? ELECTROPHORESIS. 2013;34:745-52.

[33] Hiemenz PC, Lodge TP. Polymer Chemistry, Second Edition: Taylor & Francis; 2007.

[34] Fuller DN, Gemmen GJ, Rickgauer JP, Dupont A, Millin R, Recouvreux P, et al. A general method for manipulating DNA sequences from any organism with optical tweezers. Nucleic Acids Research. 2006;34:e15.

4 MOLECULAR PROPERTIES AND SINGLE MOLECULE RELAXATION DYNAMICS OF SURFACE-TETHERED BRANCHED DNA POLYMERS[‡]

4.1 INTRODUCTION

The molecular topology of long chain polymers has long been known to influence the bulk properties of these materials [1-3]. Synthetic polymers used in commercial applications display exceedingly complex topologies, including high grafting densities of side chains, hierarchical branching, and dangling ends [4,5]. In recent years, architecturally complex polymers with well-defined structures such as multi-arm stars [6], H-polymers [7], and comb polymers [8] have been used as model systems to study the role of molecular topology on non-equilibrium flow dynamics. Recent studies have focused on the impact of macromolecular branching on the emergent, bulk-scale rheological properties of polymer solutions and melts [7, 9]. Chain branching results in complex flow properties that differ substantially from linear polymers under similar conditions, such as strain hardening in uniaxial extensional flow under relatively low strain rates [8]. Given the importance of polymeric materials in modern society, it is critical to achieve a molecular-level understanding of polymer dynamics in the context of non-linear chain topologies [1-3].

Comb polymers are an architectural subset of branched polymers consisting of side chain branches grafted to a main chain backbone [1]. Comb polymers are a particularly relevant chain architecture occurring in applications such as pharmacokinetics [10, 11], alternative energy solutions [12], and anti-fouling surface coatings [13]. The linear and non-linear viscoelastic properties of comb

[‡]Adapted with permission from D. J. Mai, A. B. Marciel, C. E. Sing, C. M. Schroeder, *ACS Macro Letters*, **4**, 446-452, 2015. Copyright (2015) American Chemical Society.

polymers have been investigated using a combination of approaches including theory, simulations, and bulk rheological experiments [2, 14-17]. Recent studies of comb polymer melts have uncovered a hierarchical stress relaxation mechanism that arises due to branched molecular architectures [17]; however, structural heterogeneity within a branched polymer sample has been shown to blur the macroscopic rheological response of branched polymer melts [7, 18]. Bulk-level experiments intrinsically average across all molecules and polymer topologies within a sample, which presents a major challenge for studying molecular-based mechanisms such as hierarchical stress relaxation. Moreover, it has been challenging to describe the non-linear rheological behavior of branched polymers using a universal constitutive model. Theoretical approaches have been used to develop constitutive stress-strain relations for linear [19] and pom-pom [20] polymers; however, the molecular details of polymer topology clearly play a key role in the emergent stress response under flow. Recently, a constitutive model has been developed for comb polymers by extending the pom-pom model to comb-shaped topologies [21].

In this Chapter, we directly observe the dynamics of branched polymers using single molecule techniques. In particular, we focus on comb polymers based on DNA, though by changing the branching distribution, we also observe three-arm stars and H-polymers. For over a decade, DNA has been used as a model system to study the dynamics of single polymer molecules in flow [22-26]. Using this approach, researchers have directly observed intriguing phenomena such as molecular individualism [27] and conformational hysteresis in flow [28]. The vast majority of single molecule DNA studies has focused on linear chain architectures [25]; however, macromolecular DNA stars and pom-poms have been generated via base pairing and hybridization

of oligonucleotides at a branched junction. In prior work, Archer and coworkers observed the dynamics of DNA-based star polymers in agarose gels under electric fields [29, 30].

4.2 MATERIALS AND METHODS

4.2.1 Branched DNA polymers

Branched DNA is synthesized as described in Chapter 3. Here, a 5'-biotin-terminated primer is included during PCR amplification to enable attachment of DNA molecules to the surface. Molecular properties of the branched DNA samples studied in this Chapter are summarized in **Table 4.1**.

4.2.2 Flow cell fabrication

An incubation buffer of 100 mM NaCl, 30 mM Tris (pH 8.0), and 2 mM EDTA was prepared. PEGylated coverslips were prepared using a mixture of biotin-PEG-NHS ester (3,500 Da) and mPEG-NHS ester (5,000 Da), as described elsewhere [31]. PEGylated glass coverslips were incubated for ~10 minutes with NeutrAvidin in incubation buffer (100 μg/mL) and a minimal amount of surfactant (1.5 μL of 1.0% Triton X) to facilitate surface tethering of biotin-terminated branched DNA polymers. Next, coverslips were rinsed with deionized water and attached to a drilled quartz slide with double-sided sticky tape and epoxy. Polyethylene tubing was epoxied into holes (~1 mm diameter) drilled into quartz slides to allow for buffer exchanges and flow through the channel. The flow channel was incubated with bovine serum albumin (BSA) in incubation buffer (final BSA concentration of 200 μg/mL) for ~10 minutes, followed by the biotin-terminated DNA sample in incubation buffer (10–40 pM) for ~30 minutes. The channel was rinsed with BSA solution prior to imaging.

4.2.3 Single molecule imaging

Imaging buffer. A viscous buffer was prepared using 62.5 or 65 wt% sucrose in incubation buffer (70 or 130 cP at 23.5 °C). This buffer was mixed with an oxygen scavenging system and a reducing agent to minimize photobleaching, consisting of glucose (5 mg/mL), β-mercaptoethanol (150 mM), glucose oxidase (0.3 mg/mL), and catalase (0.3 mg/mL). DNA molecules were labeled using SYTOX Green (200 nM).

Optical setup. Surface-tethered, fluorescently labeled DNA molecules were stretched by applying pressure-driven flow in the custom-fabricated flow cells described in 4.2.2. Single branched DNA polymers were imaged by excitation with a 488 nm laser (50 mW SpectraPhysics Excelsior Laser) or a 637 nm laser (140 mW Coherent OBIS Laser). The 488 nm optical path included absorptive neutral density filters (Thorlabs), a 488 nm long-pass dichroic mirror (ZT488rdc, Chroma), and a long-pass emission filter (BLP01-488R-25, Semrock). The intensity at the sample was ~0.1 kW/cm2. The 637 nm optical path included an absorptive neutral density filter (ThorLabs), 650 nm long-pass dichroic mirror (FF650-Di01-25x36, Semrock), and long-pass emission filter (HQ665LP, Chroma). The intensity at the sample was ~0.6 kW/cm2. Samples were detected by a 100x oil-immersion objective lens (NA = 1.40) with 1.6x additional zoom and collected by an Andor iXon Ultra 897 EMCCD camera.

4.2.4 Relaxation experiments

Single molecule relaxation experiments are conducted using the flow cell described in Section 4.2.2. A small amount of biotin-terminated linear DNA (same backbone length as branched DNA) is added as a reference. Tracer molecules are also added to the imaging buffer to monitor fluid

drift within the system; videos are discarded when drift is observed. Surface-tethered samples are stretched under strong flow, and videos are acquired during and following the cessation of flow. Multiple stretch-relax cycles are collected for each molecule; stretch-relax cycles are averaged for each molecule.

4.3 RESULTS AND DISCUSSION

4.3.1 Molecular Properties of DNA Comb Polymers

The hybrid enzymatic-synthetic approach described in Chapter 3 allows for precise control over backbone and branch molecular weights. Moreover, branch grafting density can be controlled in an average sense by tuning the relative stoichiometry of side branches during the 'graft-onto' reaction. We use single molecule fluorescence microscopy (SMFM) to directly observe branched polymers with different architectures and contour lengths. In this way, branch grafting densities and distributions are directly characterized using SMFM, which reveals polymer topologies including three-arm stars (1 branch), H-polymers (2 branches), and comb polymers (>2 branches). Branched DNA polymers are labeled with fluorescent nucleic acid dyes such as SYTOX Green or YOYO-1, thereby yielding either single-color polymers or dual-color DNA polymers in cases where branches are covalently labeled with Cy5 (red) dye and backbones are labeled with an intercalating dye (green). This approach allows for simultaneous visualization of branch and backbone dynamics using SMFM.

In these experiments, polymer molecules are specifically linked to a passivated surface by tethering one terminus of the polymer backbone to a functionalized glass coverslip coated with a mixture of polyethylene glycol (PEG) and PEG-biotin (**Figure 4.1**) [31]. PEG-biotin coverslips

are first incubated with NeutrAvidin, copiously rinsed with water, and then used to construct a custom microfluidic flow cell by affixing together with a quartz microscope slide. Buffer exchange into the flow cell is achieved using polyethylene tubing epoxied into inlet/outlet ports drilled through the glass slide. To facilitate specific tethering to the glass coverslip surface, linear and branched DNA are labeled with a biotin moiety at one terminus of the chain. Branched DNA polymers are incubated in the flow cell at a concentration of 10-40 pM, thereby generating a uniform field of single polymers via specific surface tethering. Polymer chains are stretched in pressure-driven flow using a viscous buffer (62.5% or 65% sucrose, yielding 70 or 130 cP solution viscosity, respectively) containing the nucleic acid stain SYTOX Green.

A composite image of dual-color DNA combs stretched under fluid flow is shown in **Figure 4.2**. Comb polymers are clearly indicated by the presence of Cy5-labeled side branches (red) co-localized along DNA backbones (green). Composite dual-color images can be deconstructed to identify SYTOX Green-stained backbones (488/503 nm, excitation/emission peaks) and Cy5-labeled branches (638/670 nm, excitation/emission peaks). Using this approach, we measured the molecular properties of DNA comb polymers, including the distributions of grafted branches and flow-stretched end-to-end distances of DNA backbones.

Single molecule length distributions. The average backbone end-to-end distances for branched polymers in flow are shown in **Figure 4.3**, where dotted lines indicate the expected extension of molecules in strong flows ($x/L \approx 0.8$ for $100 < Wi < 300$, where Wi is Weissenberg number) [32]. Interestingly, the average end-to-end backbone distance is fairly constant for polymers with identical backbone lengths but variable branch grafting densities in strong shear flow.

Distributions of molecular end-to-end distance are shown in **Figure 4.4**. Molecules are binned by measured lengths of 200 nm. A dotted line indicates the molecules' expected contour length in the presence of an intercalating dye, which increases the unstained contour length by a factor of ~1.3 ($L_{10k,\ unstained} \approx 3.3$ μm, $L_{10k,\ stained} \approx 4.3$ μm, $L_{20k,\ unstained} \approx 6.7$ μm, $L_{20k,\ stained} \approx 8.6$ μm). A small fraction (<25%) of the branched polymers excluded from these data showed apparent end-to-end distances <70% of the expected contour length, which can be attributed to photocleavage during laser excitation or shearing of macromolecular structures during handling.

Calculations using the distributions indicate sample dispersities ($Đ = M_w/M_n$) between 1.02 and 1.03. Weight-average molecular weight M_w and number-average molecular weight M_n were calculated using the definitions $M_w = \Sigma_i i n_i M_i$ and $M_n = \Sigma_i x_i M_i$, where i is an estimated degree of polymerization (DOP) based on bins shown in **Figure 4.4**, n_i is the number of molecules with DOP i, M_i is the theoretical molecular weight of a molecule of DOP i, and x_i is the mole fraction of molecules with DOP i.

Branch frequency distributions. SMFM allows for direct characterization of the molecular topology of branched DNA molecules over a wide range of conditions. In order to quantify the number of branches per backbone, surface-tethered DNA combs are illuminated by a red laser for several minutes; as illustrated in **Figure 4.5**. Cy5-labeled DNA branches are sufficiently bright for single molecule imaging, and branch distributions and related statistics determined from single molecule imaging experiments are shown in **Figure 4.6** and **Table 4.1**, respectively.

In most cases, a single branch can be identified as an isolated red 'spot' along the polymer backbone, given the relatively low grafting densities for the comb polymers prepared in this work. Nevertheless, it is possible that two branches could occupy the same diffraction-limited spot,

which could lead to undercounting. The contour length of a ~1 kbp DNA molecule is ~300 nm, so any single branch would appear as a diffraction-limited spot (~250 nm). The likelihood of two branches occupying the same diffraction-limited spot is generally low due to reaction stoichiometry, low grafting densities, and electrostatic and steric interactions. Moreover, the intrinsic photobleaching and photoblinking behavior of Cy5 further facilitates the observation and classification of individual branches [33]. By imaging single comb polymers until photobleaching, it is possible to resolve multi-step photobleaching trajectories from Cy5-labeled branches, thereby revealing the number of dyes per diffraction-limited spot.

From the histograms shown in **Figure 4.6**, it is clear that the overall degree of molecular branching increases upon increasing the ratio of branches to backbones in the reaction solution. The variance-to-mean ratio (VMR) of a distribution provides a measure of the degree of randomness or spread in the distribution of a process, in this case, graft-onto synthesis of DNA comb polymers via SPAAC. The VMR is defined as VMR = σ^2/μ using standard deviation σ and mean μ. As shown in **Table 4.1**, the branch VMR of each sample is less than 1, suggesting that branch addition does not follow a Poisson process. Non-zero VMRs also confirm the presence of distributions in branching, such that comb polymer samples do not exhibit uniform branching, as evidemt from the histograms in **Figure 4.6**. We note that VMRs decrease with increasing branch-to-backbone ratio. Because smaller VMR values indicate tighter distributions in a process, we infer that branch addition events are distributed more uniformly among molecules in samples with high graft densities than in samples with low graft densities.

Our single molecule data show that the average number of branches added per backbone is generally less than expected, assuming stoichiometric incorporation of chemically modified

DBCO-dUTP and addition of side branches during the ‘graft-onto’ reactions. In particular, we observe an average branch addition of <10 in all cases, however, the theoretical maximum incorporation of DBCO-dUTP in samples 10A, 10D, and 20A is 500, 1200, and 100, respectively. We hypothesize that the main source of this disparity lies in the discrimination of non-natural, chemically modified nucleotides against natural nucleotides during PCR of DNA backbones. Natural DNA polymerases exhibit an extremely high fidelity for natural nucleotides, and chemical modifications in non-natural bases are known to frustrate DNA polymerases during primer extension synthesis or in moving past a modified template region. [34, 35]. Evolved DNA polymerases can be used to preferentially incorporate non-natural bases [36]; however, such polymerases could be sensitive to the site of chemical modification on nucleotides and are generally less suitable for long-range PCR used in this work.

In general, we observe decreased PCR product yields upon substitution of chemically modified nucleotides, which can be overcome by modifying reaction conditions as described in Chapter 3. Incorporation of chemically modified DBCO-dUTP especially hinders efficient replication of higher molecular weight amplicons; for example, in long-range PCR synthesis of 20 and 30 kbp backbones, only 1% substitution of natural dTTP with 5-DBCO-dUTP is tolerated in the reaction under these conditions. In addition to PCR inefficiencies using non-natural bases, it is possible that steric hindrance and electrostatic repulsion results in decreased grafting densities, in particular, linking negatively-charged DNA branches onto DNA backbones during SPAAC reactions.

4.3.2 Topology-Controlled Relaxation of Single Branched Polymers

We used SMFM to directly observe the conformational relaxation dynamics of surface-tethered branched polymers. Here, we monitor the relaxation of branched polymers from high stretch

(>80% contour length) following cessation of flow, and we report the impact of branch number and position on the relaxation of branched polymers. In this particular experiment, we focus on branched polymers with 30 kbp backbones and 10 kbp branches using single-color fluorescence. The dimensions of these polymers permit visual counting of side branches as the molecules explore conformational space during relaxation processes. Importantly, these experiments highlight the ability to independently characterize branch and backbone behavior during a dynamic process for branched polymers.

A series of time-lapse images showing the relaxation process for a single surface-tethered branched polymer is shown in **Figure 4.7**. In addition, we provide a schematic illustrating the characteristic branched polymer topologies observed during this process and corresponding stages of relaxation based on quantitative visual analysis of molecular end-to-end distance (x). We note that the schematic and stages are specific to the molecular dimensions observed in this study, and that changes in branch and/or backbone sizes would subsequently change the observed relaxation processes.

Prior to cessation of shear flow (*Stage 0*), polymer molecules exist in a highly extended conformation. At short times following the cessation of flow (*Stage I*), both the backbone and the branches exhibit a simultaneous and rapid entropic response characterized by a sharp decrease in fractional extension with respect to time. At intermediate times in the relaxation process (*Stage II*), we observe mixed modes including branch and backbone relaxation dynamics, such that branches explore various conformational 'breathing modes' while the backbone relaxes. We expect mixing of relaxation modes for these molecular topologies, in which branches and backbones are similar in size. At longer times (*Stage III*), the longest mode of relaxation dominates,

which corresponds to relaxation of the main chain backbone for this specific molecular architecture, and polymer molecules ultimately appear as fluctuating random coils with non-linear topologies. These visual observations empirically suggest that two timescales govern the relaxation process, with the duration of *Stage II* related to the branch relaxation time and the duration of *Stage III* associated with the backbone relaxation time.

Molecular relaxation processes can be quantified by measuring the end-to-distance of the main chain backbone over time. Here, we plot fractional backbone extension (x/L) by normalizing the instantaneous chain extension by the backbone contour length ($L_{30k,\ stained}$ = 13.6 μm). Single molecule relaxation trajectories of linear reference polymers (30 kbp) are shown in **Figure 4.8**, where the bold line indicates the time-dependent ensemble average of fractional extension. Ensemble averages of branched DNA polymer relaxation are shown in **Figure 4.9**.

Interestingly, single molecule dynamics clearly show that relaxation processes are dependent on molecular topology. In particular, we observe slower chain relaxation for branched polymers (1, 2, or 3 side branches) compared to a linear reference polymer with identical backbone molecular weight. We quantify this relaxation process to further probe chain topology effects. The longest relaxation time (*Stage III*) is dominated by the slowest mode at relatively small fractional extensions (*e.g.*, $x/L < 0.30$). The longest relaxation time can be determined by fitting backbone relaxation data over this region to a Rouse-inspired single exponential decay: $(x/L)^2 = c_1 \exp(-t/\tau) + c_2$, where τ is the longest relaxation time of the linear polymer and c_1 and c_2 are fitting constants [32, 37, 38]. Due to the separation of timescales observed in **Figure 4.7** for the branch (10 kbp) and backbone (30 kbp) motions, we interpret this long-time relaxation as that of the backbone experiencing extra frictional drag due to fully relaxed side branches. Based on this

reasoning, we can determine the longest relaxation time of the comb polymer backbone using a single exponential fit between fractional extensions $0.14 < x/L < 0.30$, such that the low end of this range corresponds to distances over which backbone stretch can be accurately tracked using diffraction-limited fluorescence imaging. Using this approach, we determine longest relaxation times for linear polymers ($\tau_{linear,III} = 8.0 \pm 0.9$ s) and branched polymers with 1, 2, and 3 branches as $\tau_{1,III} = 8.0 \pm 0.9$ s, $\tau_{2,III} = 9.6 \pm 1.1$ s, and $\tau_{3,III} = 13.0 \pm 1.7$ s, respectively. **Figure 4.10** suggests that no other time constants emerge when the same data are fit to a multi-exponential decay, which further supports a single exponential decay function.

Comb polymer molecules with 3 side branches exhibit a significant increase in the longest relaxation time. However, the impact of 1 or 2 branches appears to be negligible in the context of the longest relaxation time, at least for this particular set of branch (10 kbp) and backbone (30 kbp) molecular weights. In order to further probe this effect, we also considered the intermediate relaxation timescale (*Stage II*). Based on multi-mode models for polymer dynamics in dilute solutions (*e.g.* Rouse model) [37, 38], we considered the possibility of multiple modes (*i.e.* multiple relaxation timescales) by fitting the relaxation data in the intermediate extension region ($0.30 < x/L < 0.50$) to a multi-exponential function. However, we found that these data were best fit to a single exponential decay with only a single time constant, which reveals a strong dependence of the relaxation time on the number of branches: $\tau_{linear,II} = 4.7 \pm 0.6$ s, $\tau_{1,II} = 4.2 \pm 0.6$ s, $\tau_{2,II} = 5.7 \pm 0.8$ s, and $\tau_{3,II} = 7.0 \pm 1.0$ s. Clearly, over these timescales, the presence of 2 or 3 branches slows intermediate relaxation processes.

In addition to branch grafting densities, our data also show that the position of the branch point along the main chain backbone has a direct impact on polymer relaxation. In **Figure 4.11**, we

consider several relaxation trajectories for molecules with a single branch located at different positions. Each curve indicates an ensemble of singly branched molecules wherein branch position is classified relative to the surface-tethered point (*e.g.*, branch point at first third of backbone near tether, middle third, and last third near the free end). Intermediate relaxation times reflect a strong dependence on branch position, such that we observe slower relaxation when a branch exists farther from the surface tether: τ_{tether} = 2.5 ± 0.5 s, τ_{mid} = 4.7 ± 0.5 s, and τ_{end} = 5.6 ± 1.0 s. Interestingly, polymers with 1 branch near the tether point appear to relax faster than the linear backbone counterparts ($\tau_{linear,II}$ = 4.8 ± 0.6 s); however, the longest relaxation times of these molecular ensembles show no significant differences compared to the linear reference polymer.

From these data, we consider two related effects on the (*Stage II*) relaxation of the branch as it pertains to the backbone relaxation probed by the flow cessation experiments. First, we hypothesize the existence of a new relaxation mode spanning from the tether point to the end of the branch. When the branch point is positioned near the end of the polymer backbone, then this mode is likely more dominant than the primary mode along the main chain backbone. In this case, the relaxation of the comb polymer backbone is slower than that of a linear chain. Second, we hypothesize the importance of hydrodynamic flow fields induced by branch relaxations. When the branch point is positioned near the tether point, the aforementioned branch-based relaxation mode induces a local fluid flow more strongly than the slowly relaxing backbone. We postulate that the branch hydrodynamically drives the relaxation of the main chain near the tether point, which can result in a more rapid relaxation of the comb polymer backbone than that of a linear chain. More elaborate branch-wall hydrodynamic coupling could be possible, similar to effects important for linear chains near surfaces [39-41]. From a broader perspective, it is important to note that these

branch effects can only be observed using single molecule experiments that can resolve branch position along a polymer chain backbone.

4.4 CONCLUSIONS

In summary, we report the direct observation of topology-controlled relaxation dynamics of branched DNA polymers. Using this approach, our work extends single polymer investigations to a new class of polymers with non-linear branched topologies. In particular, our data reveal the influence of branch grafting distributions on polymer relaxation dynamics. We observe that the relaxation of a surface-tethered polymer with 1 branch depends strongly on branch position; we also observe that surface-tethered polymers with at least 2 branches relax more slowly than linear polymers. Our results motivate intriguing questions for further study, including an investigation of the relaxation modes within a branched polymer and the dynamic stretching behavior of single branched polymers in free-solution flows.

From a broader perspective, the versatility of the synthetic approach described in Chapter 3 enables a broad design space for branched polymer synthesis for single molecule studies. For example, long-range PCR can readily yield chemically modified branch and backbone molecules approaching 50 kbp [42]. The application of SMFM to this design space enables in-depth studies of single molecule dynamics of branched polymers. In this way, experimental work with these polymers will enable a fundamental molecular-based understanding of the non-equilibrium dynamics of branched polymers.

4.5 FIGURES AND TABLES

Table 4.1. Molecular properties of branched DNA polymers

Sample	Backbone length (kbp)	Branch length (bp)	Substitution of dTTP (%)†	Molar excess of branches‡	Number of branches*	Branch VMR
10 Linear	10	--	0	0	--	--
10 A	10	951	10.	5	2.0 ± 1.3	0.79
10 B	10	951	10.	10	3.4 ± 1.3	0.51
10 C	10	951	10.	20	5.1 ± 1.0	0.21
10 D	10	951	25	50	7.3 ± 1.2	0.19
20 Linear	20	--	0	0	--	--
20 A	20	951	1.0	10	3.8 ± 1.7	0.72
20 B	20	951	1.0	20	4.6 ± 1.5	0.51
20 C	20	951	1.0	50	5.4 ± 1.6	0.49
20 D	20	951	1.0	100	7.4 ± 1.7	0.39
30 Linear	30	--	0	0	--	--
30 Branched	30	10,052	1.0	15	1.5 ± 0.7	--

†Percentage of dTTP nucleotide replaced by 5-dUTP-DBCO during PCR to generate DNA backbones; ‡molar excess of branch molecules in comparison to backbone molecules in SPAAC graft-onto reactions; *mean ± standard deviation. These measurements exclude molecules of stretched end-to-end distances less than 3 or 6 μm for 10 kbp or 20 kbp backbones, respectively. For all samples, the measurements are based on averages over $N > 100$ molecules, except for the 30 kbp branched sample ($N = 45$).

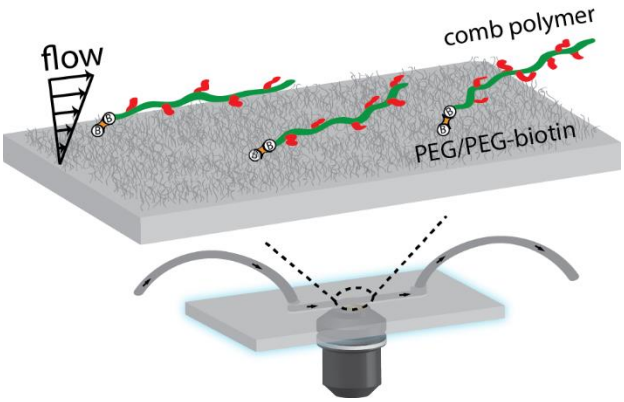

Figure 4.1. Schematic of experimental setup showing surface chemistry and custom-built microfluidic flow cell. Glass coverslips are functionalized with a mixture of PEG/PEG-biotin and NeutrAvidin prior to tethering linear or comb-shaped DNA via a terminal biotin moiety.

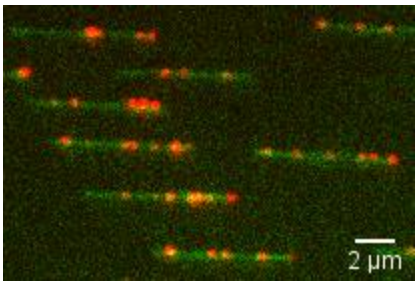

Figure 4.2. Single molecule image of dual-color DNA comb polymers tethered to a surface and stretched under shear flow. Composite image generated by co-localization of SYTOX Green-stained backbones and branches (green) and Cy5-labeled branches (red).

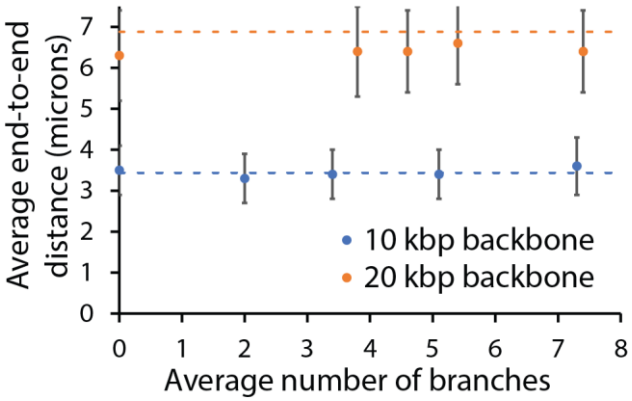

Figure 4.3. Average backbone end-to-end distances for DNA comb polymers stretched under fluid flow; error bars reflect standard deviation. Dotted lines indicate the expected extension of linear DNA molecules stretched under tethered shear flow with a flow strength of $100 < Wi < 300$ [32].

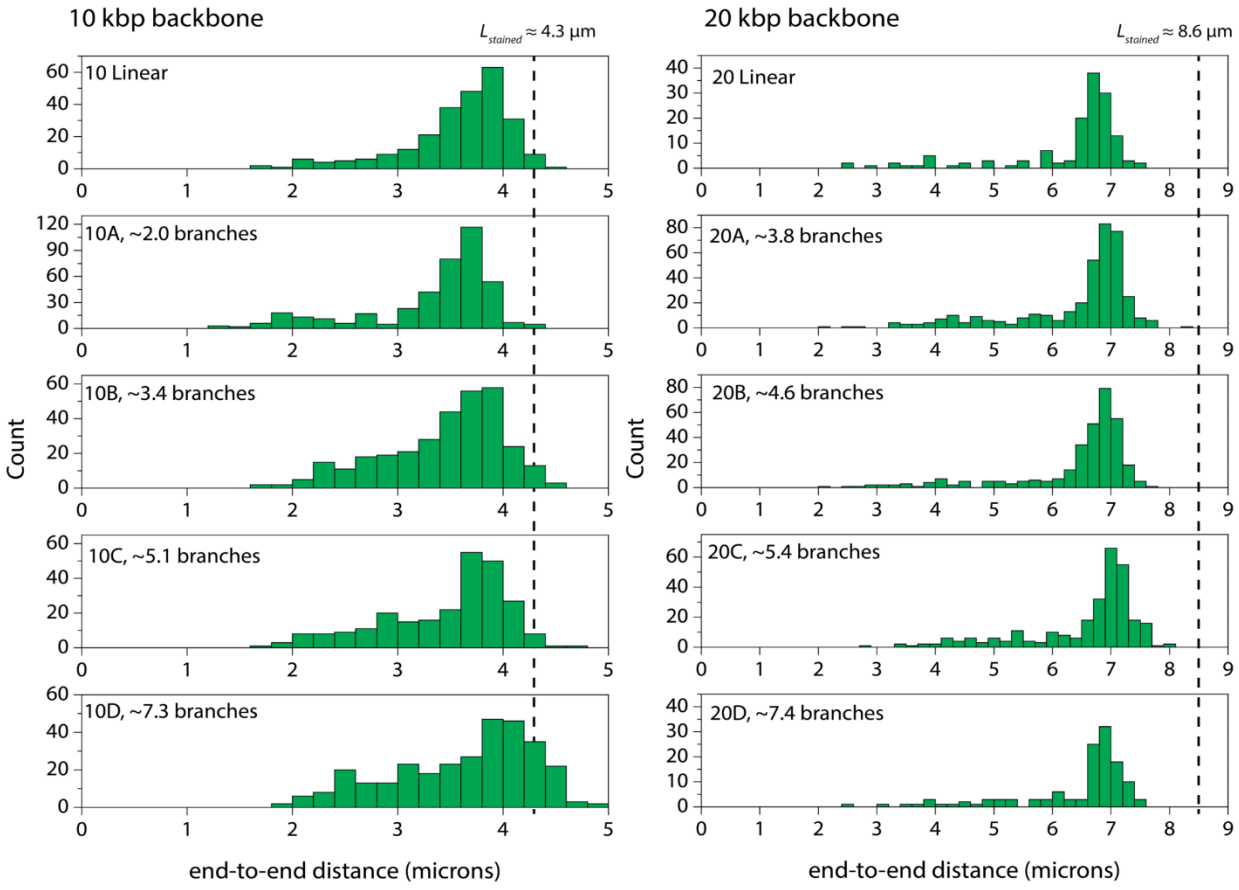

Figure 4.4. Distribution of backbone end-to-end distances for linear and branched DNA polymers stretched under fluid flow, as determined by single molecule experiments described in **Table 4.1**. The dotted line indicates the expected contour length in the presence of an intercalating dye.

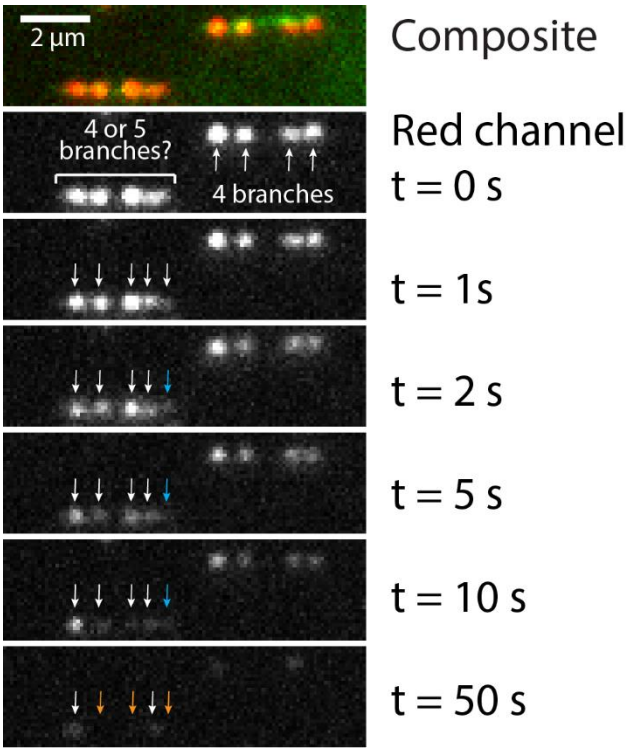

Figure 4.5. Time lapse of images acquired for branch counting. A 'photoblinking' event is observed between 2 and 10 seconds (blue arrows), and 'photobleaching' events are shown after 50 seconds (orange arrows).

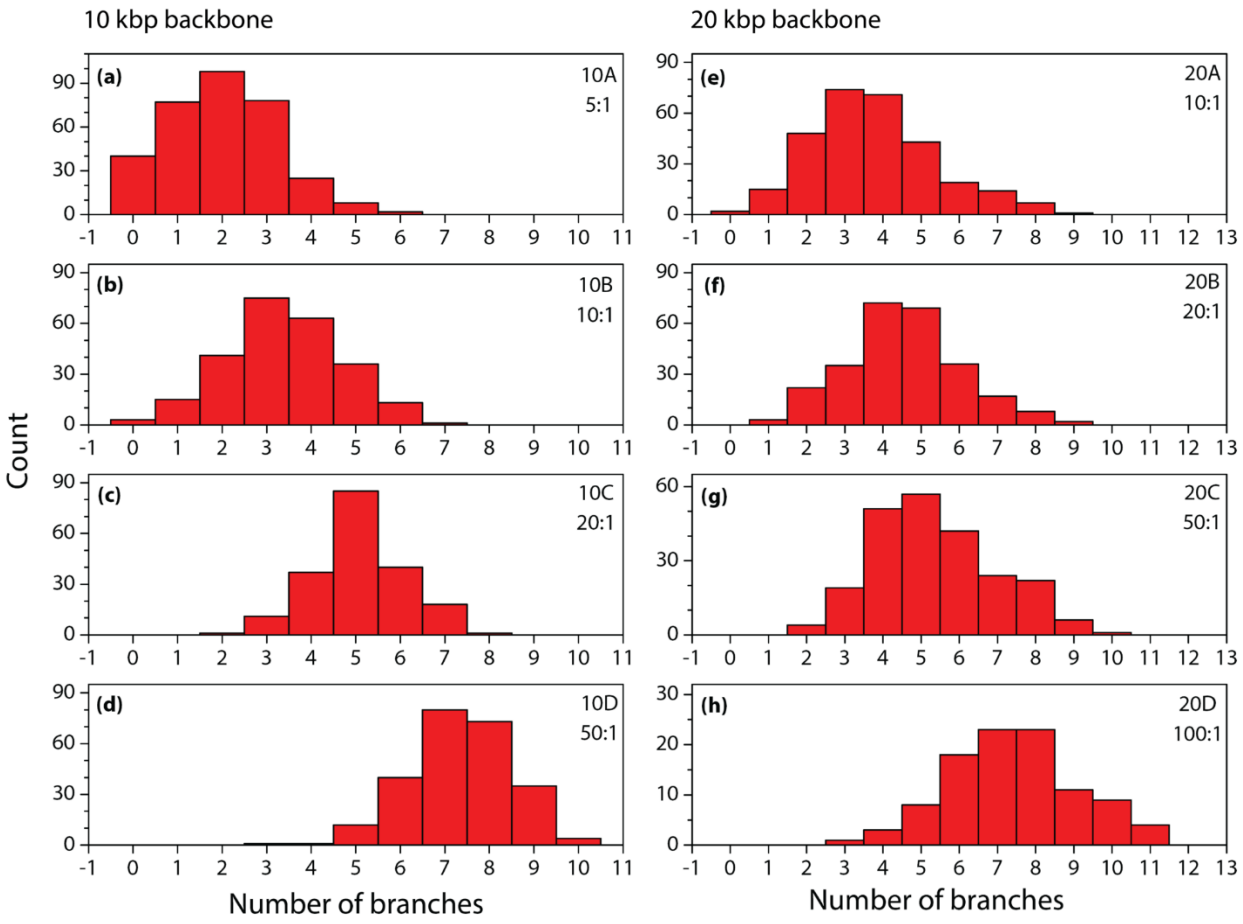

Figure 4.6. Branch frequency distributions for dual-color DNA combs described in **Table 4.1**. (a)-(d) represent samples with backbone length of 10 kbp and end-to-end length greater than 3 μm, and (e)-(h) represent samples with backbone length of 20 kbp and end-to-end length greater than 6 μm. In all cases, larger molar excesses of branch molecules compared to backbone molecules results in higher branching frequencies.

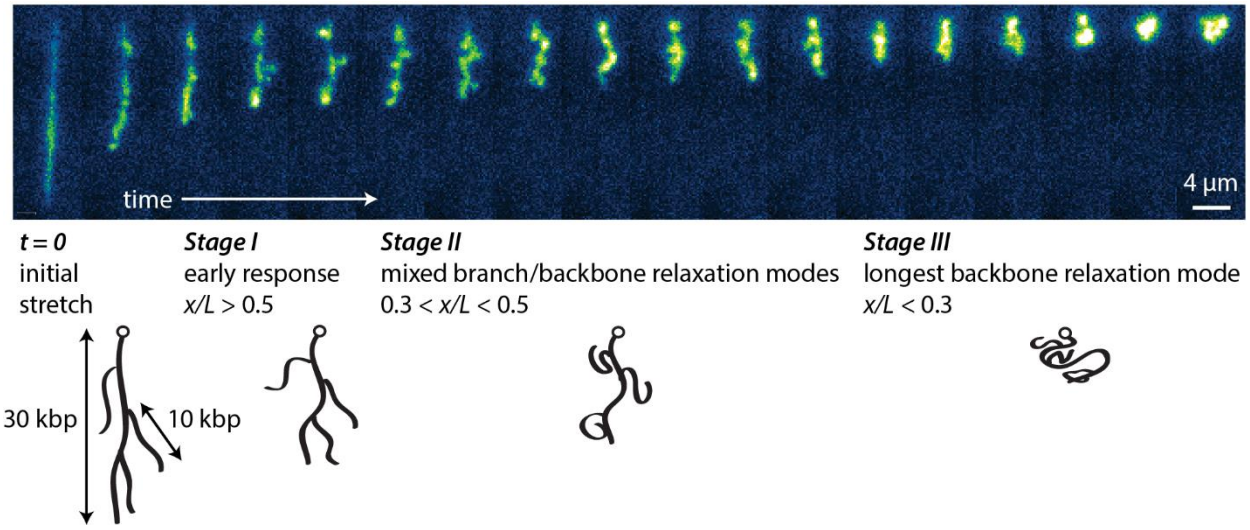

Figure 4.7. Relaxation dynamics of surface-tethered branched polymer molecules (solvent viscosity $\eta \approx 125$ cP). Time lapse images showing relaxation of a 30 kbp comb polymer with 10 kbp branches after the cessation of shear flow, with corresponding schematic of relaxation mechanisms. Images taken 2.5 seconds apart.

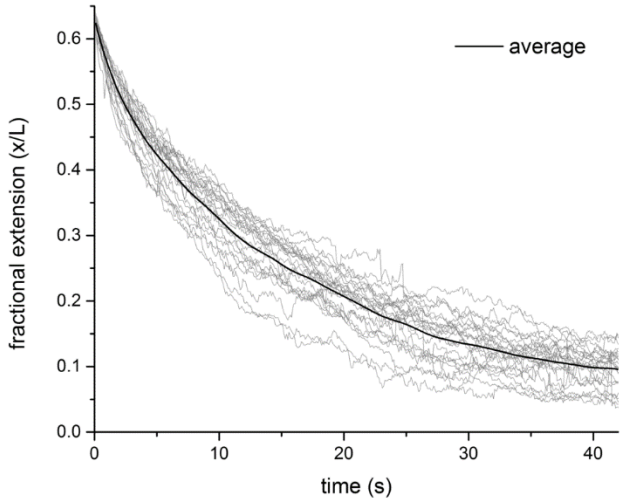

Figure 4.8. Relaxation of surface-tethered linear polymers ($\eta \approx 125$ cP). Single molecule relaxation trajectories are shown in gray, and the bold line indicates the time-dependent ensemble average of fractional extension.

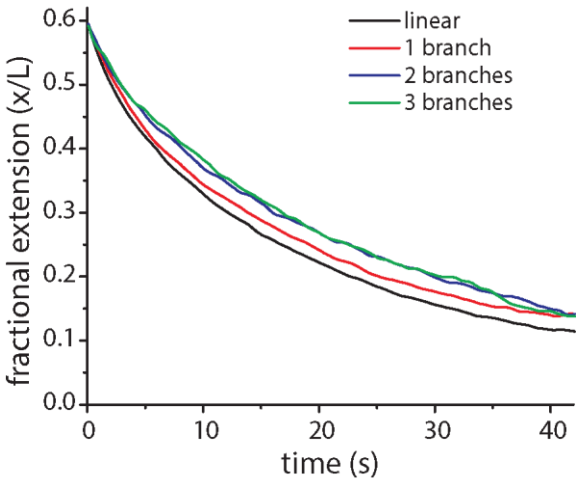

Figure 4.9. Ensemble-averaged time-dependent fractional extension of molecules with varying degrees of branching indicate that relaxation processes are dependent on molecular topology. Branched polymers exhibit slower chain relaxation compared to a linear reference polymer with identical backbone molecular weight.

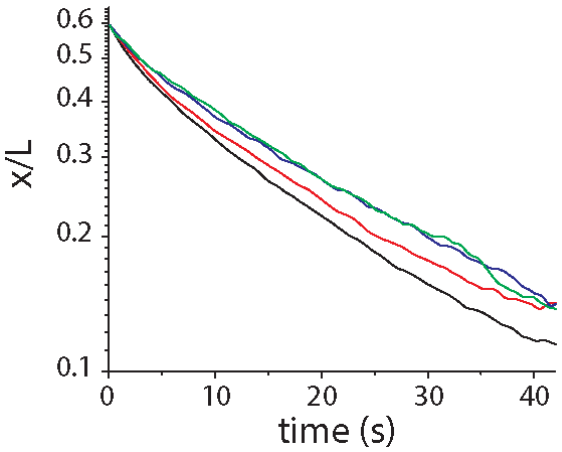

Figure 4.10. Semi-log representation of the time-dependent fractional extension of single branched and linear polymers during relaxation. These data are identical to those shown in **Figure 4.9**. This representation suggests that no other time constants emerge upon fitting to a multi-exponential decay, thereby supporting the use of a single exponential decay function to determine relaxation times.

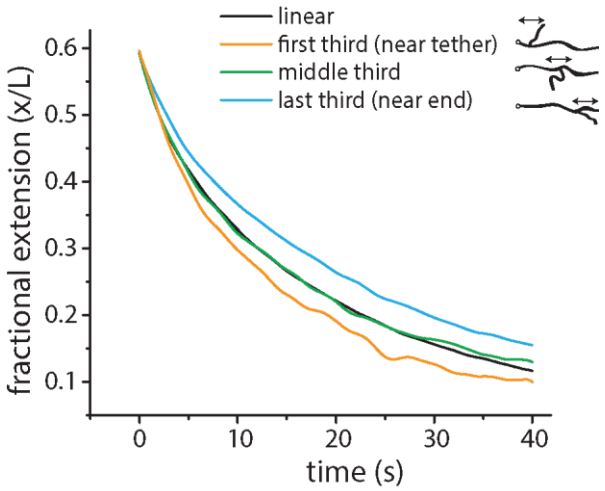

Figure 4.11. Ensemble-averaged relaxation trajectories for molecules with a single branch, where the branch position varies along a main chain. While polymers with a branch near the tether point appear to relax faster than the linear backbone counterparts, the longest relaxation times of these molecular ensembles show no significant differences compared to the linear reference polymer.

4.6 REFERENCES

[1] Dealy JM, Larson RG. Structure and Rheology of Molten Polymers. Cincinnati, OH: Hanser Publications; 2006.

[2] Zimm BH, Kilb RW. Dynamics of branched polymer molecules in dilute solution. Journal of Polymer Science. 1959;37:19-42.

[3] Larson RG. The Structure and Rheology of Complex Fluids. New York: Oxford University Press; 1998.

[4] Bovey FA, Schilling FC, McCrackin FL, Wagner HL. Short-Chain and Long-Chain Branching in Low-Density Polyethylene. Macromolecules. 1976;9:76-80.

[5] Voit BI, Lederer A. Hyperbranched and Highly Branched Polymer Architectures—Synthetic Strategies and Major Characterization Aspects. Chemical Reviews. 2009;109:5924-73.

[6] Snijkers F, Ratkanthwar K, Vlassopoulos D, Hadjichristidis N. Viscoelasticity, Nonlinear Shear Start-up, and Relaxation of Entangled Star Polymers. Macromolecules. 2013;46:5702-13.

[7] van Ruymbeke E, Lee H, Chang T, Nikopoulou A, Hadjichristidis N, Snijkers F, et al. Molecular rheology of branched polymers: decoding and exploring the role of architectural dispersity through a synergy of anionic synthesis, interaction chromatography, rheometry and modeling. Soft matter. 2014.

[8] Lentzakis H, Vlassopoulos D, Read D, Lee H, Chang T, Driva P, et al. Uniaxial extensional rheology of well-characterized comb polymers. Journal of Rheology (1978-present). 2013;57:605-25.

[9] Larson RG. Predicting the Flow of Real Polymers. Science. 2011;333:1834-5.

[10] Chen B, van der Poll DG, Jerger K, Floyd WC, Fréchet JMJ, Szoka FC. Synthesis and Properties of Star-Comb Polymers and Their Doxorubicin Conjugates. Bioconjugate Chemistry. 2011;22:617-24.

[11] Chen B, Jerger K, Fréchet JMJ, Szoka Jr FC. The influence of polymer topology on pharmacokinetics: Differences between cyclic and linear PEGylated poly(acrylic acid) comb polymers. Journal of Controlled Release. 2009;140:203-9.

[12] Chen Y, Thorn M, Christensen S, Versek C, Poe A, Hayward RC, et al. Enhancement of anhydrous proton transport by supramolecular nanochannels in comb polymers. Nat Chem. 2010;2:503-8.

[13] de Vos WM, Leermakers FAM, Lindhoud S, Prescott SW. Modeling the Structure and Antifouling Properties of a Polymer Brush of Grafted Comb-Polymers. Macromolecules. 2011;44:2334-42.

[14] Chambon P, Fernyhough CM, Im K, Chang T, Das C, Embery J, et al. Synthesis, Temperature Gradient Interaction Chromatography, and Rheology of Entangled Styrene Comb Polymers. Macromolecules. 2008;41:5869-75.

[15] Kapnistos M, Vlassopoulos D, Roovers J, Leal LG. Linear Rheology of Architecturally Complex Macromolecules: Comb Polymers with Linear Backbones. Macromolecules. 2005;38:7852-62.

[16] Daniels DR, McLeish TCB, Crosby BJ, Young RN, Fernyhough CM. Molecular Rheology of Comb Polymer Melts. 1. Linear Viscoelastic Response. Macromolecules. 2001;34:7025-33.

[17] Kapnistos M, Kirkwood KM, Ramirez J, Vlassopoulos D, Leal LG. Nonlinear rheology of model comb polymers. Journal of Rheology (1978-present). 2009;53:1133-53.

[18] Snijkers F, van Ruymbeke E, Kim P, Lee H, Nikopoulou A, Chang T, et al. Architectural Dispersity in Model Branched Polymers: Analysis and Rheological Consequences. Macromolecules. 2011;44:8631-43.

[19] McLeish TCB. Tube theory of entangled polymer dynamics. Advances in Physics. 2002;51:1379-527.

[20] McLeish TCB, Larson RG. Molecular constitutive equations for a class of branched polymers: The pom-pom polymer. Journal of Rheology (1978-present). 1998;42:81-110.

[21] Lentzakis H, Das C, Vlassopoulos D, Read DJ. Pom-pom-like constitutive equations for comb polymers. Journal of Rheology (1978-present). 2014;58:1855-75.

[22] Mai DJ, Brockman C, Schroeder CM. Microfluidic systems for single DNA dynamics. Soft matter. 2012;8:10560-72.

[23] Marciel AB, Schroeder CM. New directions in single polymer dynamics. Journal of Polymer Science Part B: Polymer Physics. 2013;51:556-66.

[24] Shaqfeh ESG. The dynamics of single-molecule DNA in flow. Journal of Non-Newtonian Fluid Mechanics. 2005;130:1-28.

[25] Latinwo F, Schroeder CM. Model systems for single molecule polymer dynamics. Soft Matter. 2011;7:7907-13.

[26] Brockman C, Kim SJ, Schroeder CM. Direct observation of single flexible polymers using single stranded DNA. Soft matter. 2011;7:8005-12.

[27] Perkins TT, Smith DE, Chu S. Single Polymer Dynamics in an Elongational Flow. Science. 1997;276:2016-21.

[28] Schroeder CM, Babcock HP, Shaqfeh ES, Chu S. Observation of polymer conformation hysteresis in extensional flow. Science. 2003;301:1515-9.

[29] Heuer DM, Saha S, Archer LA. Electrophoretic dynamics of large DNA stars in polymer solutions and gels. ELECTROPHORESIS. 2003;24:3314-22.

[30] Saha S, Heuer DM, Archer LA. Electrophoretic mobility of linear and star-branched DNA in semidilute polymer solutions. ELECTROPHORESIS. 2006;27:3181-94.

[31] Selvin PR, Ha T. Single-molecule techniques: a laboratory manual. Cold Spring Harbor, New York: Cold Spring Harbor Laboratory Press; 2008.

[32] Ladoux B, Doyle PS. Stretching tethered DNA chains in shear flow. Europhys Lett. 2000;52:511-7.

[33] Bates M, Huang B, Dempsey GT, Zhuang X. Multicolor Super-Resolution Imaging with Photo-Switchable Fluorescent Probes. Science. 2007;317:1749-53.

[34] Augustin MA, Ankenbauer W, Angerer B. Progress towards single-molecule sequencing: enzymatic synthesis of nucleotide-specifically labeled DNA. Journal of Biotechnology. 2001;86:289-301.

[35] Zhu Z, Waggoner AS. Molecular mechanism controlling the incorporation of fluorescent nucleotides into DNA by PCR. Cytometry. 1997;28:206-11.

[36] Ramsay N, Jemth A-S, Brown A, Crampton N, Dear P, Holliger P. CyDNA: Synthesis and Replication of Highly Cy-Dye Substituted DNA by an Evolved Polymerase. Journal of the American Chemical Society. 2010;132:5096-104.

[37] Doi M, Edwards SF. The theory of polymer dynamics. Oxford Oxfordshire

New York: Clarendon Press ;

Oxford University Press; 1986.

[38] Rouse PE. A Theory of the Linear Viscoelastic Properties of Dilute Solutions of Coiling Polymers. J Chem Phys. 1953;21:1272-80.

[39] Brenner H. The Slow Motion of a Sphere through a Viscous Fluid Towards a Plane Surface. Chem Eng Sci. 1961;16:242-51.

[40] Ma HB, Graham MD. Theory of shear-induced migration in dilute polymer solutions near solid boundaries. Phys Fluids. 2005;17.

[41] Sing CE, Alexander-Katz A. Theory of Tethered Polymers in Shear Flow: The Strong Stretching Limit. Macromolecules. 2011;44:9020-8.

[42] Fuller DN, Gemmen GJ, Rickgauer JP, Dupont A, Millin R, Recouvreux P, et al. A general method for manipulating DNA sequences from any organism with optical tweezers. Nucleic Acids Research. 2006;34:e15.

5 SINGLE MOLECULE DYNAMICS OF COMB POLYMERS

5.1 INTRODUCTION

The increasing prevalence of branched polymers in commercial applications has drawn recent and broad interest toward understanding the impact of molecular structure on physical behavior [1-3]. Comb and brush polymers, which consist of a main polymer backbone with grafted side chains, are chemically versatile and attractive for applications ranging from drug delivery [4, 5] to supramolecular nanocomposites [6] to desalination membranes [7]. Comb polymers exhibit rich rheological behaviors compared to their linear counterparts [1-3]. This behavior includes distinct linear viscoelastic signatures [8-12], nonlinear relaxation of stress following a step strain [13, 14], stress overshoots in the startup of shear flow [15, 16], and enhanced strain hardening in uniaxial extensional flow [17, 18].

Interestingly, comb polymers exhibit both shear thinning and strain hardening behaviors, which seem contradictory but result in favorable processing behaviors in comparison to their linear analogues [3, 19]. Shear thinning refers to the decrease in a complex fluid's viscosity η upon increasing the steady shear rate $\dot{\gamma}$ [2]. Shear-thinning materials can pass through an extruder easily by becoming more liquid-like at high shear rates [3, 19]. While most polymeric melts exhibit shear-thinning behavior, the onset of shear thinning occurs at lower strain rates for branched polymers than for linear polymers of identical molecular weight [20].

In extensional flows, polymer architecture plays a different role in material response. Here, the response of a material to transient uniaxial extensional flow can be described by a tensile-stress growth coefficient η_E^+, defined according to Eq. 5.1 [3],

$$\eta_E^+ \equiv \sigma_E/\dot{\varepsilon} \qquad (5.1)$$

where σ_E is the net tensile stress, which is a function of time and extensional strain rate $\dot{\varepsilon}$. The linear response is defined by the limit of η_E^+ as $\dot{\varepsilon}$ approaches zero. Strain hardening refers to deviations in η_E^+ from the linear response at finite $\dot{\varepsilon}$. Strain hardening of polymeric materials enables the stabilization of films and fibers during extensional flow-dominated processes [19]. Comb polymers exhibit strain hardening behavior at lower strain rates than linear polymers; this behavior is enhanced as the length of a side branch increases [17, 18].

We note that shear thinning describes steady-state behavior in shear flow, whereas strain hardening is a dynamic process occurring at the start-up of extensional flow. From a molecular perspective, the contribution of branches to the physical underpinnings of both phenomena remain unclear.

Recent advances in comb synthesis and purification have enabled detailed probes of the rheological response of model branched polymers [16-18, 21, 22]. These studies reveal dramatic effects of molecular-scale architectural defects on bulk rheological measurements. In this way, slight changes in local connectivity vastly impact global material response. Although bulk-scale rheological measurements enable orders of magnitude of measurement in the time and space domains, these techniques lack direct visualization of physical phenomena at the molecular level.

In this Chapter, we report the direct observation of comb polymer dynamics in planar extensional flow. After synthesis and purification of DNA comb polymers, we utilize microfluidic devices to stretch single comb polymer molecules in planar extensional flow. Planar extensional flow is a strong flow analogous to uniaxial extensional flow used to study the strain-hardening behavior of polymer melts. Our experimental platform enables simultaneous visualization of polymer

backbones and branches during steady-state extension and transient stretch in the startup of extensional flow.

5.2 MATERIALS AND METHODS

5.2.1 Synthesis and preparation of DNA for single molecule imaging

DNA comb polymers are synthesized as described in Chapter 3. In this Chapter, combs consist of either 30 kbp backbones with 951 bp branches, 40 kbp backbones with 951 bp branches, or 40 kbp backbones with 2200 bp branches. All branches are labeled with Cy5. Bulk absorbance measurements determined that 951 bp branches contain 7-8 dyes/branch and 2200 bp branches contain 14-16 dyes/branch. Linear DNA templates (30 kbp template, 40 kbp template, or λ-phage DNA) are also utilized as references to evaluate the impact of branching on dynamics.

DNA polymers are fluorescently labeled by incubation with YOYO-1 (Invitrogen) at a dye-to-base-pair ratio of 1:4 in an aqueous incubation buffer (30 mM Tris, pH 8.0, 5 mM NaCl, 2 mM EDTA) for at least 1 hour in the dark. Viscous imaging buffers (50–60 wt% sucrose, 30 mM Tris, pH 8.0, 5 mM NaCl, 2 mM EDTA) are mixed with an oxygen scavenging system and a reducing agent to minimize photobleaching, consisting of glucose (5 mg/mL), glucose oxidase (0.3 mg/mL), catalase (0.3 mg/mL), and β-mercaptoethanol (150 mM). In some studies, the small-molecule photostabilizer Trolox is added to the imaging buffer in excess of its solubility limit (4 mM) at 4 °C overnight, followed by syringe filtering (0.2 μm, PALL Acrodisc) to remove excess trolox prior to mixing with labeled DNA. Labeled DNA and imaging buffers are rotationally mixed for 30 minutes prior to injection into a microfluidic device.

5.2.2 Fabrication and characterization of microfluidic hydrodynamic trap

A two-layer, microfluidic cross-slot device is fabricated using standard soft-lithography techniques [23-25]. Schematics of this device are shown in **Figure 5.1**. Master molds are patterned on silicon wafers using photomasks (3600 dpi, Delta Graphics) and SU-8 photoresist (Microchem). The resulting feature heights range from 80–100 μm, and molds are coated with trichloro(1H,1H,2H,2H-perfluorooctyl)silane (Sigma-Aldrich) by vapor deposition to prevent delamination during subsequent fabrication steps. Polydimethylsiloxane (PDMS, RTV615, Momentive) is mixed at 15:1 or 5:1 resin to crosslinker ratios to cast fluidic and control layers, respectively. For the fluidic layer, uncured PDMS is deposited by spin-coating such that the PDMS thickness exceeds the feature height by ~20 μm. For the control layer, PDMS is cast directly onto the silicon wafer to form a ~5 mm slab. Both layers are partially cured at 65 °C for 20-30 minutes. After curing, the control layer slab is removed from the master and an inlet port is formed by punching a hole using a 21 gauge luer stub. The control layer is aligned with the fluidic layer and the two layers are cured for at least 2 additional hours. Once both layers are fully cured, the entire slab is removed from the fluidic layer master and inlet and outlet ports are formed for the fluidic layer. Each PDMS device is trimmed to fit a glass coverslip and bonded to a coverslip after oxygen plasma cleaning.

Pressure-driven flow is used to drive fluid through the PDMS device, generating a planar extensional flow field near the center of the cross slot (Eqs. 5.2 and 5.3, **Figure 5.1**), where v_x is velocity in the x direction, v_y is fluid velocity in the y direction, and $\dot{\varepsilon}$ is the fluid strain rate.

$$v_x = -\dot{\varepsilon}x \tag{5.2}$$

$$v_y = \dot{\varepsilon}y \tag{5.3}$$

The *y*-coordinate of the stagnation point is modified by actuating the fluid pressure in the valve layer (**Figure 5.1**), and automated feedback control is implemented between the imaging platform and valve pressure transducer to enable hydrodynamic "trapping" of single molecules near the stagnation point [25, 26].

Fluid strain rates are measured via particle imaging velocimetry using 0.84 μm fluorescent beads (Spherotech) as tracer particles. Bead trajectories are imaged using a CCD camera (AVT Stingray) and analyzed in MATLAB. Strain rates are characterized as a function of fluid pressure and device height.

5.2.3 Fluorescence microscopy

Single molecule experiments are carried out on an inverted epifluorescence microscope (Olympus IX-71) with a 100× oil-immersion objective lens (NA = 1.40) and 1.6× additional zoom lens. DNA comb polymers are imaged by excitation with a 488 nm laser (50 mW, SpectraPhysics Excelsior Laser) and/or a 637 nm laser (140 mW, Coherent OBIS Laser). The 488 nm optical path includes absorptive neutral density filters (Thorlabs), a 488 nm long-pass dichroic mirror (ZT488rdc, Chroma), and a long-pass emission filter (BLP01-488R-25, Semrock). The intensity at the sample is ~0.1 kW/cm^2. The 637 nm optical path includes an absorptive neutral density filter (ThorLabs), 650 nm long-pass dichroic mirror (FF650-Di01-25x36, Semrock), and long-pass emission filter (HQ665LP, Chroma). The intensity at the sample is ~0.6 kW/cm^2.

For simultaneous two-color YOYO-1/Cy5 imaging, the 488 nm and 637 nm optical paths are modified to include a dual-band dichroic mirror (FF500/646-Di01-25x36, Semrock) and a DualView DV2 beamsplitter apparatus with a 630 nm dichroic cube (MS-630LDX-1826,

Photometrics). The short wavelength channel is passed through a band pass emission filter (FF01-550/88, Semrock), and the long wavelength channel is passed through band-pass (HQ700/75m, Chroma) and long-pass (HQ665LP, Chroma) emission filters. Relaxation and stretching dynamics of λ-DNA are imaged by excitation with a 488 nm laser and detection with an EMCCD camera.

5.3 RESULTS AND DISCUSSION

5.3.1 Effect of the photostabilizing agent Trolox on DNA

Trolox (TX) has garnered widespread use as a photostabilizing agent in single molecule fluorescence imaging due to its ability to suppress dark states and triplet states of fluorescent dyes. [27-29] In particular, TX has been shown to improve the performance of Cy5, which is used to identify branches from backbones in DNA comb polymers. Despite the popularity of TX in single molecule fluorescence experiments, the role of its interactions with biomolecules such as DNA has not been fully characterized. Moreover, the commonly used DNA intercalating dye YOYO-1 is known to impact the physical properties of DNA, specifically increasing DNA contour lengths by ~30%. [30] Here, the impact on persistence length is less clear, with results arguing for no change or an increase in persistence length. [31] For these reasons, it is important to identify and understand potential interactions between TX, YOYO, and DNA. We utilize single molecule techniques to probe the use of TX as a photoprotectant for fluorescently labeled DNA combs (**Figures 5.3 and 5.4**) and evaluate the impact of TX on the physical properties of DNA (**Figure 5.5**).

Single molecule visualization of linear and branched DNA with TX. In a single molecule comparison of DNA combs in the absence and presence of TX, we observe the expected benefits

of TX-containing buffers on DNA. Specifically, we observe enhanced photostability, shown qualitatively in **Figure 5.3**, along with an overall reduction of photocleavage events. **Figure 5.4a** demonstrates dramatic quantitative improvements to the photostability of Cy5-labeled DNA combs in the presence of TX, whereas the impact of TX on YOYO-1 fluorescent dyes appears negligible from **Figure 5.4b**. These results suggest that TX-containing buffers will be advantageous in future studies of DNA with alternate dye systems to study unexplored conformational dynamics and complex polymer topologies. [32]

Relaxation and stretching dynamics of λ-phage DNA in the presence of TX. Using the microfluidic-based hydrodynamic trap, we compare the relaxation and steady-state extension behaviors of λ-DNA in the absence and presence of TX. Changes to the physical properties of DNA (*e.g.* contour length L_c) will change the relaxation time, which subsequently affects the quantitative characterization of polymer stretching in flow. In this way, relaxation time can be used as a measure of the impact of TX on contour length.

To measure the longest relaxation time τ_1, λ-DNA molecules are stretched to at least 50% of maximum extension in flow, followed by direct observation of chain relaxation upon flow cessation. Upon cessation of flow, the time-dependent maximum projected polymer extension $x(t)$ is fit to Eq. 5.4.

$$\left(\frac{\langle x(t)\rangle}{L_c}\right)^2 = A\exp\left(\frac{-t}{\tau_1}\right) + B \qquad (5.4)$$

where A and B are fitting constants. The fit is performed over the linear entropic force regime where $\langle x(t)\rangle/L_c < 0.3$. Assuming a contour length for YOYO-1 fluorescently labeled λ-DNA of 21.1 μm, we observe differences in DNA relaxation times in the absence ($\tau_1 = 4.1 \pm 0.3$ s, $N = 15$)

and presence (τ_1 = 3.5 ± 0.2 s, N = 25) of TX. Given the known scaling of longest polymer relaxation time with molecular weight ($\tau_1 \sim N^{3\nu}$), the contour length of λ-DNA in the presence of TX is estimated as 19.2 μm using Eq. 5.5 with scaling exponent 3ν = 1.64 [33].

$$N_{TX} = N_{YOYO}\left(\frac{\tau_{TX}}{\tau_{YOYO}}\right)^{\frac{1}{1.64}} \tag{5.5}$$

After characterizing the change in longest polymer relaxation time, we compare the steady-state extension behavior of λ-DNA in the absence and presence of Trolox in **Figure 5.5** by plotting extension as a function of Weissenberg number ($Wi = \dot{\varepsilon}\tau_1$), where $\dot{\varepsilon}$ is the fluid strain rate determined by particle imaging velocimetry. The raw steady-state extension behavior of labeled λ-DNA in the absence of Trolox (red circles) agrees with previous measurements by Perkins, *et al.* (black squares). [34] The inclusion of Trolox in the imaging buffer (blue triangles) results in a clear *decrease* in DNA extension compared to the Trolox-free buffer, consistent with the change in longest polymer relaxation time. To account for this decrease in extension, we normalize the data based on the estimated contour length of 19.2 μm. Plotting fractional extension (x/L_c) as a function of Wi shows consistent steady-state extension behavior across all experiments. In subsequent estimation of DNA contour lengths in TX-containing buffers, we apply a TX correction of $L_{c,TX} = 0.91 \times L_{c,YOYO}$.

5.3.2 Longest comb polymer relaxation time

The longest polymer relaxation time of comb polymers is determined as described in Section 5.3.1. The number of branches on a DNA comb polymer is determined during the period of high stretch. Comb polymers are divided into subsets with low branching (1-4 branches) and high branching (5

or more). Relaxation times of comb and linear polymers of varying molecular topologies are summarized in **Table 5.1**.

Generally, we observe slower relaxation behavior of branched polymers with increasing branch length and branch density, even in the presence of relatively short branches. This trend is shown in **Figure 5.6**, which includes the single-exponential decay functions based on ensemble averages of single molecule relaxation trajectories. Here, the samples have identical backbone molecular weights and are measured in solutions of equal viscosity (solvent viscosity η_s = 50 cP). These observations are consistent with the notion that larger molecules require more time to relax to an equilibrium conformation following high stretch. We note that linear and comb polymers in low-viscosity solutions ($\eta_s \lesssim 25$ cP) exhibit similar longest polymer relaxation times. It is possible that differences in polymer relaxation cannot be resolved given these specific experimental conditions and molecular topologies.

5.3.3 Stretching dynamics of comb polymers

Among non-equilibrium properties, one of particular importance is the existence of a coil-to-stretch transition (CST), which has been observed for linear polymers in extensional flows. [34-36]. In **Figure 5.7**, we compare the steady-state extension of linear and comb-shaped DNA polymers as a function of fluid strain rate $\dot{\varepsilon}$. Again, DNA combs are sorted by degree of branching. The data clearly show a CST for comb-shaped DNA, and the shapes of the curves are similar to that of linear DNA, especially in the case of low branching. In the case of high branching, the onset of stretching appears to occur at lower absolute flow strengths relative to linear DNA. This is perhaps not surprising due to the added friction of branches along a DNA backbone. Remarkably, the curves collapse upon normalization of the steady-extension curves by plotting these data as a

function of Weissenberg number *Wi*, which accounts for differences in longest backbone relaxation times between linear and comb polymers, as shown in **Figure 5.8**. Here, fractional extension is plotted as a function of *Wi*, thereby accounting for differences in the longest polymer relaxation time between architectures. We also compare the steady-state extension of linear and comb-shaped DNA to λ-DNA, and the steady-state stretching behavior appears consistent across these molecular weights and topologies.

We further characterize polymer dynamics during the transient stretching process by observing the extension and dynamic conformations of single molecules. To ensure a completely random initial state for each transient stretch, we allow the molecule to relax to an equilibrium configuration by waiting ~10 τ_1 between transient extension experiments.

In one experiment, we conducted a series of transient stretching experiments on linear templates (30 kbp), as well as combs with 30 kbp backbones and 951 bp branches. **Figure 5.9** shows trajectories of molecular extension as a function of accumulated strain $\varepsilon(t) = \dot{\varepsilon}t$ for linear polymers. Here, stretching trajectories are characterized based on flow strength, with $Wi = 1.7 \pm 0.2$ shown in orange and $Wi = 2.5 \pm 0.2$ shown in navy. Variations in *Wi* reflect the propagation of uncertainties from the longest polymer relaxation time τ_1 and the observation of molecules at varying *z*-positions within the microfluidic device. **Figure 5.10** includes a plot of strain rate as a function of device height and sample fluid pressure in the channel for this experiment. During data acquisition, the pressure and *z*-position of each stretching trajectory are accounted to enable later determination of $\dot{\varepsilon}$, *Wi*, and $\varepsilon(t)$.

Single molecule stretching trajectories of linear and comb polymers are compared in **Figure 5.11**. Comb polymers are sorted by degree of branching as described before. Trajectories are shown as

an ensemble (top), as well as by flow rate, such that $Wi \approx 1.7$ (middle) or $Wi \approx 2.5$ (bottom). The different values of the average longest backbone relaxation time τ_1 for each molecular subset are accounted for when sorting trajectories by Wi. In both linear and comb polymers, we observe the well-known phenomenon of molecular individualism, wherein molecules adopt a diverse set of conformations during transient stretch [34, 35]. In this set of trajectories, conformations are characterized as half dumbbells (black), dumbbells (blue), and folded (red). In some cases, molecules begin as coils and eventually unravel via folding trajectories; these molecules are classified simply as folds.

Interestingly, our results directly show that chain branching fundamentally changes the stretching behavior of polymer molecules. In polymer chains adopting half dumbbell or dumbbell conformations, comb polymers stretch under weaker deformations than linear polymers. For these conformations, linear polymers require up to ~7 units of accumulated strain to fully extend, whereas comb polymers with low or high branching require up to ~5 or ~3 units of strain, respectively. Remarkably, highly branched comb polymers in dumbbell-like configurations undergo nearly identical stretching pathways compared to linear chains. Rapid uniform stretching can be attributed to several possible effects, including but not limited to: stiffer polymer backbones due to the presence of branches, “loose” initial conformations of the polymer coil due to steric hindrance of branches, and additional hydrodynamic drag between the surrounding fluid and branches.

For folded conformations, however, we observe fundamentally different stretching behaviors for linear and comb polymers. We find that folded conformations generally exhibit the slowest unraveling dynamics in flow; this remains true for comb polymers regardless of the degree of

branching. Surprisingly, the presence of branches does not uniformly increase the rate of unraveling in molecules adopting folded conformations. In linear polymers and highly branched polymers, we observe an initial slow unraveling of the chain, followed by a smooth (and rapid) stretching response upon escaping the fold. This unraveling behavior is reflected by the steep slope of stretching trajectories with respect to accumulated strain that occurs between regions of initial slow unfolding and steady-state extension at long times. For comb polymers containing only a few branches, our results show that stretching of folded molecules proceeds at widely varying rates.

In a separate experiment, we also investigated the response of single comb polymers with longer side branches (40 kbp backbones and 2200 bp branches) during transient stretch in extensional flow. Single molecule stretching trajectories are shown in **Figure 5.12**, where comb polymers are divided into subsets with low branching (1-4 branches) and high branching (5 or more branches). Trajectories are sorted by molecular conformations observed during stretch: kinks (green), half dumbbells (black), dumbbells (blue), and folds (red). Although we used a narrow range of strain rates in this experiment ($0.70 < \dot{\varepsilon} < 0.85$), different values of τ_1 between comb polymer populations result in $Wi_{\text{low branching}} = 3.8 \pm 0.4$ and $Wi_{\text{high branching}} = 5.4 \pm 0.4$. As before, variations in *Wi* reflect the propagation of uncertainties from the longest polymer relaxation time and strain rates within the microfluidic device. Despite these differences in *Wi*, we compare trajectories on the basis of branch frequency, rather than flow strength.

Figure 5.12 shows similar trends between comb polymers with low and high branching as described for prior data on combs with shorter ~1 kb branches. Highly branched polymers stretch quickly and uniformly upon releasing their initial conformations, and this behavior is observed for dumbbell-like or folded conformations. Comb polymers with only a few branches exhibit a broad

spectrum of conformations, including kinked conformations, which were rarely observed in molecules with shorter (30 kbp) backbones. Interestingly, molecules with folded conformations show high degrees of variability in stretching trajectories. Direct visualization of molecules during stretch reveals that the apex of a fold persists at or near a branch point, as shown in **Figure 5.13**. In this way, a branched polymer will temporarily accommodate the fold until an end becomes free, after which the polymer stretches to its steady-state extended conformation through a mechanism similar to an initially kinked conformation. This stretching mechanism is fundamentally distinct compared to the unfolding pathways of linear polymers, in which the portions of the molecule on either side of the fold continuously exchange mass during the unfolding event. Here, the apex of the fold translates along the length of the backbone until the fold is released.

5.4 CONCLUSIONS

In this Chapter, we present the first single molecule studies of comb polymer dynamics in extensional flow, which reveal unexpected molecular responses to flow. First, comb polymers exhibit slower relaxation mechanisms after stretch compared to linear polymers, even in the presence of relatively short branches. Second, comb polymer molecules stretch in fundamentally different ways and through different molecular conformations compared to linear polymers. Comb polymers exhibit enhanced stretching dynamics, such that molecules adopting initial dumbbell-like conformations stretch with greater uniformity and under weaker deformation compared to linear polymers. Here, increasing the degree of branching increases the uniformity of single molecule stretching trajectories.

Rapid stretching of single comb polymers is analogous to the well-known phenomenon of strain hardening in entangled branched polymer melts [3, 17, 18]. From a molecular perspective, strain

hardening is considered a result of enhanced alignment and orientation of polymer segments between branches. Similarly, single comb polymers undergo more rapid orientation and alignment than linear polymers in planar extensional flow, wherein rapid stretch is attributed to additional hydrodynamic drag between the fluid and branches. Extensional dynamics such as strain hardening are challenging to measure in polymer *solutions*, so ongoing work focuses on the development of rheological techniques to measure dilute polymer extensional dynamics [38]. These techniques will enable the direct comparison of single molecule stretching dynamics to bulk-scale extensional dynamics.

Interestingly, single molecule visualization also reveals different stretching mechanisms between folded linear and comb polymers. Linear polymers unravel smoothly from folded conformations by exchanging mass between portions of the molecule on either side of the fold, causing the apex of the fold to translate along the backbone until it is released. In contrast, comb polymers accommodate the fold, such that the fold apex persists at a branch point and unfolding can occur by various mechanisms. In some cases, the apex persists briefly before translating to another branch point or translating along the rest of the backbone as the chain unravels. In other cases, mass is not exchanged between the sides of the fold. Here, the fold persists until the ends of the molecule become separated, after which the fold acts like a "hinge" connecting two rapidly stretching sides of the molecule. In this way, the molecule stretches by a mechanism similar to that of a molecule with an initially kinked conformation. Remarkably, the inclusion of a local constraint (branch point) results in dramatically different global molecular behavior. Heterogeneous stretching of folded comb polymers may contribute to the challenging interpretation of bulk-scale rheological measurements, especially in the case of non-linear flows. From a broad perspective,

we note that these heterogeneities can only be observed through single molecule visualization of specific branch positions and backbone conformations during stretch.

5.5 FIGURES AND TABLES

Table 5.1. Comb polymer relaxation times

Backbone m.w.	Branch m.w.	Buffer condition	$L_{c,linear}$	Expected*	Observed**		
				$\tau_{1,linear}$	$\tau_{1,linear}$	$\tau_{1,low}$	$\tau_{1,high}$
30 kbp	951 bp	75 cP TX	12.0 μm	2.7 – 3.2 s	3.3 ± 0.2 s N = 21	3.4 ± 0.2 s N = 20	3.8 ± 0.3 s N = 21
40 kbp	951 bp	50 cP no TX	17.4 μm	3.3 – 3.9 s	3.5 ± 0.8 s N = 20	4.3 ± 0.2 s N = 17	4.8 ± 0.1 s N = 20
40 kbp	2200 bp	50 cP no TX	17.4 μm	3.3 – 3.9 s	3.5 ± 0.8 s N = 20	5.1 ± 0.3 s N = 6	6.8 ± 0.3 s N = 13
40 kbp	2200 bp	22.6 cP no TX	17.4 μm	1.5 – 1.8 s	n/a	2.7 ± 0.1 s N = 10	3.8 ± 0.2 s N = 5
40 kbp	2200 bp	23.5 cP no TX	17.4 μm	1.6 – 1.8 s	n/a	2.2 ± 0.1 s N = 31	2.5 ± 0.1 s N = 9
40 kbp	2200 bp	25.0 cP no TX	17.4 μm	1.7 – 2.0 s	2.3 ± 0.1 s N = 38	2.6 ± 0.1 s N = 14	2.2 ± 0.1 s N = 18

*Based on known scaling of DNA relaxation time with viscosity and molecular weight, $\tau_1 \sim \eta^1 N^{3\nu}$, $3\nu = 1.64$. Reference relaxation times are 0.058 – 0.068 s for λ-DNA with no YOYO-1 (L_c = 16.0 μm) at 1 cP. [37]

**average ± standard error of the mean; n/a indicates an experiment with no linear reference

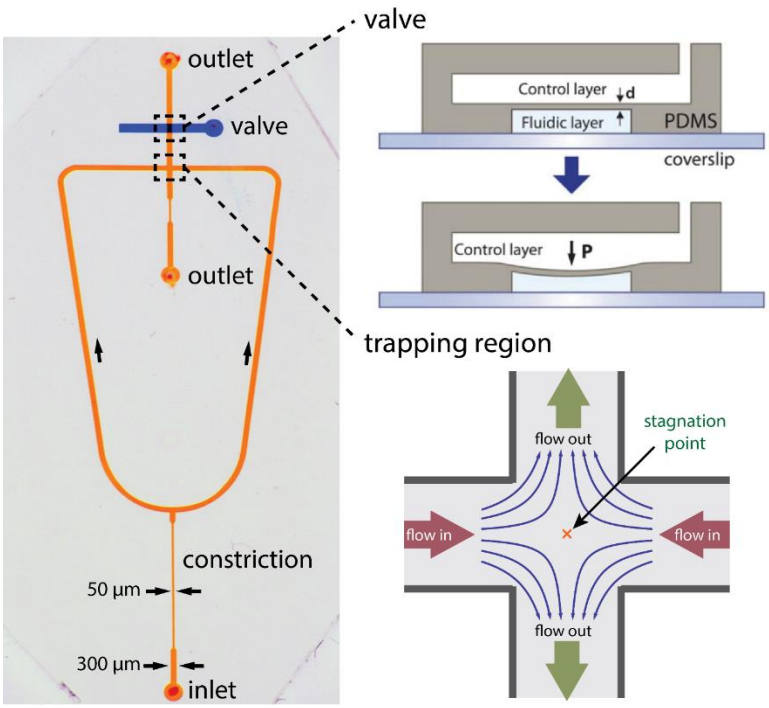

Figure 5.1. Two-layer microfluidic hydrodynamic trap. (left) Optical micrograph of device, with the fluidic layer shown in orange and the valve layer in blue. (right, top) An always-open microfluidic valve modifies the relative flow rate between two outlet channels. Increasing the valve pressure decreases the volume of the fluidic channel below the valve, thereby decreasing the fluid flow rate. Adapted with permission from M. Tanyeri and C. M. Schroeder, *Nano Letters*, 2013, **13**, 2357-2364. Copyright (2013) American Chemical Society. (right, bottom) Planar extensional flow field generated in the cross-slot region. The stagnation point position is controlled by adjusting the outlet flow rates. Automated feedback control is implemented between the imaging platform and valve pressure transducer to "trap" molecules in the stagnation point. Adapted from M. Tanyeri, E. M. Johnson-Chavarria, C. M. Schroeder, Applied Physics Letters, 2010, **96**, 224101 with the permission of AIP Publishing.

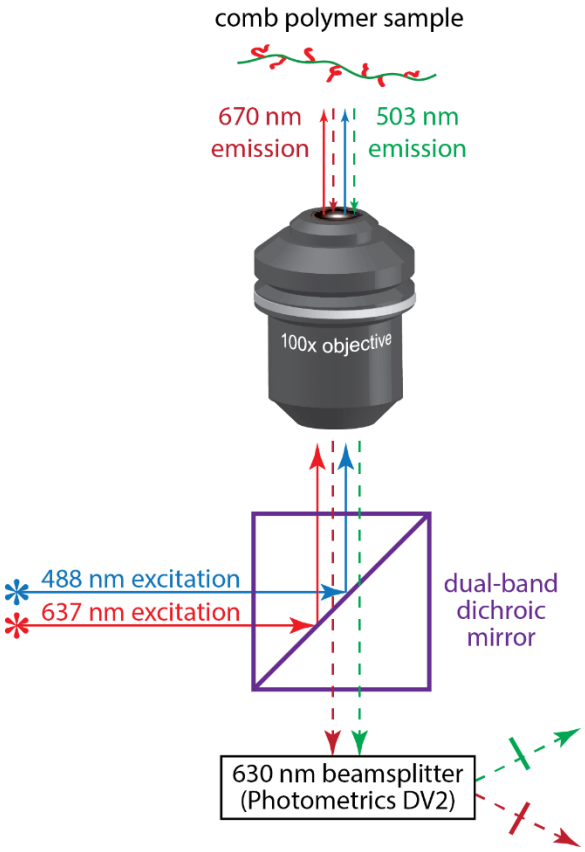

Figure 5.2. Schematic of optical setup for simultaneous branch and backbone visualization. Samples undergo simultaneous excitation at 488 nm and 637 nm. Emitted signals pass through a 630 nm beamsplitter (Photometrics DV2) and downstream bandpass filters. Channels corresponding to red and blue-green emissions are imaged side-by-side using an EMCCD camera.

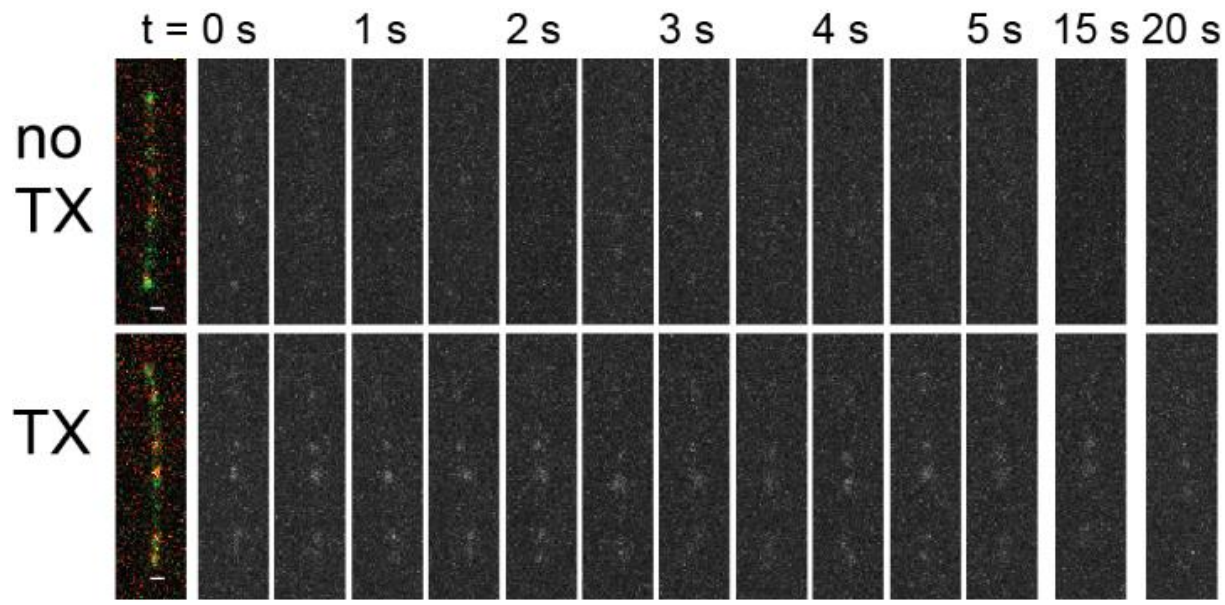

Figure 5.3. Direct single molecule visualization of DNA comb polymers in the presence and absence of TX. Stretched DNA combs, scale bars = 2.0 μm. Left: overlay of YOYO-labeled DNA (green) and Cy5-labeled branches (red).

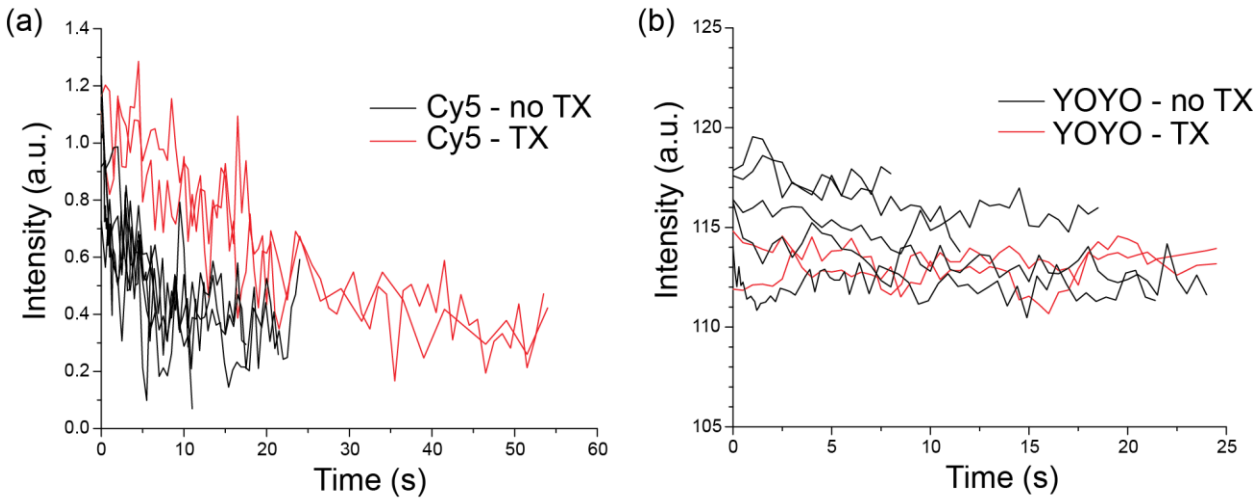

Figure 5.4. Quantitative characterization of dye photostability revealing the photostabilizing effects of TX on DNA-based combs. **(**a) Intensity of Cy5-labeled branches in the absence and presence of TX. (b) Intensity of YOYO-1 labeled DNA in the absence and presence of TX.

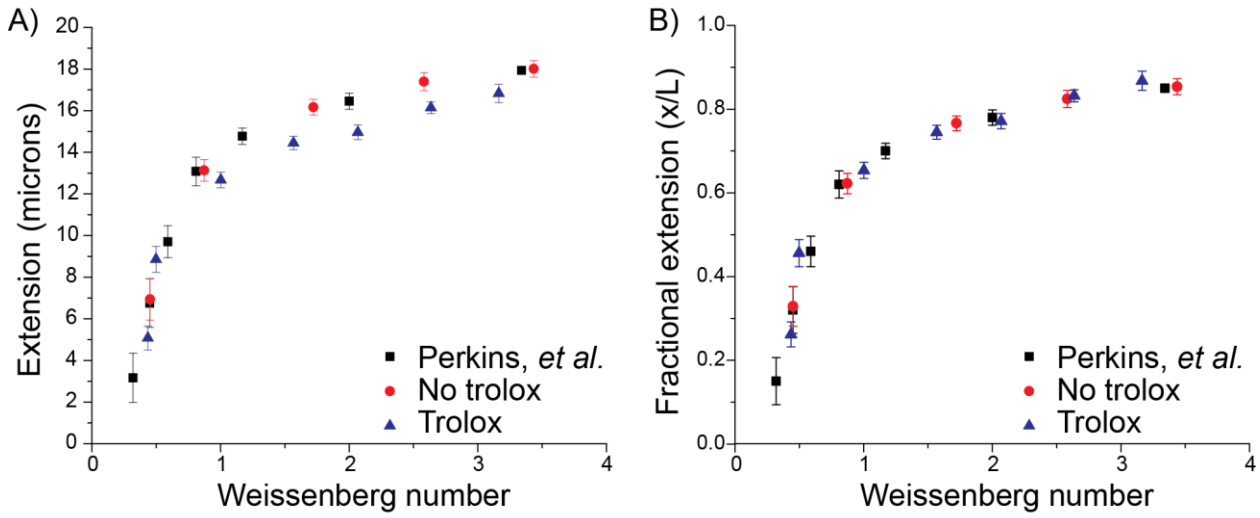

Figure 5.5. Steady state extension of λ-DNA in planar extensional flow in presence and absence of TX. (a) Steady-state extension of λ-DNA labeled with YOYO-1 as a function of *Wi* in the absence of TX (red circles) and presence of TX (blue triangles). Data from this experiment are compared to previous results of Perkins, *et al.* (black squares) [34]. (b) Steady-state fractional extension (x/L) as a function of *Wi* in the absence (L_c = 21.1 μm, τ_1 = 4.1 ± 0.3 s) and presence of TX (L_c = 19.2 μm, τ_1 = 3.5 ± 0.2 s).

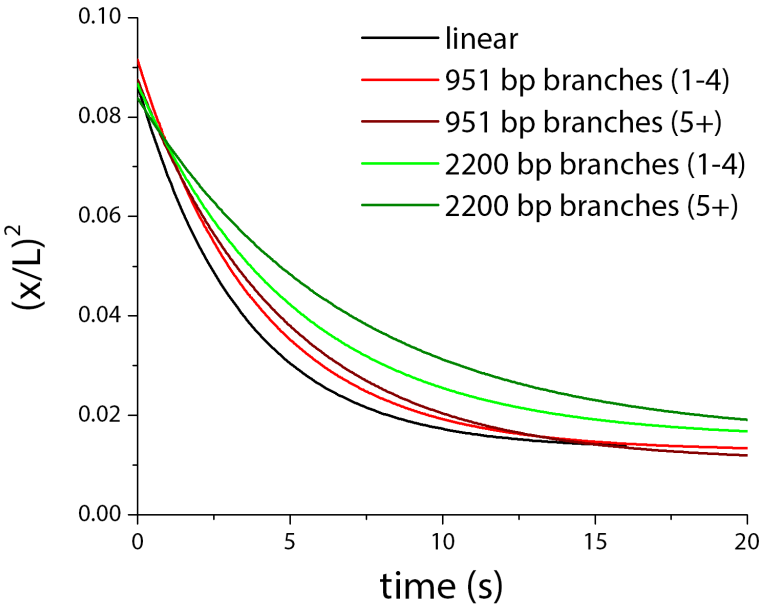

Figure 5.6. Ensemble average single molecule relaxation trajectories of 40 kbp polymers with linear backbones (black, N = 20), 40 kbp combs with 951 bp branches (red), and 40 kbp combs with 2200 bp branches (green). In all cases, η_s = 50 cP. Branched molecules are divided into subsets with low branching (1-4 branches, N_{951} = 17 and N_{2200} = 6) and high branching (5 or more, N_{951} = 20 and N_{2200} = 13). Contour length is based on labeling with YOYO-1 and imaging without TX (L_c = 17.4 μm).

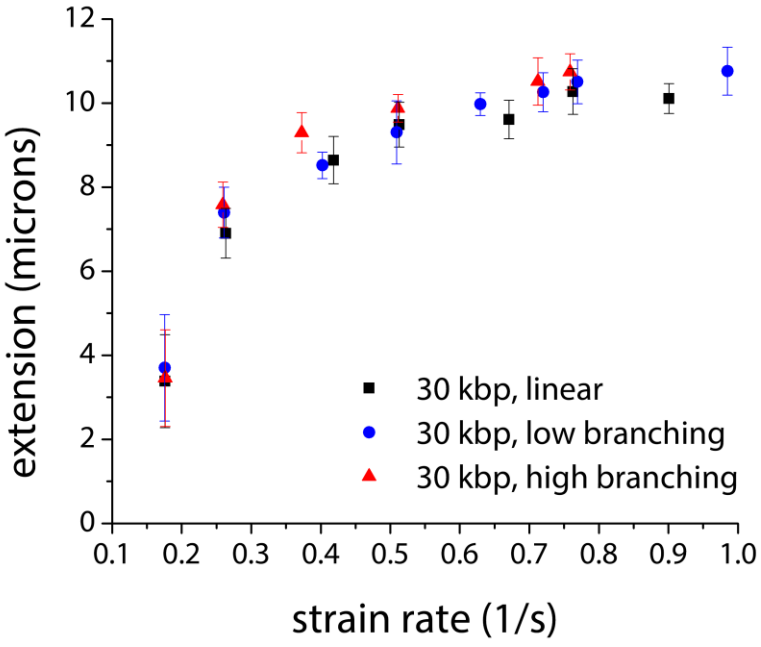

Figure 5.7. Steady-state extension of linear (black squares) and comb polymers (1-4 branches indicated by blue circles, 5 or more branches indicated by red triangles) as a function of strain rate determined by particle tracking velocimetry. Samples were labeled with YOYO-1 and observed in 75 cP buffer with TX.

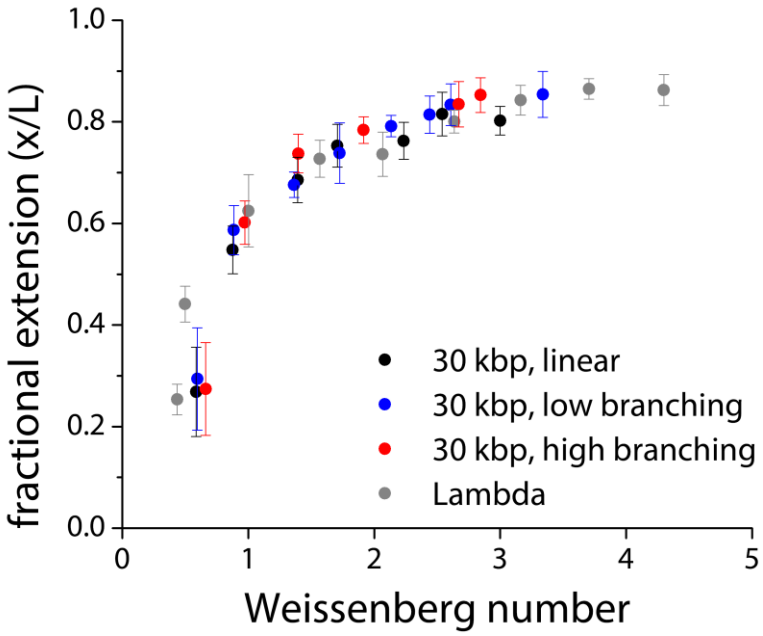

Figure 5.8. Scaled steady-state extension of linear and comb polymers. Fractional extension (x/L_c) is based on contour lengths for 30 kbp linear DNA (L_c = 12.0 μm) and λ-DNA (L_c = 19.2 μm), both of which are labeled with YOYO-1 and imaged in the presence of TX. Weissenberg numbers are defined using the average longest relaxation times for each molecular sub-population, and strain rates are determined by particle tracking velocimetry.

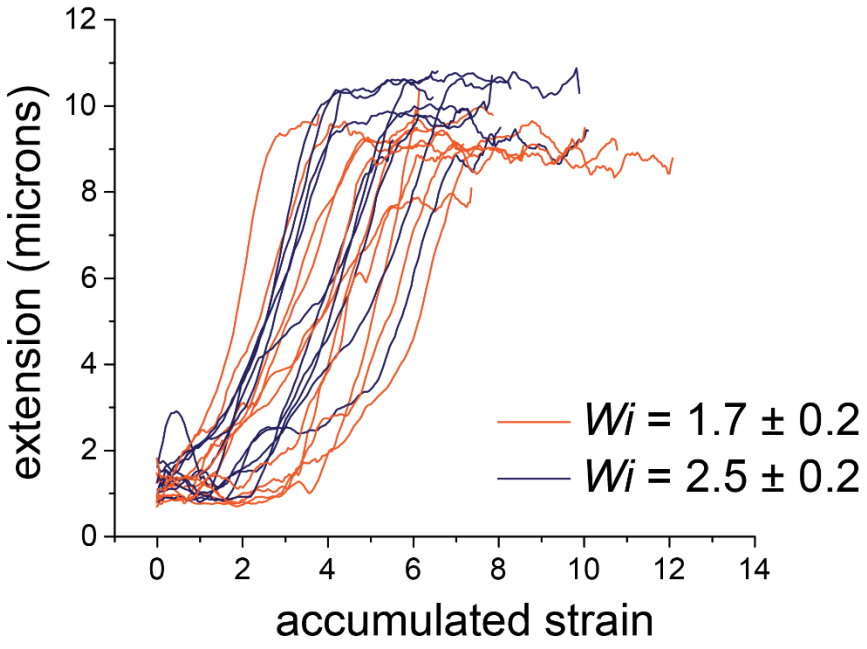

Figure 5.9. Single molecule stretching trajectories of 30 kbp linear DNA in planar extensional flow (η_s = 75 cP, DNA labeled with YOYO and imaged in the presence of TX) as functions of accumulated strain ($\dot{\varepsilon}t$). Trajectories are sorted by flow strength (Wi = 1.7 ± 0.2 in orange, Wi = 2.5 ± 0.3 in navy). Wi are expressed as average ± standard deviation; variations in Wi are due to variation in the observation of molecules at varying z-positions within the microfluidic device.

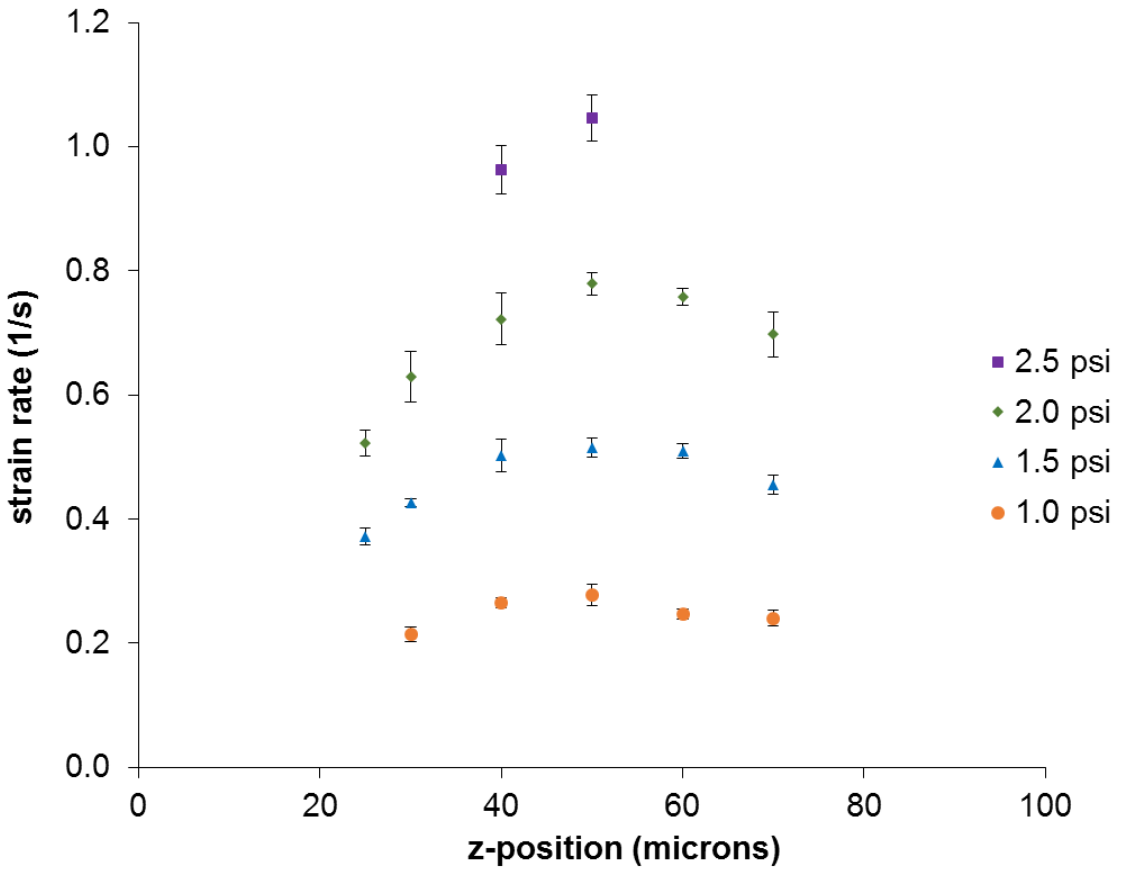

Figure 5.10. Calibration curves of strain rate in planar extensional flow as a function of *z*-position in a microfluidic device for varying fluid pressures. Data was acquired near the center of a cross-slot microfluidic device. Data points and error bars represent averages and standard deviations over triplicate videos of bead trajectories analyzed by particle tracking velocimetry.

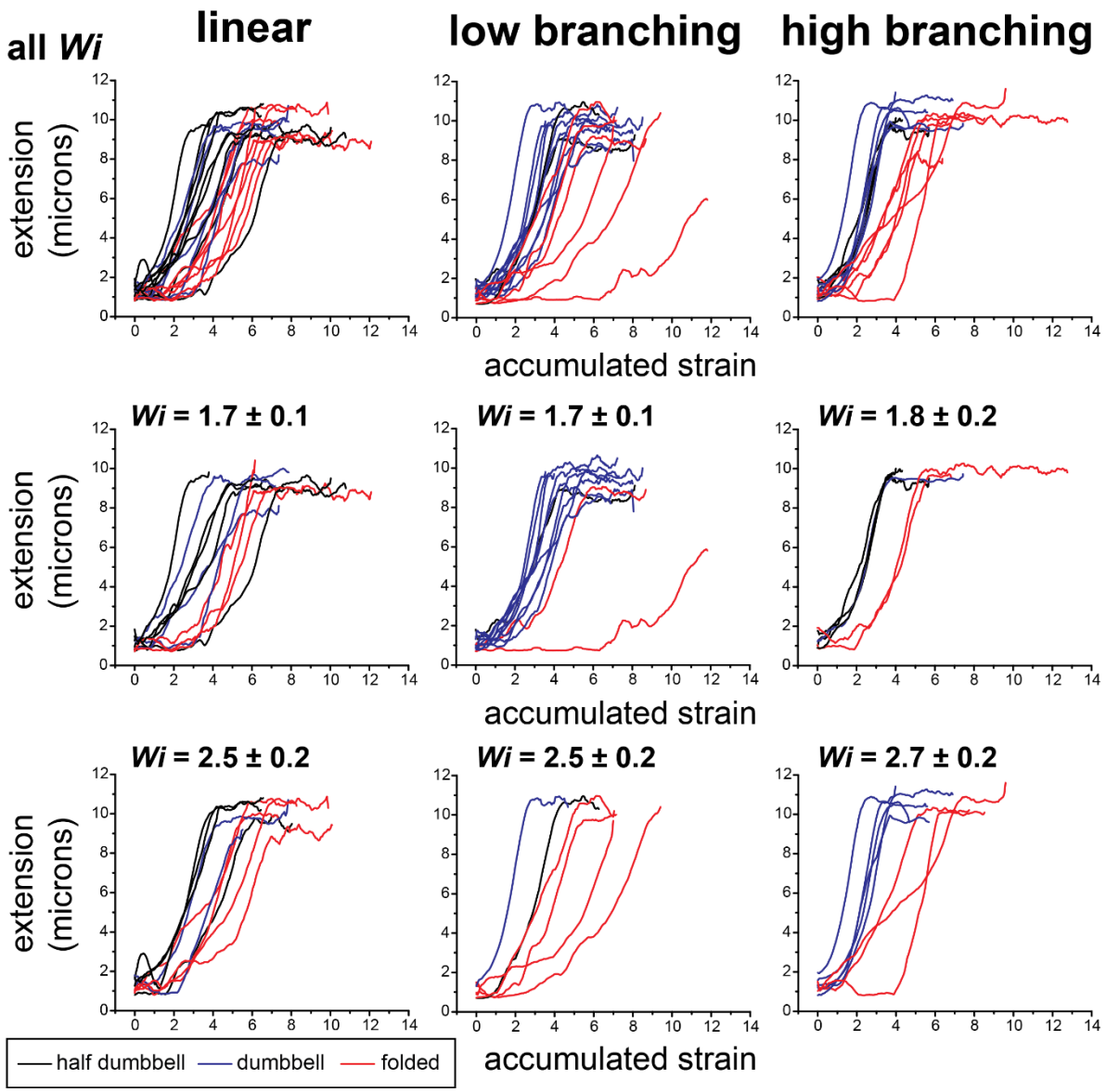

Figure 5.11. Single molecule transient stretching trajectories of linear DNA (30 kbp) or DNA combs (30 kbp backbones and 951 bp branches) in planar extensional flow (η_s = 75 cP, DNA labeled with YOYO-1 and imaged in TX-containing buffer) as functions of accumulated strain ($\dot{\varepsilon}t$). Comb polymers are divided into subsets with low branching (1-4 branches) and high branching (5 or more branches). Trajectories are sorted by flow strength (*Wi*, average ± standard deviation) and molecular conformations observed during stretch.

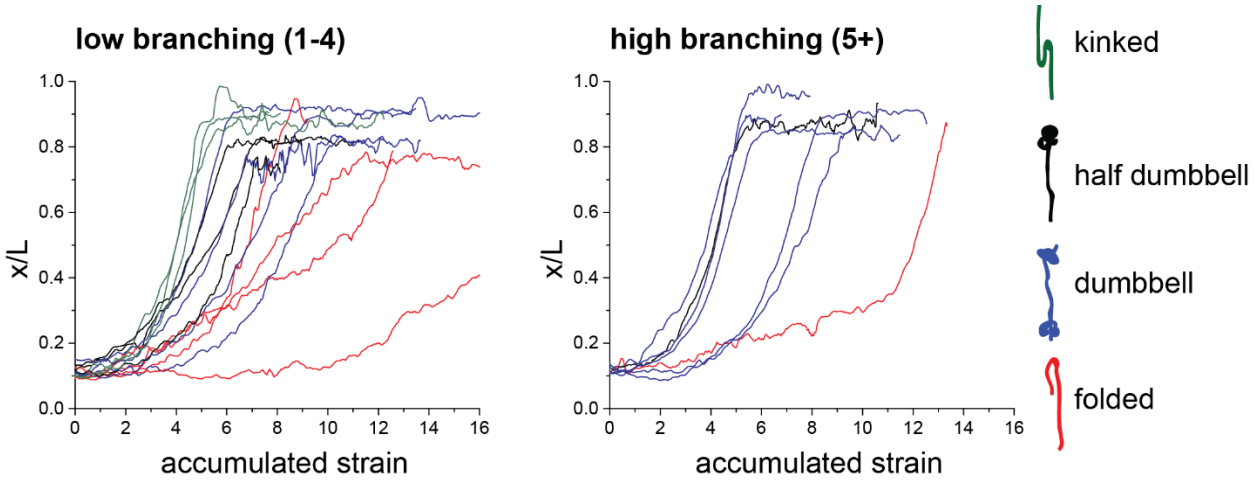

Figure 5.12. Single molecule transient stretching trajectories of DNA combs (40 kbp backbones and 2200 bp branches) in planar extensional flow (η_s = 50 cP, L_c = 17.4 μm, DNA labeled with YOYO-1 and imaged without TX) as functions of accumulated strain ($\dot{\varepsilon}t$). Comb polymers are divided into subsets with low branching (1-4 branches) and high branching (5 or more branches). Note similar strain rates used throughout this experiment ($0.70 < \dot{\varepsilon} < 0.85$) but different values of τ_1, resulting in $Wi_{\text{low branching}} = 3.8 \pm 0.4$ and $Wi_{\text{high branching}} = 5.4 \pm 0.4$. Trajectories are sorted by molecular conformations observed during stretch: kinks (green), half dumbbells (black), dumbbells (blue), and folds (red).

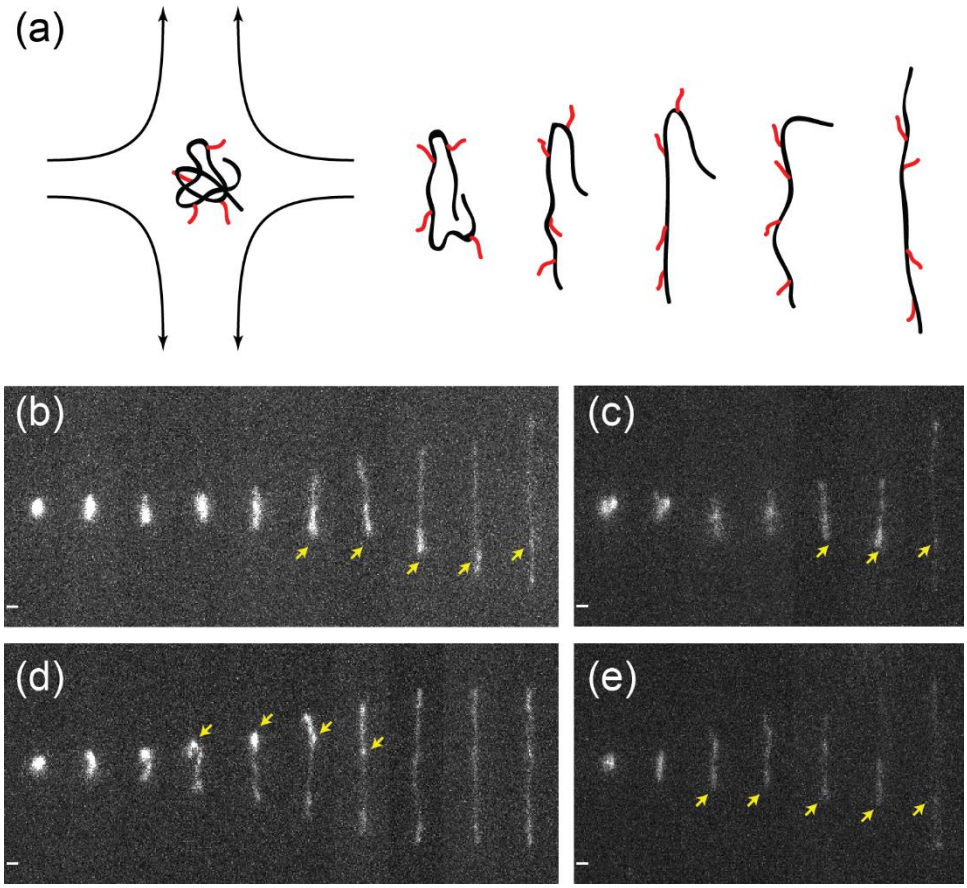

Figure 5.13. Stretching of folded comb polymer molecules in planar extensional flow. (a) Schematic of comb polymer conformations during an unfolding event. (b-d) Direct single molecule visualization of folded DNA comb polymers (40 kbp backbones with 2200 bp branches, scale bars = 1.0 μm, 2.5 s elapsed between snapshots). Yellow arrows indicate branches that persist through the apex of the fold.

5.6 REFERENCES

[1] Snijkers F, Pasquino R, Olmsted PD, Vlassopoulos D. Perspectives on the viscoelasticity and flow behavior of entangled linear and branched polymers. Journal of Physics: Condensed Matter. 2015;27:473002.

[2] Larson RG. The Structure and Rheology of Complex Fluids: OUP USA; 1999.

[3] Dealy JM, Larson RG. Structure and Rheology of Molten Polymers: From Structure to Flow Behavior and Back Again: Hanser Publishers; 2006.

[4] Duro-Castano A, Movellan J, Vicent MJ. Smart branched polymer drug conjugates as nano-sized drug delivery systems. Biomaterials Science. 2015;3:1321-34.

[5] Scholz C, Kos P, Wagner E. Comb-Like Oligoaminoethane Carriers: Change in Topology Improves pDNA Delivery. Bioconjugate Chemistry. 2014;25:251-61.

[6] Kao J, Xu T. Nanoparticle Assemblies in Supramolecular Nanocomposite Thin Films: Concentration Dependence. Journal of the American Chemical Society. 2015;137:6356-65.

[7] Choi H, Park J, Tak T, Kwon Y-N. Surface modification of seawater reverse osmosis (SWRO) membrane using methyl methacrylate-hydroxy poly(oxyethylene) methacrylate (MMA-HPOEM) comb-polymer and its performance. Desalination. 2012;291:1-7.

[8] Kapnistos M, Vlassopoulos D, Roovers J, Leal LG. Linear Rheology of Architecturally Complex Macromolecules: Comb Polymers with Linear Backbones. Macromolecules. 2005;38:7852-62.

[9] Daniels DR, McLeish TCB, Crosby BJ, Young RN, Fernyhough CM. Molecular Rheology of Comb Polymer Melts. 1. Linear Viscoelastic Response. Macromolecules. 2001;34:7025-33.

[10] Chambon P, Fernyhough CM, Im K, Chang T, Das C, Embery J, et al. Synthesis, Temperature Gradient Interaction Chromatography, and Rheology of Entangled Styrene Comb Polymers. Macromolecules. 2008;41:5869-75.

[11] Hu M, Xia Y, McKenna GB, Kornfield JA, Grubbs RH. Linear Rheological Response of a Series of Densely Branched Brush Polymers. Macromolecules. 2011;44:6935-43.

[12] Inkson NJ, Graham RS, McLeish TCB, Groves DJ, Fernyhough CM. Viscoelasticity of Monodisperse Comb Polymer Melts. Macromolecules. 2006;39:4217-27.

[13] Lee JH, Driva P, Hadjichristidis N, Wright PJ, Rucker SP, Lohse DJ. Damping Behavior of Entangled Comb Polymers: Experiment. Macromolecules. 2009;42:1392-9.

[14] Kirkwood KM, Leal LG, Vlassopoulos D, Driva P, Hadjichristidis N. Stress Relaxation of Comb Polymers with Short Branches. Macromolecules. 2009;42:9592-608.

[15] Snijkers F, Vlassopoulos D, Ianniruberto G, Marrucci G, Lee H, Yang J, et al. Double Stress Overshoot in Start-Up of Simple Shear Flow of Entangled Comb Polymers. ACS Macro Letters. 2013;2:601-4.

[16] Snijkers F, Kirkwood KM, Vlassopoulos D, Leal LG, Nikopoulou A, Hadjichristidis N, et al. Viscoelasticity and nonlinear simple shear flow behavior of an entangled asymmetric exact comb polymer solution. Journal of Rheology. 2016;60:451-63.

[17] Kempf M, Ahirwal D, Cziep M, Wilhelm M. Synthesis and Linear and Nonlinear Melt Rheology of Well-Defined Comb Architectures of PS and PpMS with a Low and Controlled Degree of Long-Chain Branching. Macromolecules. 2013;46:4978-94.

[18] Lentzakis H, Vlassopoulos D, Read DJ, Lee H, Chang T, Driva P, et al. Uniaxial extensional rheology of well-characterized comb polymers. Journal of Rheology. 2013;57:605-25.

[19] McLeish TCB. A tangled tale of topological fluids. Physics Today. 2008;61:40.

[20] Robertson CG, García-Franco CA, Srinivas S. Extent of branching from linear viscoelasticity of long-chain-branched polymers. Journal of Polymer Science Part B: Polymer Physics. 2004;42:1671-84.

[21] van Ruymbeke E, Lee H, Chang T, Nikopoulou A, Hadjichristidis N, Snijkers F, et al. Molecular rheology of branched polymers: decoding and exploring the role of architectural dispersity through a synergy of anionic synthesis, interaction chromatography, rheometry and modeling. Soft Matter. 2014;10:4762-77.

[22] Snijkers F, van Ruymbeke E, Kim P, Lee H, Nikopoulou A, Chang T, et al. Architectural Dispersity in Model Branched Polymers: Analysis and Rheological Consequences. Macromolecules. 2011;44:8631-43.

[23] Unger MA, Chou H-P, Thorsen T, Scherer A, Quake SR. Monolithic Microfabricated Valves and Pumps by Multilayer Soft Lithography. Science. 2000;288:113-6.

[24] McDonald JC, Whitesides GM. Poly(dimethylsiloxane) as a Material for Fabricating Microfluidic Devices. Accounts of Chemical Research. 2002;35:491-9.

[25] Tanyeri M, Schroeder CM. Manipulation and Confinement of Single Particles Using Fluid Flow. Nano Letters. 2013;13:2357-64.

[26] Tanyeri M, Johnson-Chavarria EM, Schroeder CM. Hydrodynamic trap for single particles and cells. Applied Physics Letters. 2010;96:224101.

[27] Altman RB, Terry DS, Zhou Z, Zheng Q, Geggier P, Kolster RA, et al. Cyanine fluorophore derivatives with enhanced photostability. Nat Meth. 2012;9:68-71.

[28] Rasnik I, McKinney SA, Ha T. Nonblinking and long-lasting single-molecule fluorescence imaging. Nat Meth. 2006;3:891-3.

[29] Cordes T, Vogelsang J, Tinnefeld P. On the Mechanism of Trolox as Antiblinking and Antibleaching Reagent. Journal of the American Chemical Society. 2009;131:5018-9.

[30] Günther K, Mertig M, Seidel R. Mechanical and structural properties of YOYO-1 complexed DNA. Nucleic Acids Research. 2010;38:6526-32.

[31] Kundukad B, Yan J, Doyle PS. Effect of YOYO-1 on the mechanical properties of DNA. Soft matter. 2014;10:9721-8.

[32] Mai DJ, Marciel AB, Sing CE, Schroeder CM. Topology-Controlled Relaxation Dynamics of Single Branched Polymers. ACS Macro Letters. 2015;4:446-52.

[33] Tree DR, Muralidhar A, Doyle PS, Dorfman KD. Is DNA a Good Model Polymer? Macromolecules. 2013;46:8369-82.

[34] Perkins TT, Smith DE, Chu S. Single Polymer Dynamics in an Elongational Flow. Science. 1997;276:2016-21.

[35] Smith DE, Chu S. Response of Flexible Polymers to a Sudden Elongational Flow. Science. 1998;281:1335-40.

[36] De Gennes PG. Coil-stretch transition of dilute flexible polymers under ultrahigh velocity gradients. The Journal of Chemical Physics. 1974;60:5030-42.

[37] Perkins T, Quake, Smith D, Chu S. Relaxation of a single DNA molecule observed by optical microscopy. Science. 1994;264:822-6.

[38] Dinic J, Zhang Y, Jimenez LN, Sharma V. Extensional Relaxation Times of Dilute, Aqueous Polymer Solutions. ACS Macro Letters. 2015;4:804-8.

6 BROWNIAN DYNAMICS SIMULATIONS OF COMB POLYMERS

6.1 INTRODUCTION

Advances in microfluidic systems and synthesis of DNA polymers with complex topologies have enabled direct observation of molecular-scale behaviors in branched polymers. Previously, single molecule experiments have been paired with coarse-grained simulations to elucidate the dynamic behavior of DNA polymers in numerous settings, including linear chains in shear flow [1, 2], knot formation in confined polymers [3, 4], and ring polymers in planar extensional flow [5, 6]. Moreover, molecular-scale models of polymers have aided the development of theories in polymer physics and rheology, such as a single-chain slip-spring model for monodisperse polymer melts [7] and molecular constitutive equations for polymers with pom-pom architectures [8].

Theories for the behaviors of dilute linear [9, 10] and star-like [11, 12] polymers have been proposed and studied for several years, but these have not been generalized to universally describe the behavior of polymers with complex architectures in non-equilibrium flows. Moreover, modern theoretical approaches for branched polymers focus on entangled solutions and melts [13-16], which exhibit different physical responses compared to single polymer molecules in dilute solutions.

In this Chapter, we present Brownian dynamics (BD) simulations to model the behavior of single comb polymers. Simulations provide a means to explore the vast design space surrounding branched polymers, with variables including but not limited to branch length, branch frequency, and branch position. The versatile nature of BD simulations will also be useful for investigating

scaling behaviors of branched polymers and developing design rules that connect microscopic and macroscopic properties of branched polymeric materials.

6.2 METHODS

6.2.1 Coarse-grained bead-spring model

In BD simulations, polymers are modeled as a series of beads (points of hydrodynamic drag) connected by entropic springs in a surrounding continuum solvent [17-19]. Coarse-grained representations improve computational efficiency compared to atomistic or molecular dynamics while retaining the underlying physics occurring at relevant time and length scales for a particular polymeric system. The underlying physics is captured by the application of Newton's equations of motions to each bead *i* (Eq. 6.1),

$$\mathbf{F}_i^{total} = m_i \mathbf{a}_i \simeq 0 \qquad (6.1)$$

where beads are assumed to have low mass m_i and negligible inertia ($m_i \mathbf{a}_i \simeq 0$). In this way, a force balance can be written for each bead (Eq. 6.2),

$$\mathbf{F}_i^{total} = \mathbf{F}_i^{drag} + \mathbf{F}_i^{Brownian} + \mathbf{F}_i^{external} \simeq 0 \qquad (6.2)$$

where the forces acting upon the bead include hydrodynamic drag forces $\mathbf{F}_i^{drag}$ from the surrounding (implicit) viscous solvent, a Brownian force $\mathbf{F}_i^{Brownian}$ from random collisions of solvent molecules with the bead, and external forces $\mathbf{F}_i^{external}$ including any spring forces, excluded volume interactions, and external body forces.

In our simulations of comb polymers, we consider the simplified case of a free-draining polymer, in which hydrodynamic interactions between beads are neglected. In this way, the drag force reduces to Stokes drag on a sphere (Eq. 6.3),

$$\mathbf{F}_i^{drag} = -\zeta\left(\frac{\mathrm{d}\mathbf{r}_i}{\mathrm{d}t} - \mathbf{u}^{\infty}(\mathbf{r}_i)\right) \tag{6.3}$$

where ζ is the drag coefficient and $\mathbf{u}^{\infty}(\mathbf{r}_i)$ is the velocity of the solvent at the bead position $\mathbf{r}_i$. As an example, $\mathbf{u}^{\infty}(\mathbf{r}_i) = 0$ in quiescent solvent, whereas the velocity field of planar extensional flow is described by Eqs. 6.4 – 6.6:

$$u_x^{\infty} = -\dot{\varepsilon}x \tag{6.4}$$

$$u_y^{\infty} = \dot{\varepsilon}y \tag{6.5}$$

$$u_z^{\infty} = 0 \tag{6.6}$$

where $\dot{\varepsilon}$ is the fluid strain rate and *x*,*y* are the distances from the fluid stagnation point along the compressional and extensional axes, respectively. Thermal forces (Brownian motion) in the system occur on time and length scales associated with the solvent molecules, which are small compared to the beads making up the polymer molecule. These forces are defined as random statistical forces (Eqs. 6.7 and 6.8) satisfying the fluctuation-dissipation theorem.

$$\left\langle \mathbf{F}_i^{Brownian}(t) \right\rangle = 0 \tag{6.7}$$

$$\left\langle \mathbf{F}_i^{Brownian}(t) \cdot \mathbf{F}_i^{Brownian}(t') \right\rangle = 2k_B T\zeta\delta_{ij}\delta(t-t')\boldsymbol{\delta} \tag{6.8}$$

Here, brackets indicate an ensemble average, k_B is the Boltzmann constant, T is absolute temperature, δ_{ij} is the Kronecker delta, $\delta(t-t')$ is the Dirac delta function, and $\boldsymbol{\delta}$ is the unit second-

order tensor. Non-random, external forces also influence the polymer beads. In our simulations of comb polymers, we consider springs forces exerted between beads according to Eq. 6.9.

$$\mathbf{F}_i^{external} = \mathbf{F}_{i-1}^{spring} - 2\mathbf{F}_i^{spring} + \mathbf{F}_{i+1}^{spring} \qquad (6.9)$$

The magnitude of these forces can be described by a variety of models, including linear Hookean springs ($F^{spring}(r) = kr$, where k is a constant describing the spring stiffness), springs with finite extensibility, or stiff springs that can be used to model inextensible bead-rod segments. DNA is known to be accurately described by a wormlike chain model for semiflexible polymers, which is well-approximated by the Marko-Siggia spring law (Eq. 6.10) [20],

$$F^{WLC}(r) = \frac{k_B T}{l_p}\left[\frac{1}{4}\left(1 - \frac{r}{L_s}\right)^{-2} - \frac{1}{4} + \frac{r}{L_s}\right] \qquad (6.10)$$

where l_p is persistence length and L_s is the spring contour length. Combining and rearranging Eqs. 6.2, 6.3, 6.8, and 6.10 results in a Langevin equation describing the overall motion of a bead (Eq. 6.11).

$$\frac{\mathrm{d}\mathbf{r}_i}{\mathrm{d}t} = \mathbf{u}^{\infty}(\mathbf{r}_i) + \frac{1}{\zeta}\left(\delta\sqrt{2k_B T\zeta} + \frac{k_B T}{l_p}\left[\frac{1}{4}\left(1 - \frac{r}{L_s}\right)^{-2} - \frac{1}{4} + \frac{r}{L_s}\right]\right) \qquad (6.11)$$

A BD simulation is carried out by integrating Langevin equations forward in time for all beads in a polymer molecule. Here, we use a simple explicit Euler time integration scheme (Eq. 6.12),

$$\mathbf{r}_i(t + \Delta t) = \mathbf{r}_i(t) + \left(\frac{\mathrm{d}\mathbf{r}_i}{\mathrm{d}t}\right)(t) \times \Delta t \qquad (6.12)$$

where Δt is chosen to be sufficiently small to prevent the possibility of a spring from stretching beyond its fully-extended length.

6.2.2 Simulation parameters for comb polymers

Bead units *i* have negligible excluded volume or mass, but we assign a characteristic length scale $a = 2\ l_k = 4\ l_p$, where l_k is the Kuhn step length and l_p is the persistence length, in order to render the governing equations as non-dimensional. In this way, the length of a fully extended spring is then defined as $L_s = 2a$, the drag coefficient as $\zeta = 6\pi\eta a$, and the characteristic time scale describing the diffusion of the bead unit as Eq. 6.13.

$$\tau_D = {6\pi\eta a^3}\Big/{k_B T} \tag{6.13}$$

The system is made dimensionless based on characteristic length a and time τ_D, such that new variables $\tilde{r}$ and $\tilde{t}$ are defined according to Eqs. 6.14 and 6.15, respectively.

$$\tilde{r} = {r}/{a} \tag{6.14}$$

$$\tilde{t} = {t}/{\tau_D} \tag{6.15}$$

The connectivity of beads dictates contributions of spring forces within the molecule (Eq. 6.9). A linear polymer in a BD simulations is defined as a single chain of *N* beads sequentially connected by $N - 1$ springs, as shown in **Figure 6.1**. In this way, bead $i = 1$ is connected only to bead $i = 2$, whereas bead $i = 2$ is connected to both beads $i = 1$ and $i = 3$. This continues, where bead *i* is connected to beads $i - 1$ and $i + 1$, until bead $i = N$, which is only connected to bead $i = N - 1$. The connectivity rules outlined above do not hold for a branched polymer, in which branch junctions require three or more beads to be connected. To address multiple points of connectivity for a single bead, we build a connectivity matrix to describe the molecular architecture of a polymer. Simplified connectivity matrices for star and comb polymers are shown in **Figure 6.2**.

Comb polymers consist of a broad design space, with the primary parameters of interest being the backbone molecular weight M_{bb}, branch molecular weight M_{br}, branch frequency n, and branch position. Coarse-graining in BD simulations converts M_{bb} and M_{br} to the number of beads in a backbone or branch, N_{bb} and N_{br}, respectively. Here, we maintain a constant backbone $N_{bb} = 40$ beads while varying N_{br} and n, such that $N_{br} = 1$, 2, 5, 10, or 20 beads and $n = 5$, 10, or 15 branches. Branches are spaced regularly along the length of the polymer backbone. Within this parameter space, some cases are excluded to limit the total molecular size to $N \leq 200$. The linear case is also tested, such that $N_{br} = n = 0$.

Comb polymer beads are initialized according to a random walk. BD simulations are stepped forward using a time step size $\Delta t = 10^{-4}\tau_D$ for a total of 10^8 Langevin steps and sampled at every τ_D. The first 10^7 steps are discarded for equilibration. Planar extensional flow is applied for 10^7 steps according to Eqs. 6.4 – 6.6 using dimensionless elongation rate $\dot{\varepsilon}\tau_D = 0.05$. This dimensionless elongation rate is distinct from the Weissenberg number $Wi = \dot{\varepsilon}\tau_R$, where τ_R is the longest relaxation time of the entire molecule. Finally, flow is stopped and the polymer is sampled for 8×10^7 steps in the absence of flow. BD simulations are repeated to generate 50 trajectories for each polymer configuration.

6.3 Results and Discussion

In the context of the Rouse polymer model, a single polymer chain is considered to exhibit a spectrum of relaxation times associated with a corresponding spectrum of length scales. Within this spectrum are N individual 'modes' of relaxation. The zeroth mode describes the polymer's center-of-mass motion, which depends on molecular weight and the characteristic timescale according to Eq. 6.16.

$$\tau_R = N^2 \tau_D \qquad (6.16)$$

This leaves $N - 1$ *internal* modes of relaxation, in which the first mode refers to rearrangement at the length scale of the entire chain, the second mode is related to half the length of the chain, and so on. In this way, the pth mode is related to configurational rearrangement of a chain segment of size N/p for $1 < p < N - 1$, where p must be an integer. For a polymer at equilibrium, the relaxation of the end-to-end vector $\mathbf{R}(t)$ can be described as a sum of the internal relaxation modes (Eq 6.17).

$$\langle \mathbf{R}(0) \cdot \mathbf{R}(t) \rangle \sim \sum_{p>1} e^{-t/\tau_p} \qquad (6.17)$$

Brownian dynamics simulations enable the direct calculation of all relaxation modes for an equilibrium polymer chain, but the mode structure of branched polymers remains unclear. As a first step toward understanding the mode structure of branched polymers, we compare the relaxation of linear and comb polymers at equilibrium. Here, we calculate $\langle \mathbf{R}(0) \cdot \mathbf{R}(t) \rangle$ for $t > 3 \times 10^3$ τ_D in the BD simulation, such that we neglect the stretching portion of the simulated trajectory. For comb polymers, $\mathbf{R}(t)$ is defined as the end-to-end vector of the backbone chain. Single molecule trajectories of an ensemble of linear polymers ($N = 40$) and comb polymers ($N_{bb} = 40$, $N_{br} = 5$, $n =$ 10 branches) are compared in **Figure 6.3**. In general, comb polymers relax more slowly than linear polymers, and comb polymers also exhibit greater variation between trajectories.

In **Figure 6.4**, we compare the impact of branch number on relaxation with a constant branch length $N_{br} = 5$. Each curve represents an ensemble average of 50 trajectories. The observed trend is consistent our experimental findings, such that increasing the degree of branching increases the relaxation time. This trend holds across all simulated branch lengths, as shown in **Figure 6.5**. Here,

ensemble averages of relaxation times are determined by fitting each trajectory to a single exponential decay (Eq. 6.18), and error bars reflect standard error of the mean.

$$\langle \mathbf{R}(0) \cdot \mathbf{R}(t) \rangle = c_1 e^{-t/\tau} + c_2 \qquad (6.18)$$

In **Figure 6.6**, we also compare the impact of branch length on relaxation with a constant branch number n = 10 branches. Perhaps not surprisingly, increasing the branch length increases the backbone relaxation time. This trend is shown for all branch numbers in **Figure 6.7**.

We evaluate data from all of the simulations in a consistent way by comparing relaxation times to the total number of beads in a molecule, $N_{tot} = N_{bb} + n \times N_{br}$. These data are shown in **Figure 6.8**, and molecules are colored based on the number of branches. For this range of architectures and these model parameters (no hydrodynamic interactions, excluded volume interactions, or intrachain crossing events), the scaling $\tau \sim N_{tot}$ emerges. Interestingly, this scaling contrasts the known scaling for free-draining linear chains, $\tau \sim N^2$, which is recovered from simulations of linear polymers of varying backbone lengths (N = 10, 40, 50, 100, 150, or 200 beads, average over 10 trajectories). These findings suggest that while the addition of branches to a comb polymer backbone does indeed slow the overall relaxation time, a branched polymer relaxes more quickly than a linear polymer of equivalent molecular weight. This trend is consistent with the weaker dependence of the mean-squared radius [11] and viscosity [12] on total molecular weight for unentangled branched polymers, and it would be interesting to verify this trend with more realistic model parameters or experiments.

Finally, we use BD simulations to compare the relaxation of comb polymers after stretch to the relaxation time at equilibrium. We compare τ determined by Eq. 6.18 to an analog of the

experimentally measured longest polymer relaxation time τ_1 described in Chapters 4 and 5. Here, a single-exponential decaying function is fit to the time-dependent 2D projection of extension over the interval $x(t)/L_c < 0.3$ (Eq. 6.19).

$$\left(\frac{\langle x(t)\rangle}{L_c}\right)^2 = A \exp\left(\frac{-t}{\tau_1}\right) + B \qquad (6.19)$$

Figure 6.9 compares τ and τ_1, which scale linearly such that $\tau \sim 2\tau_1$. The factor of two is due to the squared functional dependence on time in Eq. 6.19 (*e.g.* $\langle x(t)\rangle^2$) compared to the linear dependence on time in Eq. 6.18 (*i.e.* $\langle \mathbf{R}(t)\cdot\mathbf{R}(0)\rangle$). The general agreement between τ and τ_1 suggests the applicability of BD simulations to further studies of comb polymer dynamics.

6.4 CONCLUSIONS

In this Chapter, we present relaxation dynamics of free-draining comb polymer molecules at equilibrium and after high stretch using Brownian dynamics simulations. We find that simulation results are qualitatively consistent with experiments, wherein relaxation of the comb polymer backbone slows with increasing comb polymer size, whether by branch length or branch density. Interestingly, the scaling of equilibrium relaxation time with overall polymer molecular weight is weaker for comb polymers than expected for linear polymers. Finally, we find agreement between the relaxation behavior of equilibrium comb polymers and highly stretched comb polymers. Simulations enabled exact control of polymer architecture and a systematic comparison between molecular structure and dynamics.

In ongoing work, we seek to use simulation data to determine the structure of internal relaxation modes in branched polymers. We expect different behavior compared to linear polymers stemming from the connectivity of branches, and understanding these differences will lead to an

understanding of the dependence of relaxation time on specific parameters within the broad design space of branched polymers. BD simulations can also be extended beyond the simple case of free-draining comb polymers by including more complex branched architectures, chain uncrossability, hydrodynamic interactions, and/or excluded volume effects. Furthermore, new methods in BD simulations enable studies inter-molecular interactions that arise as the polymer concentration increases [21-23].

Overall, Brownian dynamics simulations provide a suitable platform for exploring the parameter space of comb polymers far beyond the scope of experimental feasibility. In this way, BD simulations can be used to improve physical intuition behind experimental observations and potentially guide future experiments.

6.5 FIGURES AND TABLES

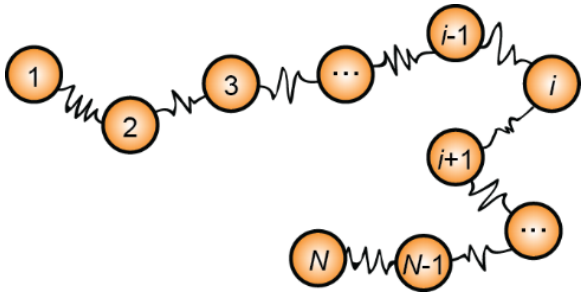

Figure 6.1. Coarse-grained bead-spring representation of a linear polymer. A spring connects bead $i = 1$ to bead $i = 2$, bead 2 is connected to beads 1 and 3, and so on. Overall, the polymer is considered to have N beads and $N - 1$ springs.

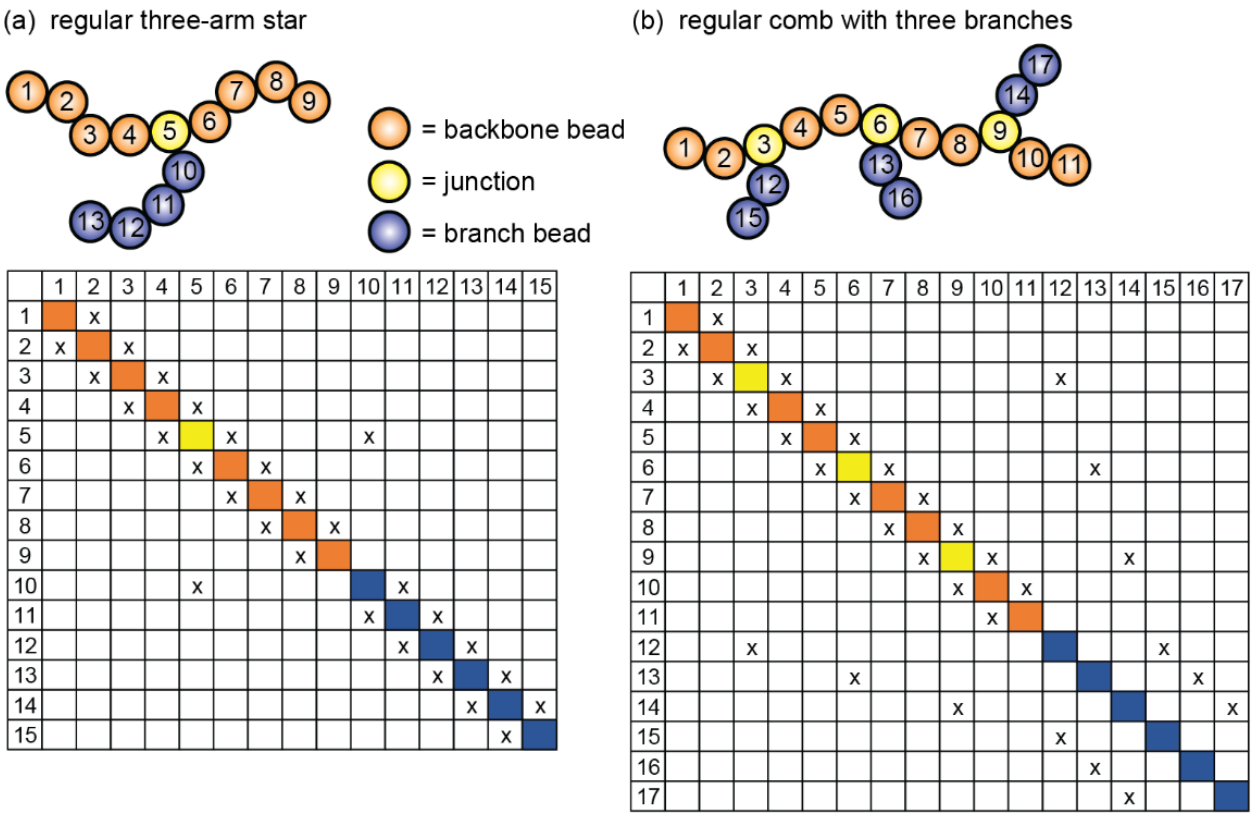

Figure 6.2. Connectivity matrices of model branched polymer molecules, where bead connections are indicated as x's. A bead cannot be connected to itself, so the self-correlations are colored for clarity with the schematics. (a) A regular three-arm star has a single junction, represented here by bead 5, which is connected to beads 4, 6, and 10. Beads at the ends of branches have a single connection (beads 1, 9, and 13) and all other beads have two connections. (b) A comb with three regularly spaced branches has three junctions (beads 3, 6, 9). Similarly, ends have only a single connection and all other beads have two connections.

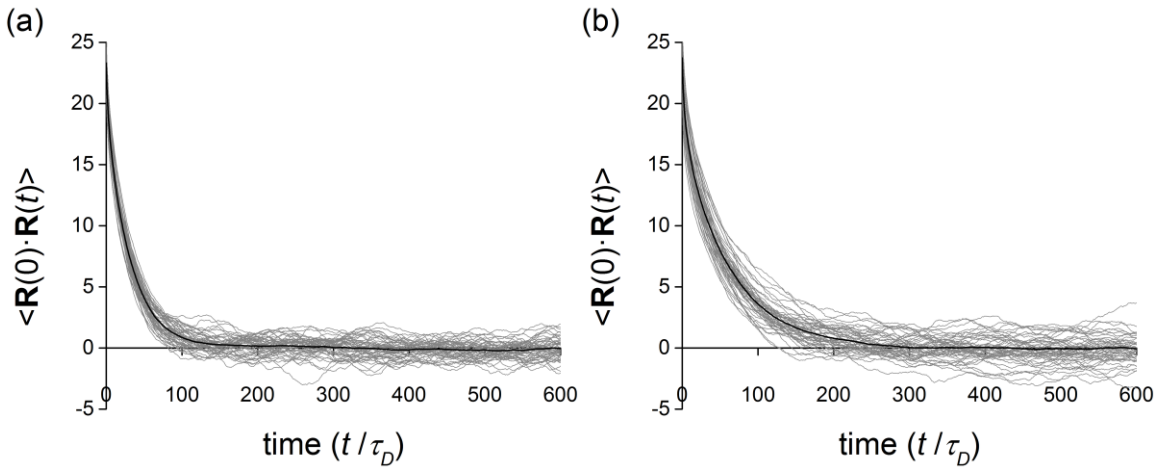

Figure 6.3. Relaxation of (a) linear polymers (N = 40) and (b) comb polymers (N_{bb} = 40, N_{br} = 5, n = 10 branches) at equilibrium. Single molecule trajectories are shown in gray, and the time-dependent ensemble average is bolded. Comb polymers with these dimensions relax more slowly and exhibit greater variation between trajectories when compared to linear polymers of equal backbone length.

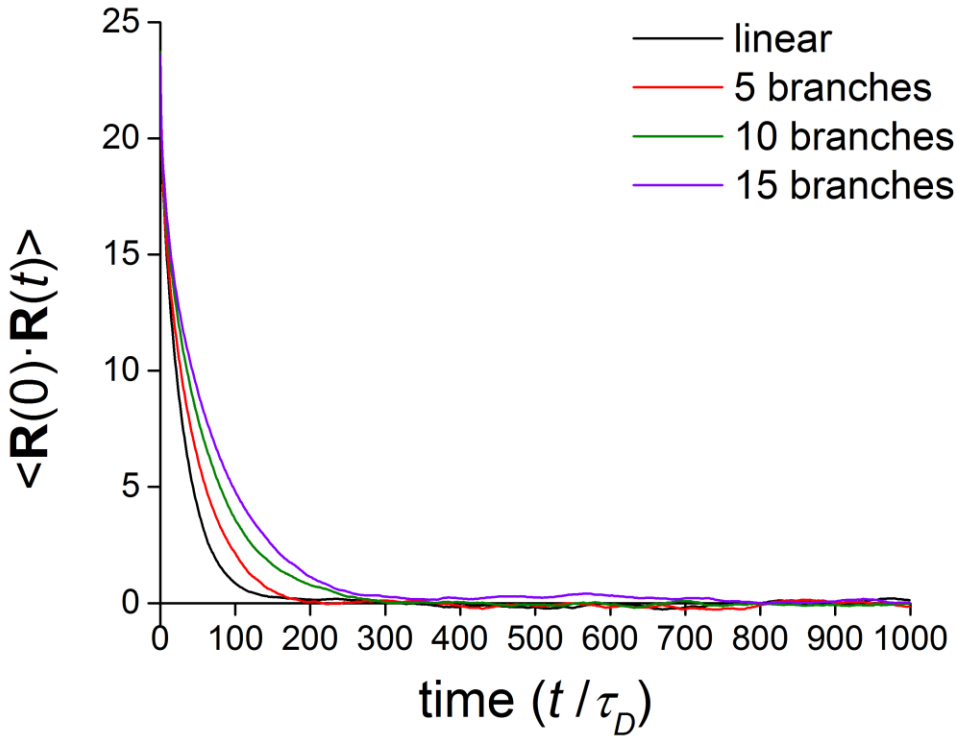

Figure 6.4. Relaxation of comb polymers (N_{bb} = 40) with constant branch length (N_{br} = 5) and varying branch number (n = 5, 10, or 15 branches). Each curve represents an ensemble average of 50 single molecule trajectories, as demonstrated in **Figure 6.3**.

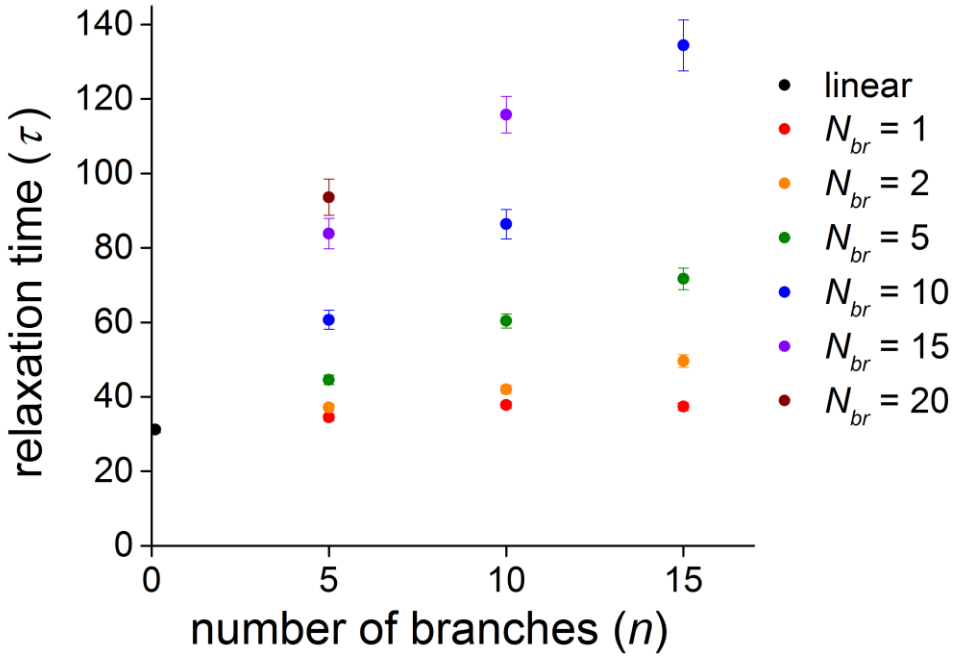

Figure 6.5. Relaxation times of comb polymers (N_{bb} = 40) with constant branch lengths and varying numbers of branches (n = 5, 10, or 15 branches). Each colored series indicates a branch length (N_{br} = 1, 2, 5, 10, 15, or 20), and each point represents an ensemble-averaged relaxation time calculated according to Eq. 6.18. Error bars reflect standard error of the mean.

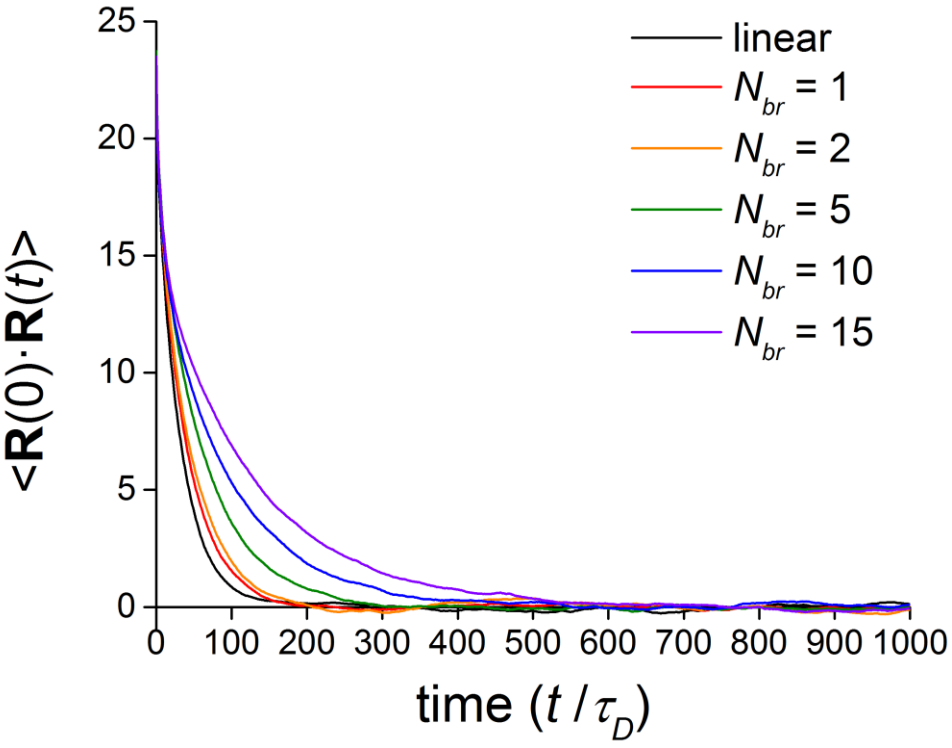

Figure 6.6. Relaxation of comb polymers (N_{bb} = 40) with constant branch number (n = 10 branches) and varying branch length (N_{br} = 1, 2, 5, 10, or 15). Each curve represents an ensemble average of 50 single molecule trajectories, as demonstrated in **Figure 6.3**.

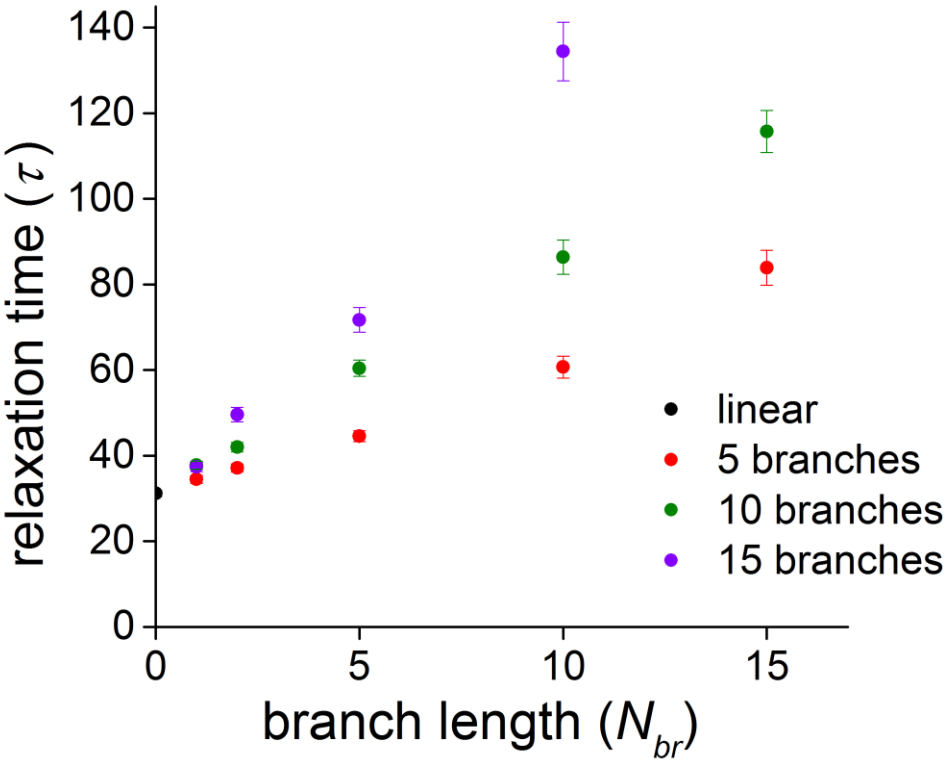

Figure 6.7. Relaxation times of comb polymers (N_{bb} = 40) with constant branch frequency and varying branch lengths (N_{br} = 1, 2, 5, 10, 15, or 20). Each colored series indicates a branch frequency (n = 5, 10, or 15 branches), and each point represents an ensemble-averaged relaxation time calculated according to Eq. 6.18. Error bars reflect standard error of the mean.

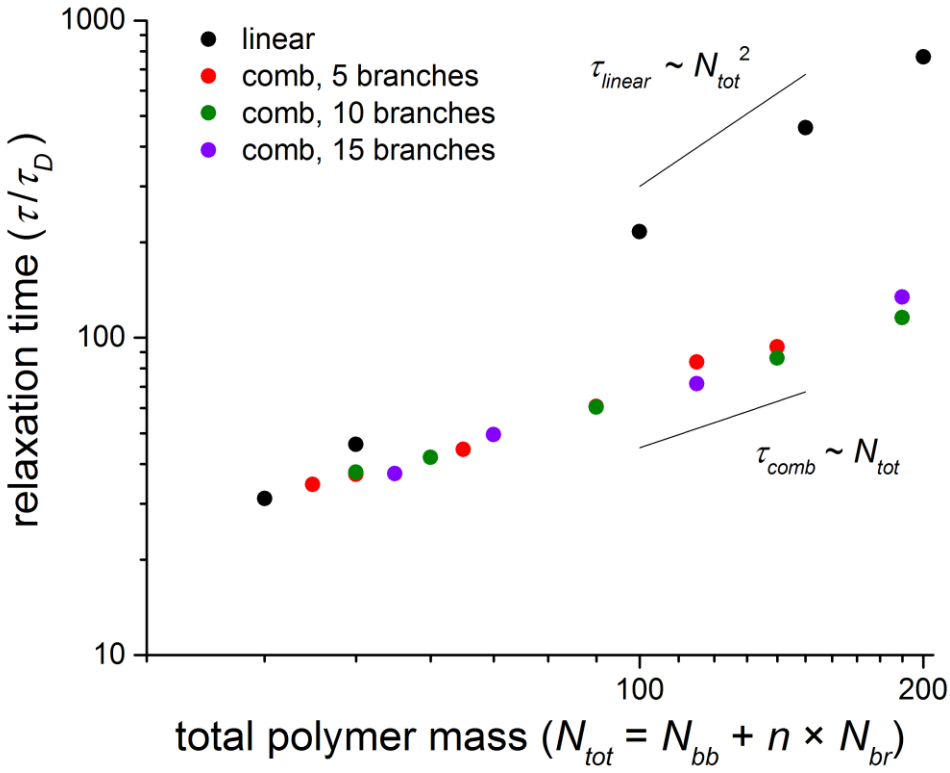

Figure 6.8. Comb polymer relaxation time as a function of total comb polymer mass, determined by $N_{tot} = N_{bb} + n \times N_{br}$. Each colored series indicates a branch frequency (n = 5, 10, or 15 branches), and each point represents an ensemble-averaged relaxation time calculated according to Eq. 6.18. Linear scaling emerges between τ and N_{tot} for comb polymers, compared to $\tau \sim N_{tot}^2$ for linear polymers.

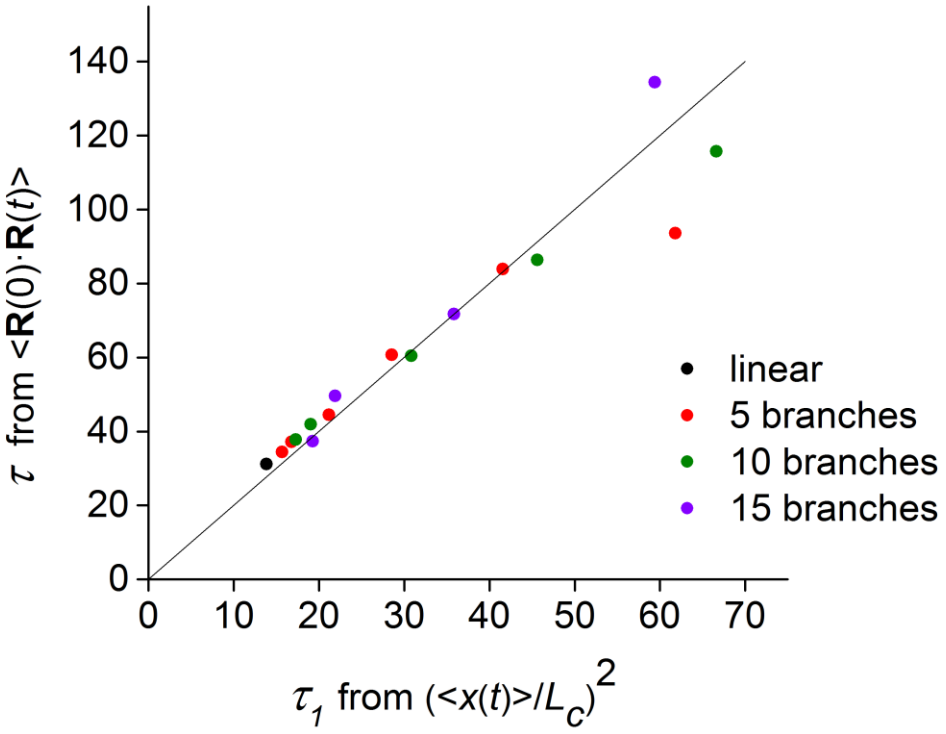

Figure 6.9. Comparison of comb polymer relaxation at equilibrium (vertical axis) and after stretch (horizontal axis). Each colored series indicates a branch frequency (n = 5, 10, or 15 branches), and each point represents ensemble-averaged relaxation times calculated according to Eq. 6.18 and Eq. 6.19. The black line corresponds to $\tau = 2\tau_1$.

6.6 REFERENCES

[1] Schroeder CM, Teixeira RE, Shaqfeh ES, Chu S. Dynamics of DNA in the flow-gradient plane of steady shear flow: observations and simulations. Macromolecules. 2005;38:1967-78.

[2] Schroeder CM, Teixeira RE, Shaqfeh ESG, Chu S. Characteristic Periodic Motion of Polymers in Shear Flow. Physical Review Letters. 2005;95:018301.

[3] Antonio S, Enzo O, Cristian M. Knotting dynamics of DNA chains of different length confined in nanochannels. Journal of Physics: Condensed Matter. 2015;27:354102.

[4] Micheletti C, Orlandini E. Knotting and Unknotting Dynamics of DNA Strands in Nanochannels. ACS Macro Letters. 2014;3:876-80.

[5] Hsiao K-W, Schroeder CM, Sing CE. Ring Polymer Dynamics Are Governed by a Coupling between Architecture and Hydrodynamic Interactions. Macromolecules. 2016;49:1961-71.

[6] Li Y, Hsiao K-W, Brockman CA, Yates DY, Robertson-Anderson RM, Kornfield JA, et al. When Ends Meet: Circular DNA Stretches Differently in Elongational Flows. Macromolecules. 2015;48:5997-6001.

[7] Likhtman AE. Single-Chain Slip-Link Model of Entangled Polymers: Simultaneous Description of Neutron Spin−Echo, Rheology, and Diffusion. Macromolecules. 2005;38:6128-39.

[8] McLeish TCB, Larson RG. Molecular constitutive equations for a class of branched polymers: The pom-pom polymer. Journal of Rheology. 1998;42:81-110.

[9] Rouse PE. A Theory of the Linear Viscoelastic Properties of Dilute Solutions of Coiling Polymers. The Journal of Chemical Physics. 1953;21:1272-80.

[10] Zimm BH. Dynamics of Polymer Molecules in Dilute Solution: Viscoelasticity, Flow Birefringence and Dielectric Loss. The Journal of Chemical Physics. 1956;24:269-78.

[11] Zimm BH, Stockmayer WH. The Dimensions of Chain Molecules Containing Branches and Rings. The Journal of Chemical Physics. 1949;17:1301-14.

[12] Zimm BH, Kilb RW. Dynamics of branched polymer molecules in dilute solution. Journal of Polymer Science. 1959;37:19-42.

[13] Dealy JM, Larson RG. Structure and Rheology of Molten Polymers: From Structure to Flow Behavior and Back Again: Hanser Publishers; 2006.

[14] McLeish TCB. Tube theory of entangled polymer dynamics. Advances in Physics. 2002;51:1379-527.

[15] Sussman DM, Schweizer KS. Microscopic theory of entangled polymer melt dynamics: Flexible chains as primitive-path random walks and supercoarse grained needles. Physical Review Letters. 2012;109:168306.

[16] Ramirez-Hernandez A, Muller M, de Pablo JJ. Theoretically informed entangled polymer simulations: linear and non-linear rheology of melts. Soft Matter. 2013;9:2030-6.

[17] Larson RG. The Structure and Rheology of Complex Fluids: OUP USA; 1999.

[18] Rubinstein M, Colby RH. Polymer Physics: OUP Oxford; 2003.

[19] Doyle PS, Underhill PT. Brownian dynamics simulations of polymers and soft matter. Handbook of Materials Modeling: Springer Netherlands; 2005. p. 2619-30.

[20] Marko JF, Siggia ED. Stretching dna. Macromolecules. 1995;28:8759-70.

[21] Saadat A, Khomami B. Computationally efficient algorithms for incorporation of hydrodynamic and excluded volume interactions in Brownian dynamics simulations: A comparative study of the Krylov subspace and Chebyshev based techniques. The Journal of Chemical Physics. 2014;140:184903.

[22] Saadat A, Khomami B. Matrix-free Brownian dynamics simulation technique for semidilute polymeric solutions. Physical Review E. 2015;92:033307.

[23] Saadat A, Khomami B. Molecular based prediction of the extensional rheology of high molecular weight polystyrene dilute solutions: A hi-fidelity Brownian dynamics approach. Journal of Rheology (1978-present). 2015;59:1507-25.

7 CONCLUSIONS AND FUTURE DIRECTIONS

Single molecule studies enable the direct observation of polymer chain dynamics at the molecular level; however, the vast majority of single polymer studies have only focused on linear DNA molecules. In our research, we extend single molecule techniques to study the dynamics of branched polymers, which effectively bridges the gap between bulk-scale rheological properties and molecular scale behavior. Our approach enables us to interrogate the impact of distributions in molecular size and architecture, thereby holding the potential to fundamentally change our understanding of the rheological response of topologically complex polymers.

In this dissertation, I first review recent studies of single molecule studies of polymers with complex topologies and architectures (Chapter 2). Experimental, computational, and theoretical advances have enabled fascinating single molecule studies of topologically complex DNA, ranging from new molecular conformations to intermolecular interactions and topology-dependent dynamics.

In our research, we specifically develop a platform to synthesize branched DNA polymers appropriate for single molecule studies (Chapter 3). We utilize a two-step 'graft-onto' synthesis method, by which we produce star, H-shaped, and comb-shaped polymers. We take advantage of the templated nature of DNA to create monodisperse polymer backbones and branches, and we control the branch distribution in an average sense. The resulting materials have suitable dimensions for direct visualization using single molecule techniques (Chapters 4 and 5). Our imaging approach enables simultaneous tracking of polymer branches and backbones. In this way, we quantify molecular properties such as branch frequency distributions and contour lengths of comb polymers.

Beyond characterization, we utilize single molecule fluorescence microscopy to study single ranched polymers in flow. We observe topology-controlled relaxation dynamics of surface-tethered branched polymers, such that molecular-scale relaxation is strongly dependent on the number and position of branches (Chapter 4). We also observe the impact of branching on relaxation of comb polymers in free solution, even in the presence of very short branches (Chapter 5). Interestingly, comb polymers in planar extensional flow exhibit different stretching mechanisms from linear polymers. From all of our single molecule experiments, we observe that the inclusion of a local constraint (branch point) results in dramatically different global molecular behavior. Heterogeneous behaviors in comb polymers may contribute to the challenging interpretation of bulk-scale rheological measurements, especially in the case of non-linear flows. We note the unique ability of single molecule techniques to provide deeper views into conformational heterogeneity and molecular response.

Finally, we probe the design space beyond our current experimental capabilities with Brownian dynamics simulations (Chapter 6). In this way, we apply a coarse-grained polymer model to investigate the impact of polymer branching on relaxation. This simple, free-draining model suggests that branched polymers exhibit a weaker dependence of relaxation on molecular weight in comparison to linear polymers, and the model is easily extended to study non-equilibrium dynamics of comb polymers.

Overall, we present molecular-scale investigations of branched polymer dynamics. Our work contributes to molecular-based understanding of topologically complex polymers in flow, thereby holding the potential to advance the large-scale production of polymers. Our results also motivate intriguing questions for further study, as the vast parameter space of branched polymeric systems

remains relatively unexplored by single molecule techniques. Progress towards preparing branched DNA at high yield and purity will enable systematic molecular-scale exploration of the impact of branching on polymer structure, properties, and dynamics. Single molecule visualization of comb polymers also hold potential for visualization of dynamic assembly processes, such that grafted branches with varying chemical properties could drive the formation of micelles, vesicles, or other assembled structures. Other areas of interest include broadening the experimental polymer design space with larger branched structures and specific labeling of backbone and/or branch ends, investigating the coil-to-stretch transition of comb polymers in various flows, and exploring the impact of branching in entangled solutions by increasing polymer concentration. In this way, an improved fundamental understanding of recently observed rheological phenomena will provide insights toward the molecular-scale design of topologically complex polymers.